NUI MAYNOOTH

Ollscoil na hÉireann Má Nuad

Near-Infrared Spectroscopy for

Brain Computer Interfacing

by

Shirley Marie-Claire Coyle

A thesis presented for the degree of

Doctor of Philosophy (Ph.D.)

National University of Ireland, Maynooth

Department of Electronic Engineering

May 2005

Head of Department: Prof. John Ringwood

Supervisors: Dr. Tomás Ward

Dr. Charles Markham

Abstract

A brain-computer interface (BCI) gives those suffering from neuromuscular impairments a means to interact and communicate with their surrounding environment. A BCI translates physiological signals, typically electrical, detected from the brain to control an output device. A significant problem with current BCIs is the lengthy training periods involved for proficient usage, which can often lead to frustration and anxiety on the part of the user and may even lead to abandonment of the device. A more suitable and usable interface is needed to measure cognitive function more directly. In order to do this, new measurement modalities, signal acquisition and processing, and translation algorithms need to be addressed. This work implements a novel approach to BCI design, using non-invasive near-infrared spectroscopic (NIRS) techniques to develop a user-friendly optical BCI. NIRS is a practical non-invasive optical technique that can detect characteristic haemodynamic responses relating to neural activity. This thesis describes the use of NIRS to develop an accessible BCI system requiring very little user training. In harnessing the optical signal for BCI control an assessment of NIRS signal characteristics is carried out and detectable physiological effects are identified for BCI development. The investigations into various mental tasks for controlling the BCI show that motor imagery functions can be detected using NIRS. The optical BCI (OBCI) system operates in real-time characterising the occurrence of motor imagery functions, allowing users to control a switch – a "Mindswitch". This work demonstrates the great potential of optical imaging methods for BCI development and brings to light an innovative approach to this field of research.

Declaration

I hereby declare that this thesis is my own work and has not been submitted in any form for another award at any university or other institute of tertiary education. Information derived from the published and unpublished work of others has been acknowledged in the text and a list of references is given.
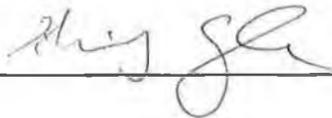
Signature: _____ Date: 07/09/05

Dedicated to the memory of my Grandmother, Mary Banche.

Acknowledgements

First of all I must thank two great supervisors, Dr. Tomás Ward and Dr. Charles Markham for all their ideas, direction and support. Their enthusiasm has prevailed from day one of this project, making my experience here an enjoyable one. The working environment here in Maynooth has been ideal and I am grateful to all those within the department who create such an amiable atmosphere. Thanks to Mr. John Maloco who can always fix a problem or find that vital component and to Mr. Karl Monaghan for being one of the first optical BCI users. I am really grateful to Mr. Bill Lanigan in the Department of Experimental Physics for all his help, which extended from troubleshooting circuits to revamping a car-seat. Thanks to Dr. Seán McCloone and Dr. Joseph Timoney for their signal-processing suggestions. I would also like to thank the other members of the Biomedical Optics Research Group, Dr. Solomiya Lebid, Mr. Ken Humphreys and Dr. Ray O'Neill, for all their help.

Thanks to all the friends that I work with for their great company, chats, sporting challenges and most importantly the welcome tea-break reliefs. I am also indebted to those who are nearest and dearest, my parents, Peter and Ghislaine, sister, Linda, and Declan, for all their help and support throughout the years.

Table of Contents

Chapter 3

Brain Computer Interfacing

Chapter 4

Basis of Near-Infrared Imaging

Chapter 5

NIRS System Design

Chapter 6

Mental strategy for BCI control

Chapter 7

Optical Brain Computer Interfacing - Applications

Chapter 8

Conclusions

Appendix A

Appendix B

Appendix C

Appendix D

References

List of Tables

List of Figures

Nomenclature

α specific absorption coefficient ($M^{-1}m^{-1}$)

A_λ attenuation at a wavelength λ

β differential pathlength (m)

B_{780nm} differential pathlength factor at 780nm

$B_{N,\lambda}$ differential pathlength factor at a wavelength λ normalised to B_{780nm}

Δc_{Hb} change in Hb concentration

Δc_{HbO} change in HbO concentration

ε specific extinction coefficient ($M^{-1}m^{-1}$)

Hb   De-oxygenated haemoglobin

HbO   Oxygenated haemoglobin

I_o incident light

I   transmitted light

L   inter-optode distance

μ_a absorption coefficient (m^{-1})

μ_s scattering coefficient (m^{-1})

List of abbreviations

ALS	Amyotrophic Lateral Sclerosis
APD	Avalanche Photodiode
BOLD	Blood Oxygenation Level Dependent
BCI	Brain Computer Interface
CCD	Charge-coupled device
CNS	Central Nervous System
CSF	Cerebrospinal Fluid
DOT	Diffuse Optical Tomography
EEG	Electroencephalography
EMG	Electromyography
EP	Evoked Potential
ER	Event Related Synchronisation
ERP	Event Related Potential
ERD	Event Related De-synchronisation
EROS	Event Related Optical Signal
fMRI	Functional Magnetic Resonance Imaging
LED	Light Emitting Diode
MEG	Magnetoencephalography
NIRS	Near-Infrared Spectroscopy
PMT	Photo-multiplier Tube
PNS	Peripheral Nervous System
OBCI	Optical Brain Computer Interface
SCP	Slow Cortical Potential
SQUID	Super Conducting Quantum Interference Device
SSVEP	Steady-state Visual Evoked Potential

List of publications arising from this work

Conference/Workshop

Coyle, S., C. Markham, W. Lanigan and T. Ward (2005). A mechanical mounting system for functional near-infrared spectroscopy brain imaging studies. Opto-Ireland 2005, non-paginated CD-ROM.

Lebid, S., R. O'Neill, C. Markham, T. Ward and S. Coyle (2005) Multi-timescale measurements of brain responses in visual cortex during functional stimulation using time-resolved spectroscopy, Opto-Ireland 2005, non-paginated CD-ROM.

Coyle, S., T. Ward and C. Markham (2004). "An Optical Brain Computer Interface." Biomedizinische Technik, Proceedings of the 2nd International Brain-Computer Interface Workshop and Training Course **49**: 45-46.

Lebid, S., R. O'Neill, C. Markham, T. Ward and S. Coyle (2004). Functional Brain Signals: A photon counting system for brain activity monitoring, IEE Conference Proceedings of The Irish Signals and Systems Conference 2004, Belfast, Northern Ireland, 469-474.

Lebid, S., R. O'Neill, C. Markham, T. Ward and S. Coyle (2004). Acquiring functional brain signals with photon counting systems: A time domain approach for pattern reversal steady-state visual evoked potentials at multiple time scales, European Workshop on Optical Fibre Sensors '04, Santander, Spain, non-paginated CD-ROM.

Coyle, S., T. Ward and C. Markham (2004). Physiological Noise in Near-infrared Spectroscopy: Implications for Optical Brain Computer Interfacing. The 26th Annual International Conference of the IEEE Engineering in Medicine and Biology Society, San Francisco, non-paginated CD-ROM.

Coyle, S., T. Ward and C. Markham (2003). Cerebral Blood Flow Changes related to Motor Imagery, using Near-infrared Spectroscopy (NIRS). World Congress on Medical Physics and Biomedical Engineering, Sydney, non-paginated CD-ROM.

Coyle, S., T. Ward, C. Markham and G. McDarby (2003). "On the suitability of Near Infrared Systems for Next Generation Brain Computer Interfaces." World Congress on Medical Physics and Biomedical Engineering 2003 **25**: 815-822.

Coyle, S., T. Ward, C. Markham, B. Roche, G. McDarby and S. F. McCloone (2003d). The use of Near-Infrared Spectroscopy in measuring general autonomic arousal. World Congress on Medical Physics and Biomedical Engineering, Sydney, Australia, non-paginated CD-ROM.

Peer-reviewed Journals

Coyle, S., T. Ward, C. Markham and G. McDarby (2003). "On the suitability of Near-Infrared Systems for Next Generation Brain Computer Interfaces." Physiological Measurement Special Issue: World Congress on Medical Physics and Biomedical Engineering 2003 **25**: 815-822.

Coyle, S., T. Ward and C. Markham (2003). "Brain-Computer Interfaces: A Review." Interdisciplinary Science Reviews **28**(2): 112-118.

Chapter 1

Introduction

"Tús maith leath na hoibre."

1.1 Preface

A Brain Computer Interface (BCI) is a communication and control channel that does not rely on the normal output pathways of the brain, namely the peripheral nerves and muscles. Instead, a BCI gives users the freedom to communicate via thought process alone. This can provide a valuable lifeline to those suffering from severe motor disabilities where a breakdown can occur in the neuronal network between the brain and muscular system, as may occur as a result of trauma, stroke or a degenerative neuromuscular disease such as amyotrophic lateral sclerosis (ALS). The most extreme manifestation of such a breakdown is known as "locked-in syndrome".

The term "locked-in syndrome" was first introduced by Plum and Posner in 1966 referring to a neurological condition manifested by quadriplegia, lower cranial nerve paralysis and mutism (Gauger 1980). Locked-in patients may experience no impairment of consciousness, may retain sensory functions and yet have little

or no capacity to interact with their environment. If there is any motor function under voluntary control it can be harnessed by using various augmentative communication technologies, e.g. head movements directing a light beam; detection of eye-blinks or eye gaze (Farwell and Donchin 1988; Burke 2001). In these scenarios one motor function substitutes another. However in cases where there is no residual motor function, signals must be detected directly from the brain in order to provide a means of communication and control. This is the objective of a brain computer interface (BCI), which makes it distinct from other augmentative communication technologies that require some form of motor control (Wolpaw *et al.* 2000). The purpose of a BCI is to provide an alternative communication and control channel for the body to interact with its surroundings. In the case of severe motor disabilities such as "locked-in" syndrome, a BCI may be the only possible communication channel, whereby the user learns to control an external device through thought process alone.

1.2   Objectives and Approaches

The objective of this thesis is to test the feasibility of using optical measurements of brain activity for the purpose of building a BCI. Most of the current BCIs measure electrical activity from the head, which can be difficult for users to learn to control. It is an aim of this work to develop a BCI that is safe, practical and accessible. Optical techniques are ideal for these requirements. The approach taken will be to use Near-Infrared Spectroscopy (NIRS), which can be used to detect various cognitive functions. This work investigates the possibility of using such signals to control an external device, presenting a novel approach to BCI research and development – An Optical Brain Computer Interface (OBCI). The term optical used in conjunction with BCI throughout this thesis refers to a system using NIRS to measure brain activity in order to control an output channel.

1.3 Contributions

While the main contribution of this thesis is the development of an optical BCI, a number of other contributions can be described as follows:

> ➤ An investigation into the suitability of NIRS for BCI development.
> ➤ A demonstration of motor imagery responses using NIRS.
> ➤ The design of custom NIRS instrumentation suitable for a BCI application, including the design of a mechanical framework for connecting sensors to the head.
> ➤ An assessment of NIRS signal characteristics and detectable physiological effects for BCI development.
> ➤ An evaluation of haemodynamic responses measured during functional activation experiments.
> ➤ The development of methods to classify events of functional brain activity for BCI deployment.
> ➤ An implementation of an OBCI application and evaluation of performance.

1.4 Outline

This thesis is organised into eight chapters. Chapter 2 gives some background information regarding the physiology and functioning of the human brain. Various functional brain imaging methods that have been developed throughout the years are also compared, and the optical imaging approach is introduced. Chapter 3 discusses the conceptual framework of a BCI and reviews current state of the art implementations. Chapter 4 focuses on NIRS and examines the physiological effects that affect the interaction of NIR light with biological tissue. Chapter 5 presents the principal factors to be considered in designing NIRS instrumentation suitable for a BCI application. Chapter 6 discusses possible mental tasks detectable using NIRS and reports the results of mental

3

imagery experiments. Chapter 7 describes the development of real-time BCI applications based on the findings of the motor imagery experiments. Conclusions and suggested future work are given in Chapter 8.

Chapter 2

The Brain – Anatomy, Function and Imaging Methods

"It is the mind that makes the body rich"

(William Shakespeare, Taming of the Shrew)

2.1   Introduction

The brain is a complex organ that scientists and philosophers have aspired to understand for centuries.   Thanks to the inquisitive nature of many pioneering researchers we now have a good understanding of its intricacies.   Today there are a number of imaging technologies that are commonplace in clinical settings for diagnosis.   This chapter outlines the body's nervous system, focusing on the brain in particular, in terms of its structure, functional organisation, connectivity, vascular schemes and signalling networks.   A knowledge of these features is important to understand the basis of functional brain imaging methods such as positron emission tomography (PET), functional magnetic resonance imaging (fMRI), electroencephalography (EEG), magnetoencephalography (MEG) and optical imaging.   The history and physiological basis of these methods is presented and the suitability of each approach for BCI development is discussed.

5

2.2 The Physiology of the Nervous System

The nervous system is a complex, highly organised network of billions of nerve cells (neurons). This section presents the histology and functionality of neurons and their organisation within the body's nervous system.

2.2.1 The Neuron

The fundamental building block of the nervous system is the nerve cell or neuron. Neurons are highly specialised cells that transmit nerve impulses from one part of the body to another. The human brain is thought to consist of 10^{11} neurons (Stevens 1979). Each neuron is fed by hundreds of other neurons and it in turn feeds into hundreds of other neurons. There are different types of neurons for performing different functions. Sensory neurons carry signals from the periphery of the body into the central nervous system. Motor neurons carry signals from the central nervous system to the muscles, skin and glands. Receptors sense the environment (chemicals, light, sound, touch) and encode this information into electrochemical messages that are transmitted by sensory neurons. Interneurons connect various neurons within the brain and spinal cord. While there are different categories of neurons, they are made up of the same basic structure and surrounded by glial cells that provide structural and metabolic support to the neurons. Neurons are comprised of three main constituents – a cell body, dendrites and an axon, as shown in figure 2.1. Each part has a specific function. The cell body is the main nutritional and metabolic centre. The dendrites branch out from the cell body and constitute the main area that receives incoming signals from other neurons. The axon generates and transmits nerve impulse or action potential to other cells. It extends away from the cell body, providing a pathway for signals to be sent to other parts of the brain and nervous system. The axon can vary in length from a couple of millimetres to over a metre depending on its signalling function. When an impulse is transmitted across to another neuronal cell the signal transfer occurs at points of contact known as synapses. The synapse is a small gap separating neurons. It consists

of a pre-synaptic ending and a postsynaptic ending with a synaptic cleft in-between, as shown in figure 2.2. Signals from the pre-synaptic ending of one neuron flows to the post-synaptic ending of another neuron across the synaptic cleft.
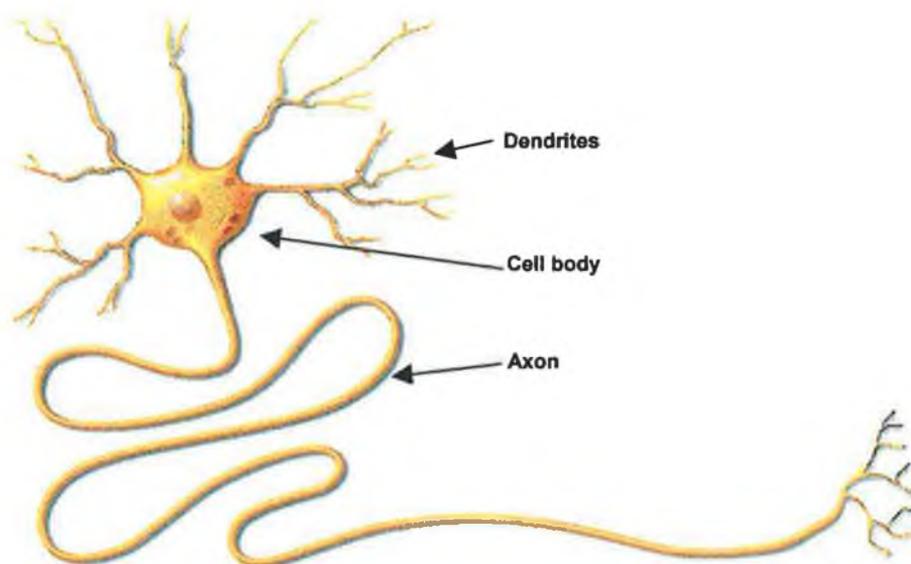
Figure 2.1 Structure of a Neuron. (Reproduced from Lancraft 2002)

The signalling event with which neurons communicate is both an electrical and chemical one. Axon transport electrical impulses, action potentials, along their fibres travelling at speeds over 100m/s. To heighten the speed of nerve impulses an insulating layer, known as myelin sheath, envelopes some axons. The action potential is produced by changes in the potentials of cell membranes, which depends on the movement of charged ions across the membrane. When a neuron is excited the permeability of the cell membrane to sodium ions increases which causes a change in the membrane potential, known as depolarisation. If a threshold of excitation is reached the neuron initiates and transmits an action potential. The action potential is either propagated over the entire axon or else it isn't propagated at all. Almost immediately after the sodium ions are allowed into the cell the membrane permeability changes, preventing sodium ions from entering but allowing potassium ions to diffuse through the membrane. This restores the resting potential of the cell and a sodium-potassium pump restores

the balance of sodium and potassium ions within the cell. When the action potential reaches the end of the axon at the synapse with another neuron the signal is transferred not as an electrical impulse, but by a chemical signal. When the action potential reaches its axonal endings vesicles containing molecules of transmitter substances are released at the pre-synaptic ending. The neurotransmitters travel across the synaptic cleft and bind to the post-synaptic ending of another neuron. The molecules affect the permeability of that neuronal membrane which in turn initiates an action potential to be transmitted to its next point of call.
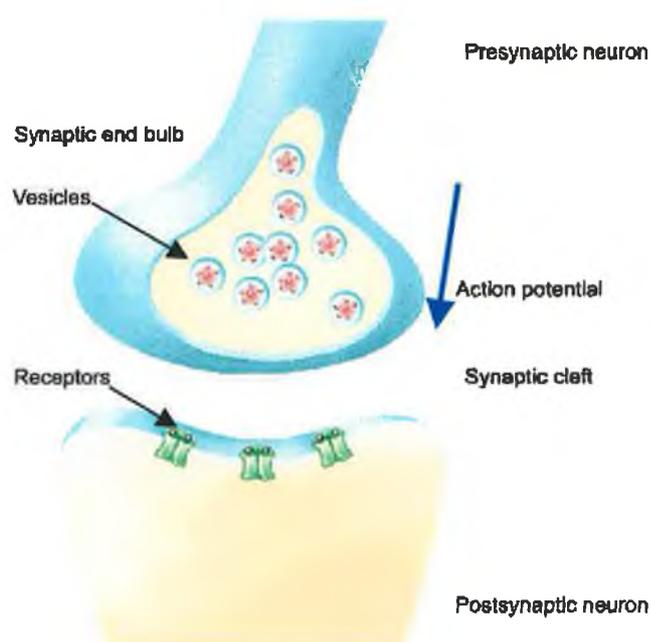
Figure 2.2 Synaptic Junction between neurons. (Reproduced from Lancraft 2002)

2.2.2 Organisation of the Nervous System

The nervous system has two subdivisions, the central nervous system (CNS) consisting of the brain and spinal cord, and the peripheral nervous system (PNS), which consists mainly of nerves linked to the spinal cord. The PNS serves as a communication line between the body's muscles and glands to the CNS, availing of millions of sensory receptors to monitor changes occurring both inside and outside the body. Sensory input is relayed to the CNS via afferent nerves where

8

the information can then be processed and interpreted. The CNS initiates a response to activate muscles or glands, carried by efferent nerves. The efferent nerves may be part of the somatic nervous system, i.e. control of voluntary movement, or the autonomic nervous system that regulates involuntary functions e.g. cardiac muscle activity. The network of nerve cells ensures that the CNS is constantly updated with sensory information from its surroundings and communicates appropriate responses as commanded by the CNS.
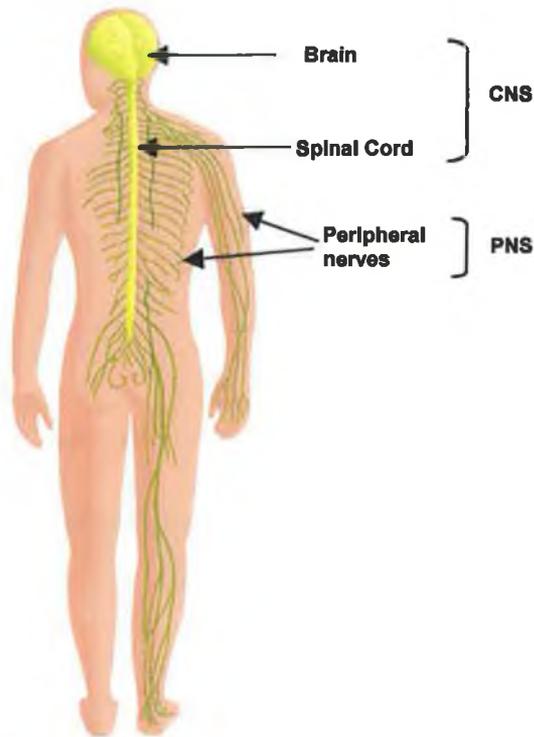
Figure 2.3 Structure of the Nervous System. (Rush University Medical Centre 2005)

2.3 The Brain

"I hold that the brain is the most powerful organ of the human body.....eyes, ears, tongue, hands and feet act in accordance with the discernment of the brain"

(Hippocrates, The Sacred Disease, Book XVII)

There is no doubt that the human brain is the essence of our being, functioning as the control centre of the body on a number of levels, assimilating information from the five senses and commissioning necessary reactions. As recognised by Hippocrates, the brain initiates and co-ordinates movements of all other body parts. The brain is central to the entire nervous system – its role is discussed in this section and also the natural safeguards that protect this vital organ to ensure homeostasis within the body.

2.3.1 Anatomy and Function

The brain performs many functions including maintaining homeostasis, assimilation of information, control of physical movement and the ability to think and experience emotions. The brain is structured into different regions each responsible for certain functions. The brain consists of four major parts – cerebrum, brain stem, cerebellum and diencephalons as shown in figure 2.4. The functionality of each region is described below.
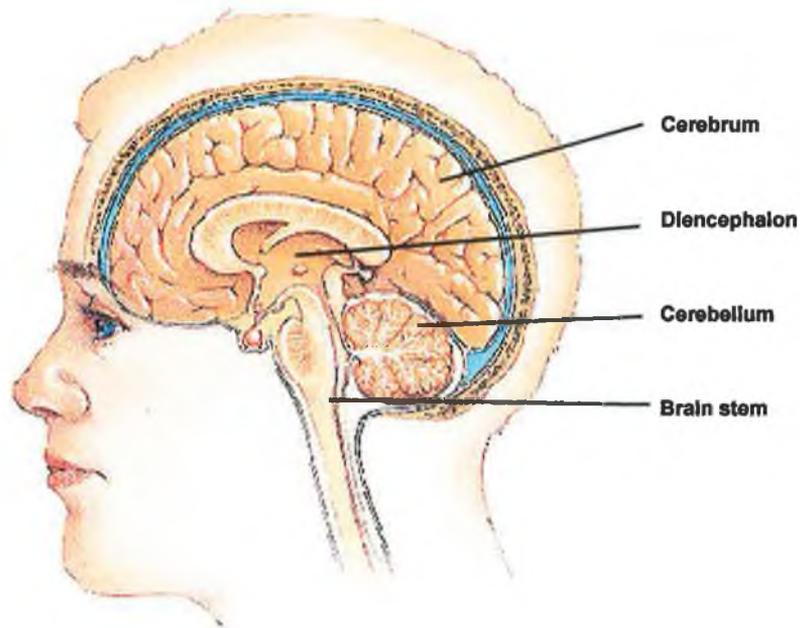
Figure 2.4 Structure of the human brain. (Reproduced from Lancraft 2002)

2.3.1.1   Brain Stem

The brain stem consists of the midbrain, pons and medulla oblongata. It provides a pathway for fibre tracts and also contains neuronal nuclei that form the cranial nerves. The midbrain contains nuclei that link the various sections of the brain involved in motor functions (cerebellum, basal ganglia, cerebral cortex), eye movements and auditory control. The pons contains nuclei that relay movement and position information from the cerebellum to the cortex. It also contains nuclei that are involved in breathing, taste and sleep. The medulla oblongata contains nuclei for regulating blood pressure and breathing, as well as nuclei for relaying information from the sense organs that comes in from the cranial nerves.

11

2.3.1.2   Cerebellum

The cerebellum is dorsal to the occipital lobe of the cerebrum. Like the cerebrum it has two hemispheres and a convoluted surface. It receives sensory input from the spinal cord, motor input from the cortex and basal ganglia and positional information from the vestibular system. The cerebellum then integrates this information and influences outgoing motor pathways from the brain to coordinate movements. It provides precise timing for skeletal muscle activity and controls balance; ensuring body movements are smooth and coordinated.

2.3.1.3   Diencephalon

The diencephalon lies above the brain stem and is enclosed by the cerebral hemispheres. It is made up of the thalamus, hypothalamus and epithalamus. The thalamus is a relay station for sensory impulses passing to the sensory cortex and participates in motor-information exchange between the cerebellum, basal ganglia and cortex. The hypothalamus is the centre for many emotions and also regulates the release of hormones from the pituitary gland, part of the endocrine system. The epithalamus is involved in forming cerebrospinal fluid.

2.3.1.4   Cerebrum

The cerebrum or cerebral hemispheres forms the outermost portion of the brain. It constitutes the largest part of the brain and is responsible for co-ordinating a number of higher-level functions. The cerebrum is divided into two hemispheres that are connected by a wide band of axons, the corpus callosum. The surface of the cerebrum is highly convoluted with folds (gyri), deep grooves (fissures) and some superficial grooves (sulci). The outer rim of grey matter, the cerebral cortex (cortex is Latin for "bark") is only 2-4mm but taking into account its multitude of convolutions it has a surface area of around $0.25m^2$ and contains

approximately one hundred billion neurons (Guyton 1987). The inner region of the cerebrum is known as white matter, so called because of the bright appearance of the myelinated axons, containing the grey matter nuclei deep within it. The longitudinal fissure divides the two cerebral hemispheres, while other fissures and sulci appear to divide the brain into different regions – frontal, temporal, parietal and occipital lobes, named after the skull bone under which they lie. Neuronal networks within the cerebral cortex are specialized, and certain functions can be roughly allotted to anatomical regions, as shown in figure 2.5, e.g. primary motor area is anterior to the central sulcus in the frontal lobe; the temporal lobe contains the primary auditory cortex which receives sensory information from the ear. Regions with specialised functions include the motor cortex, somatosensory cortex, visual cortex and auditory cortex. There are also association cortices that lie outside the primary motor or sensory areas but have reciprocal connections with these regions. The association cortices do not communicate directly with sensory or motor neurons but integrate information and inform other parts of the cortex.

The functions of the cerebral lobes are outlined as follows:

Parietal Lobe - The parietal lobes contain the primary and association cortices for somatosensory functions that receive and process all somatosensory input from the body such as touch and pain. A region called Wernicke's area, distal to the temporal lobe, is important for understanding the sensory (auditory and visual) information associated with language.

Frontal Lobe - The frontal lobe is involved in motor skills, including speech, and cognitive functions. The motor cortex, located anterior to the parietal lobe receives connections from the somatosensory cortex, processes and initiates motor functions. The frontal lobes are also important for language skills. Broca's area, a region on the left side of the frontal lobe, is involved in processing language and controlling the muscles responsible for speech (Martin 1997). Other functions of the frontal lobes include learning, thought and memory.

Occipital Lobe - The occipital lobe receives and processes visual information directly from the eyes and relates this information to Wernicke's Area in the parietal lobe and the motor cortex.

Temporal Lobe - The temporal lobe processes auditory information from the ears and relates it to Wernicke's area of the parietal lobe and the motor cortex of the frontal lobe.
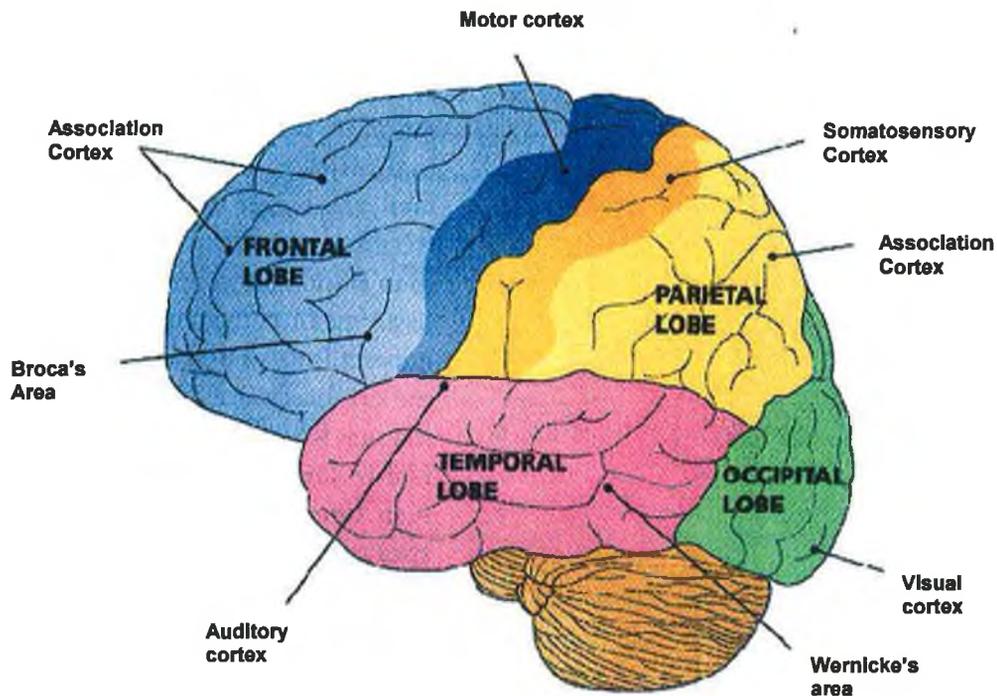
Figure 2.5 Lobes of the cerebral cortex and associated functions.

2.3.1.5   Protection of the Brain

Nature has ensured to carefully protect the brain from damage in a number of ways. Nervous tissue is very soft, delicate and unlike other cells neurons cannot be regenerated. Therefore it is vital that this tissue is carefully protected. The insulating structures must first be contended with when attempting to image the brain therefore an overview the protection mechanisms is given below.

14

Nervous tissue is shielded by bone, membranes and cushioning fluid, shown in figure 2.6. The cranium that encloses and protects the brain tissue is composed of eight bones connected to each another by interlocking immovable joints. Within the cranium are three connective tissues known as meninges. The meninges protect the brain and spinal cord from rubbing against the bones of the skull and spine. The meninges consist of dura mater, arachnoid matter and pia mater. The dura mater has two layers, one connects to the skull forming the periosteum, while the other, the meningeal, forms the outermost covering of the brain. The dural layers are fused together except for three areas where the dural sinuses collect venous blood. Arachnoid villi protruding though the dura mater are responsible for absorbing the venous blood into the dural sinuses. The arachnoid mater is made up of threadlike extensions attaching it to the pia mater ("gentle mother"). Within the subarachnoid space space is cerebrospinal fluid (CSF) which is a fluid similar to blood plasma. The CSF forms a watery cushion protecting the nervous tissue from blows and other trauma. The CSF is continually formed from blood, circulates around the brain and is returned to the blood through the arachnoid villi into the dural sinuses (Guyton 1987; Tortora and Grabowski 2003).

In addition to the structural safeguards around the brain a feature known as the blood-brain barrier provides further protection. Because nerve impulses are dependent on various ion concentrations and some amino acids, unpredictable neural activity could result if the brain tissue was exposed to fluctuations in chemicals such as hormones, ions or nutrients. Therefore the capillaries serving brain tissue are less permeable than capillaries in the rest of the body, allowing only water, glucose and essential amino acids to pass through the capillary walls and preventing urea, toxins, proteins and most drugs from entering the brain tissue. This ensures a constant internal environment within the brain.
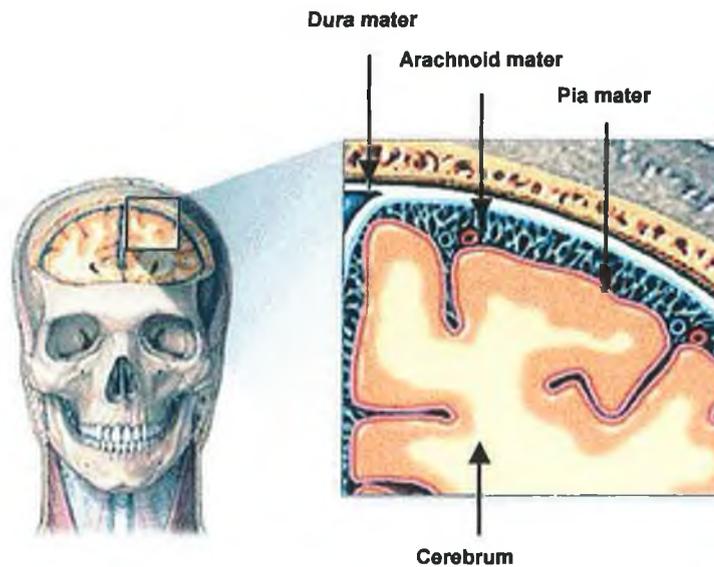
Figure 2.6 Meninges protecting brain tissue.

2.4 Brain blood supply

As the optical techniques used in this work rely on haemodynamic changes associated with brain function a description of the blood supply system is given in this section.

2.4.1 Cerebral Blood Flow

A consistent and regulated supply of blood to the brain is crucial in maintaining normal function of this complex and vital organ. The flow of blood to the brain delivers nutrients and removes metabolic by-products. The brain has highest priority in the body for the blood, even if other organs need blood, the body attempts to supply the brain with a constant flow of blood. Blood flow to the brain constitutes 15% of the total resting cardiac output, even though the brain only accounts for approximately 2% of the total body mass. Therefore brain tissue is highly perfused, with normal blood flow through the adult brain

averaging at 50-55ml/min per 100g of brain. In contrast, blood flow through skeletal muscle during rest averages 3-4ml/min per 100g of muscle (Guyton 1987).

Four major arteries, the two carotid and the two vertebral arteries, supply the brain and unite to form the circle of Willis, shown in figure 2.7. This arrangement allows adequate perfusion of the entire brain in the case of any of the four arterial vessels becoming obstructed. Adequate perfusion is critical as disruption of the cerebral blood flow for as little as 5s can result in a loss of consciousness, while ischemia lasting a few minutes results in irreversible tissue damage (Berne and Levy 2000).

Cerebral arteries

Circle of Willis

Cerebral arteries

Internal carotid artery

Basilar artery

Vertebral artery

External carotid artery

Common carotid artery

Blood supply from the heart
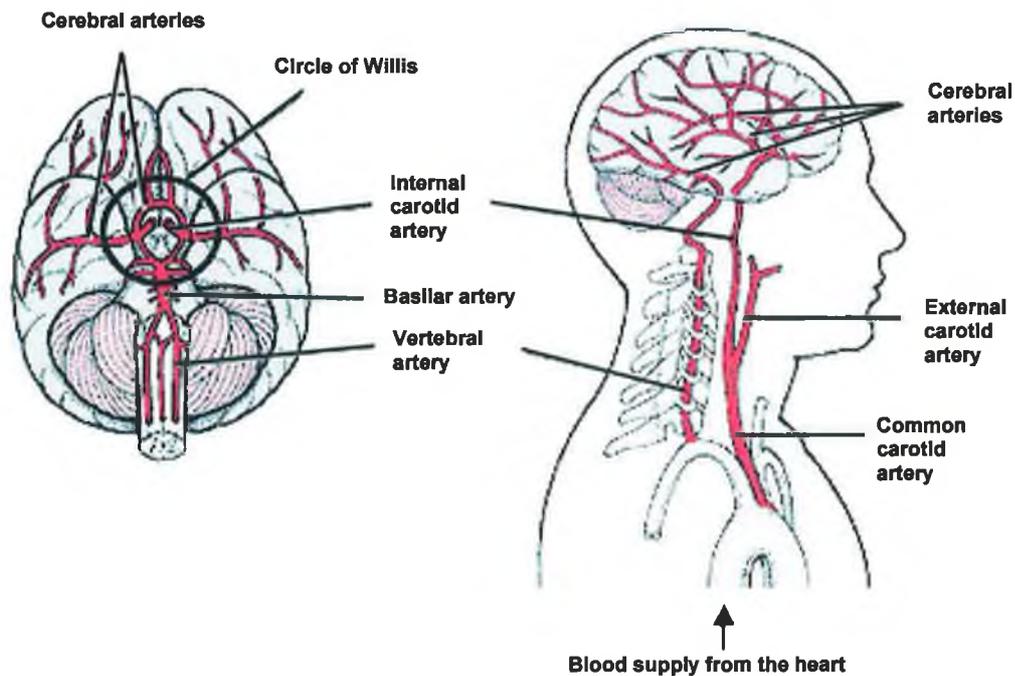
Figure 2.7 Blood supply to the brain.

The vascular organisation of the brain has been of interest to researchers for some time, particularly to establish reasons for the susceptibility of different brain areas to pathological conditions. The distribution of capillaries within the central nervous system is heterogeneous, but in a structured manner. The capillary density within a region is correlated to the number of synapses in the region. Brain areas that have a high basal level of glucose use and blood flow

17

such as the cerebral cortex have a high density of capillaries. The cortical microvasculature is correlated to anatomical arrangements within the cerebral cortex. Arterioles penetrate the cortex at right angles to the surface and give rise to capillaries at all laminae through a vertical columned arrangement, as shown in figures 2.8 and 2.9.
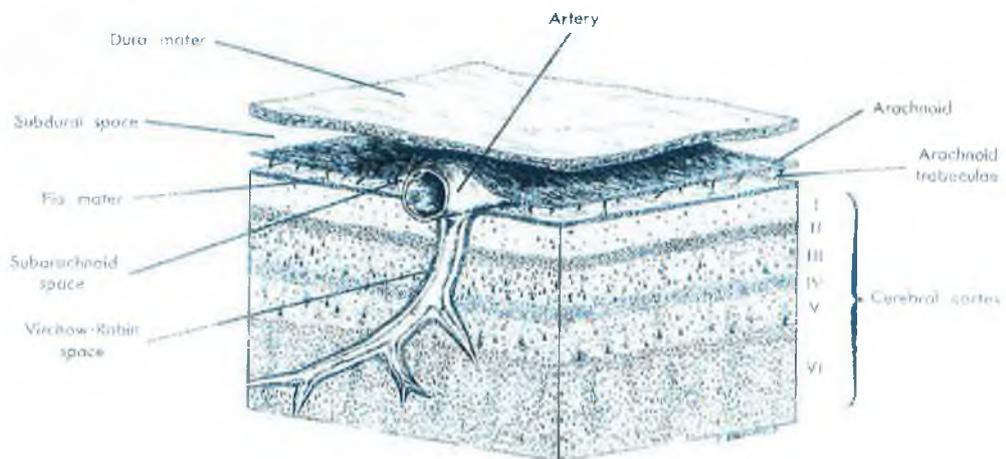
Figure 2.8 Arteriole penetrating the cortex at a right angle to the surface. Reproduced from Berne and Levy (2000).
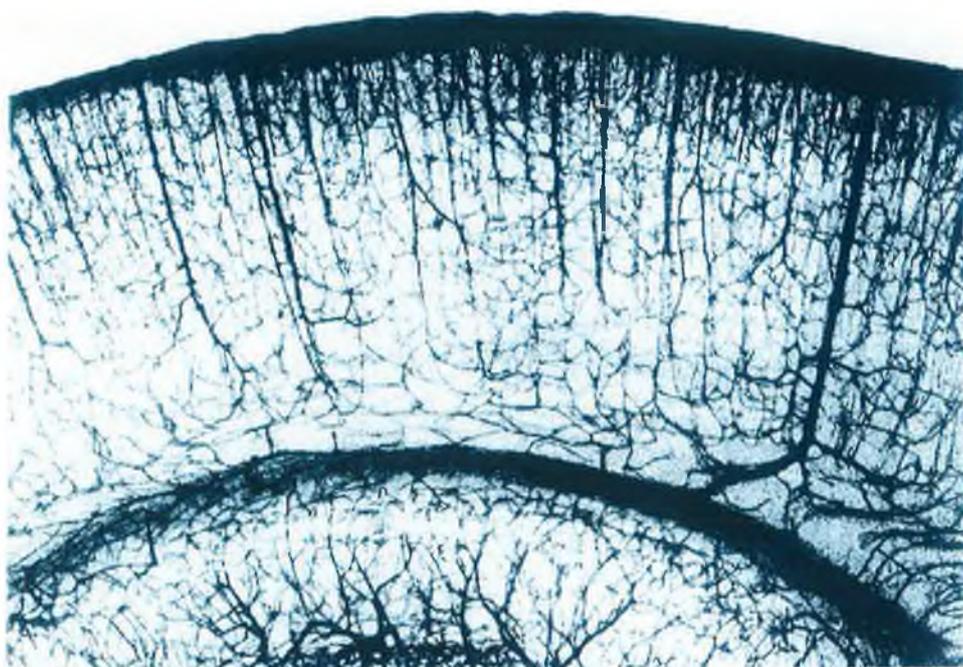
Figure 2.9 Cortical arteriolar organisations in the rat. The orientation of the vasculature at right angles to the pial surface can be seen. Reproduced from Berne and Levy (2000).

Blood flow to the brain must remain consistent in spite of any changes in perfusion pressure i.e. the pressure difference between the arteries supplying the brain and the intracranial pressure. If this were not the case low arterial pressure would cause hypoxia, while a high arterial pressure would cause brain edema. An autoregulatory mechanism takes care of this. Autoregulation of most organs is generally defined as the capacity of an organ to regulate its blood supply according to its functional or metabolic needs. The volume of blood and extravascular fluid in most body tissues can expand or contract but the brain is within the rigid cranium meaning that its contents are incompressible. The blood volume within the cranium must remain relatively constant and therefore autoregulation of cerebral circulation incorporates a protective mechanism to ensure this by regulating the resistance across the vascular bed (Edvinsson and Krause 2002).

2.4.2 Factors affecting cerebral blood flow

Overall cerebral blood flow remains generally constant but regional cortical blood flow changes in association with regional neural activity (Berne and Levy 2000). Functional activation causes dilation of arterioles in activated brain regions (Ngai *et al.* 1988), increasing cerebral blood flow within the region. The underlying mechanisms that couple the vascular response to neural activity in the activated regions are still poorly understood and continue to be debated. This is discussed in more detail in Chapter 4. The main factors affecting cerebral blood flow are carbon dioxide, hydrogen ion and oxygen concentrations (Guyton 1987).

Carbon dioxide combines with water to form carbonic acid, which subsequently dissociates to form hydrogen ions.

Hydrogen ions greatly depress neuronal activity and therefore an increase in hydrogen ion concentration consequently calls for an increase in blood flow to maintain a constant concentration level and steady level of neuronal activity. Similarly any substance that increases the acidity of brain tissue,

e.g. lactic acid, pyruvic acid (by-products of metabolism), thereby increasing hydrogen ion concentrations, causes an increase in cerebral blood flow by affecting the vasodilation of the blood vessels.

Oxygen deficiency is also a factor that affects cerebral blood flow. During hypoxia and increased oxygen consumption the formation of Adenosine, a vasodilating substance, is greatly increased. A reduction in the oxygen supply to the brain, or an increase in the brain's oxygen requirements causes formation of adenosine in the cerebral tissue within five seconds (Berne and Levy 2000), thereby maintaining a consistent oxygen supply to meet metabolic demands.

2.5   Imaging the Brain – History and Methods

"The brain is a tissue. It is a complicated, intricately woven tissue, like nothing else we know of in the universe, but it is composed of cells, as any tissue is. They are, to be sure, highly specialized cells, but they function according to the laws that govern any other cells. Their electrical and chemical signals can be detected, recorded and interpreted and their chemicals can be identified; the connections that constitute the brain's woven feltwork can be mapped. In short, the brain can be studied, just as the kidney can."

(David H. Hubel, 1981 Nobel Prize Winner)

Within the last century functional brain imaging has given us great insight into the workings of the brain. Although in the past its role was underestimated by cardiocentrists who believed that thought, sensation and behaviour originated in the heart and that the brain was there to *"make the heat and boiling in the heart well blent and tempered"* – Aristotle (384-322BC) (Martin 1997), today the brain is recognised to be the control centre of the body. Modern imaging techniques can provide an insight into the brain's anatomical structure and also

20

its functional operation. Each imaging method is based on a different principle, thereby giving complementary information regarding the brain and providing a vital window for medicine.

Before the availability of brain imaging methods that allow for *in situ* investigations, studies relied on laboratory animals and patients with localised brain injuries (Martin 1997). Brains were examined post mortem in cases of behavioural anomaly or studies were carried out on living subjects suffering injuries that left them with defects in their skulls or even exposed brain tissue. In this way behavioural defects were attributed to lesions of the brain (Posner and Raichle 1996; Toga and Mazziotta 2002).

Today we can safely visualise the functional activity of the brain, the main techniques used are positron emission tomography (PET), functional magnetic resonance imaging (fMRI), electroencephalography (EEG), magnetoencephalography (MEG) and optical imaging. Some of these methods measure neuronal activity directly, namely EEG and MEG, while the other modalities use indirect measures resulting from neural activity i.e. blood flow and metabolic effects.

2.5.1 Positron Emission Tomography (PET)

PET measures blood flow in the brain, based on the techniques used by Seymour Kety in the 1940s (Raichle 1994). The technique involved injecting cats with radioactive diffusible tracers, decapitating them after a minute, and then analysing the brain slices to view the tissue distribution of the radiolabel. PET has become a widely used measure of brain function even though in its early stages Kety and his colleagues underrated the merit of their technique at a meeting of the American Neurological Association in 1955 with the following statement.

"Of course we recognise that this is a very second-hand way of determining physiological activity; it is rather like trying to measure

what a factory does by measuring the intake of water and the output of sewage."

<div align="right">(William Landau as quoted by Toga and Mazziotta 2000.)</div>

PET can be used to provide a measure of brain function through measurement of brain oxygen consumption, blood flow and glucose metabolism and also probe other biochemical pathways such as protein synthesis and dopamine uptake (Toga and Mazziotta 2002). A radioactive isotope, e.g. labelled water (hydrogen combined with oxygen 15), is injected into a vein in the arm. Within a minute the radioactive water reaches the brain, and as it decays it emits positrons. Positrons combine with electrons, annihilating each other and releasing two gamma rays in the process (positron emission). The gamma rays travel in almost opposite directions, and detection devices around the head can locate their origin with an accuracy of a few millimetres. In regions where neurons are more active, more blood flows to these areas, containing the labelled water, and more glucose and oxygen is taken up. To investigate the location of brain activity images of blood flow are taken before and during a task. Comparison of images pre-task and during the task give an indication of the brain activity involved in performing the task (Raichle 1994). This is shown by PET scans taken during a visual study shown in figure 2.10. The control condition (looking at a static fixation point) is subtracted from the stimulation condition (looking at a flashing checkerboard pattern). PET data can be aligned with anatomical MRI images. The main advantage of PET is good spatial resolution and activation mapping of structures deep within the brain. However PET has poor temporal resolution. The radioactive isotopes generally have a half-life of 2 minutes and the entire substance almost entirely decays after 10 minutes. The short scanning time limits the number of events that can be recorded in a study. In an individual subject 6-18 blood flow scans are usually recorded, with at least 2 or 3 in the control or activated state. To improve signal to noise ratios intra subject averaging of events is usually needed. If this does not give sufficient signal integrity inter subject averaging is used to augment the number of events, although this is susceptible to variations in anatomy between subjects. The main disadvantage of PET is that it is an invasive technology and is therefore not

<div align="center">22</div>

viable in vulnerable subject populations such as children and the elderly, and is not suitable for studies of extensive time periods.
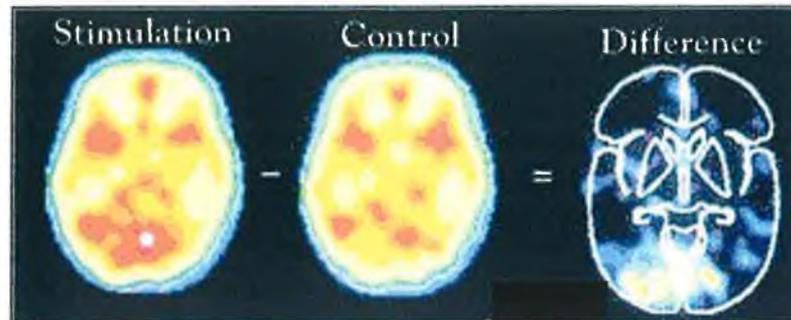
Figure 2.10 PET images demonstrating the effect of visual stimulation. (Posner and Raichle 1996)

2.5.2 *Functional Magnetic Resonance Imaging (fMRI)*

fMRI is also an indirect method of brain imaging, identifying haemodynamic changes within the brain. fMRI evolved from Magnetic Resonance Imaging (MRI), which is a widely used method that provides anatomical information. MRI is based on changes in the magnetic properties of atoms. The technique was originally developed to observe the activity of atomic nuclei, and originally termed Nuclear Magnetic Resonance Imaging (NMR). (The term "nuclear" was dropped due to its connotations of radioactivity.) Protons and some nuclei behave like tiny bar magnets that can align in parallel if placed in a magnetic field. To apply this to compounds within the human body consider each water molecule (H_2O) each containing two hydrogen nuclei. The hydrogen nuclei act as magnetic dipoles and when placed in a strong magnetic field (typically >1.5T) the dipoles become aligned. A short radio-frequency (RF) pulse can perturb the atoms from their preferred alignment. When they return to their original position they release RF energy at their resonance frequency, which is then detected and amplified by receiver coils. MRI has become a widely used clinical tool for imaging tissue since the first MRI camera was developed in the 1970s. In the following decades the growing interest in PET for functional brain imaging

triggered attempts to detect brain activity using MRI techniques. To investigate cerebral blood flow a group of researchers injected intravenously an agent that was known to enhance MRI signals from blood vessels, and they were able to monitor changes in local blood volume. In the early 1990s Siege Ogawa discovered that the concentration of deoxygenated blood affected the MRI signal (Ogawa *et al.* 1990). This was due to the fact that oxygenated blood and deoxygenated blood have different magnetic properties. Oxygen "neutralises" the effect of the iron molecule in haemoglobin. De-oxyhaemoglobin on the other hand has paramagnetic properties that cause different magnetic susceptibility between blood vessels and the surrounding tissue (Ogawa *et al.* 1990). This generates magnetic field gradients across and near the boundaries of the areas containing de-oxyhaemoglobin. For this reason de-oxyhemoglobin is sometimes referred to as an endogenous contrast-enhancing agent and serves as the source of the signal for fMRI. Changes in de-oxyhaemoglobin concentrations, associated with neuronal activity, alter the intensities of the received signals. This blood oxygenation level-dependent (BOLD) contrast is the most commonly used method of fMRI and gives an indirect measure of neuronal activity. An fMRI image based on the BOLD response is shown in figure 2.11. The image shows activated regions during a left finger-tapping task.

Figure 2.11 fMRI image during left hand movement task.

2.5.3 Electroencephalography (EEG)

Electroencephalography (EEG) measures electrical activity ("electro") of the brain ("encephalo") directly. In the late 19th century, Richard Caton discovered that electrical signals could be picked up from animals' heads by probing the surface of exposed brains of animals. In 1929 Dr. Hans Berger was the first to demonstrate this in humans (Toga and Mazziotta 2002).

Surface EEG records electrical activity non-invasively by means of electrodes placed on the surface of the scalp. The signal arises mostly from the activity of billions of nerve cells in the region below the electrode, typically of magnitudes up to 75uV. Placement of electrodes is usually conducted in accordance with the standardised "10-20 system" (Jasper 1958), shown in figure 2.12, whereby each position is assumed to be consistent with its underlying cerebral cortical structure (Homan *et al.* 1987; Steinmetz *et al.* 1989).
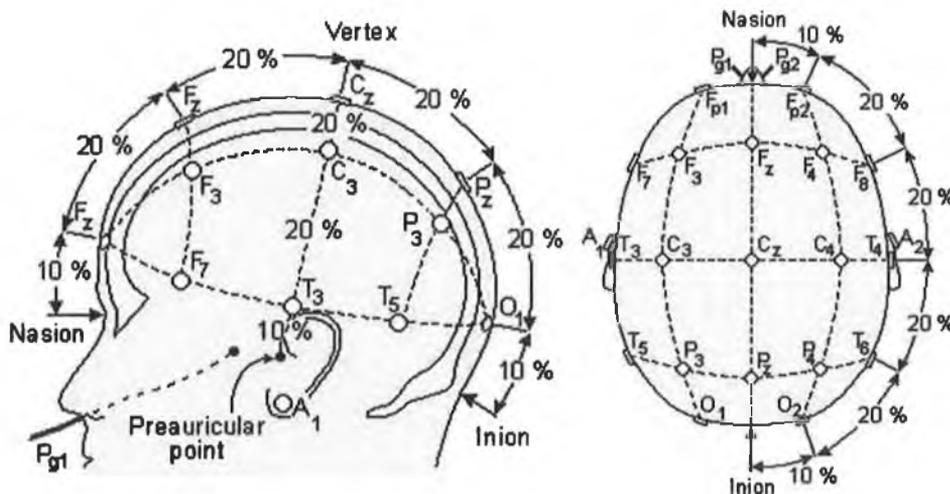
Figure 2.12 Electrode 10-20 Placement System.

EEG signals are usually analysed either in the time domain as voltage versus time, or in the frequency domain as voltage or power versus frequency. Both time-domain and frequency domain methods have been used in a number of EEG-based BCIs. In the time domain, changes in voltage that are evoked by a stimulus are known as evoked potentials. The DC level of EEG signals can also

change over a period of time, and is known as slow cortical potential. In the frequency domain, EEG signals are conventionally described by four frequency bands - delta (1-4Hz), theta (5-7Hz), alpha (8-12Hz), beta (13-35Hz). Each waveband, or rhythm is associated with different tasks, e.g. alpha wave are more prominent when the body is in a relaxed state whereas mu and beta rhythms are associated with movement. Multiple electrodes recordings can be used to create a topographic map of brain activity as shown in figure 2.13.
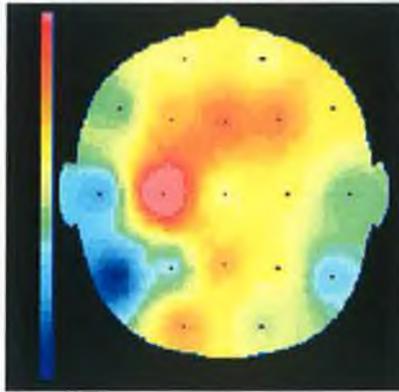
Figure 2.13 EEG topographic map acquired from a geometrical array of electrodes.

2.5.3.1 *EEG Rhythms*

EEG signals are often analysed in the frequency domain, and can be classed by their spectral peak into different bands or rhythms. Abnormalities in EEG rhythms may result from injury, disease, infection or surgery and is therefore an important tool in neuropsychological testing (Martin 1997). In functional analysis the EEG rhythms may be affected by different thoughts, actions or state of mind, e.g. planning to perform a movement can attenuate the mu band. The various EEG bands, their main locations and associated behavioural traits are listed in table 2.1

Band	Frequency (Hz)	Location	Associated tasks/ Behaviour
Delta	<4	Regional	Stages 3-4 of sleep, deeply relaxed state
Theta	4-7	Frontal, central and posterior regions	Sleep/drowsiness, emotional processes
Alpha	8-13	Posterior regions of head, stronger over occipital cortex	Physical relaxation, best seen with eyes closed
Mu	8-13	Precentral and postcentral regions	Motor functions
Beta	14-30	Mostly frontal and central regions, central beta related to mu rhythm	Central beta associated with motor function and tactile stimulation. 18 - 25Hz beta activity enhanced during stages I and II sleep
Gamma	>30	Precentral and postcentral regions	Binding sensory information and sensorimotor integration, establish rapid coupling between spatially separated cell assemblies

Table 2.1 Characteristics of the EEG frequency bands.

2.5.3.2   Evoked Potentials

Surface EEG signals are fluctuations in the electrical potential collected from the scalp, resulting from activity in the underlying cortical tissue. Embedded in this activity, which is spatially distributed over the head, are tiny signals known as evoked potentials (EPs) or event related potentials (ERPs). These are small perturbations in the EEG signal due to a particular stimulus. They are typically only a few microvolts in amplitude and occur due to sensory stimuli (visual, auditory, somatosensory and olfactory); cognitive factors and voluntary movement. Due to their low amplitudes repeated presentation of stimuli is

usually needed to enable signal averaging techniques. The waves are generally given names such as N100, N200, P200 and P300, based on their polarity and time of onset. The amplitude and timing peaks of ERP waves give information about the sequence and timing of task-related processes. One of the first reported ERP events was in the 1960s and referred to as the contingent negative variation – a low frequency negative wave preceding an expected stimulus (Martin 1997). Around the same time a positive wave peaking at 300ms was found to occur after infrequent, task-relevant stimuli. This "P300" is commonly referred to as the "oddball" paradigm, as it occurs due to an unanticipated rare event, which happens amongst a number of common events (Sutton *et al.* 1965). Early waves such as the N100 and P200 are thought to represent stimulus processing, typically due to exogenous stimuli, while the later waves reflect endogenous processes such as decision-making, cognitive processing or context updating (Martin 1997). For this reason the P300 is often used to evaluate cognitive deterioration in neuropsychiatric disorders and degenerative disorders.

2.5.3.3   *Slow Cortical Potentials (SCPs)*

Electrical signals from the brain that vary in amplitude slowly are known as slow cortical potentials (SCPs). These are DC shifts in the EEG signal lasting from a few hundred milliseconds up to several seconds or minutes. Negative SCPs are typically associated with movement and other functions involving cortical activation, while positive SCPs are usually associated with reduced cortical activation. Subjects can learn to control their SCPs by means of visual or auditory feedback.

2.5.3.4   *Implanted electrodes*

Electrical signals recorded from the surface of the scalp originating from millions of neurons are subjected to much noise and undergo considerable distortion due to the skull. In order to achieve better signal to noise ratios microelectrodes can be placed either on the surface of the cerebral cortex or within the cortex.

Electrocorticography (EcoG) involves the placement of electrodes over the dural surface, and was first used in the 1940s to identify the location of epileptogenic zones prior to neurosurgical treatment of partial epilepsies. EcoG can be used to record the brain's electrical activity, and also provide electrical stimulation to brain tissue. Electrical stimulation is used in locating epileptogenic zones, as these areas can show increased excitability to electrical stimulation. Electrical stimulation can also be used for cortical functional mapping. Penfield and his co-workers mapped speech areas and somatosensory areas during surgery on epileptic patients under local anaesthesia (Penfield and Jasper 1954). Subdural electrode arrays are also used for prolonged monitoring of patients' EEG patterns. A more invasive approach that probes deeper into the brain, to isolate fewer neurons, uses electrodes implanted into the cerebral cortex. This has been performed in animal trials and a limited number of human cases. However this approach has significant risks of infection and tissue damage.

2.5.4 Magnetoencephalography (MEG)

MEG is closely related to EEG given that both signals under investigation with these methodologies are generated by the same neuronal activities. Neuronal currents generate electric and magnetic fields in accordance with Maxwell's equations. Electric fields are detected using EEG while magnetic fields are picked up with MEG. The magnetic signals generated by the cortical currents can be picked up with super-conducting coils connected to SQUIDs (super-conducting quantum interference devices), which are ultra-sensitive detectors of magnetic fields, shown in figure 2.14. The detected magnetic fields are the result of activity from a large number of neurons, as magnetic fields from single neurons would be very weak. The main advantage of MEG over EEG is that the skull and scalp do not distort magnetic signals and it is therefore easier to locate the source of the signals. The sources of brain activity can be mapped on a 3-D image of the subject's head. MEG is a non-invasive technology however the instrumentation is bulky and expensive.

As the magnetic signals from the brain are extremely weak a magnetically shielded room is required to reject external disturbances which exist due to fluctuations in the earth's geomagnetic field; moving vehicles and elevators; radio, television and microwave transmitters and power-line fields.
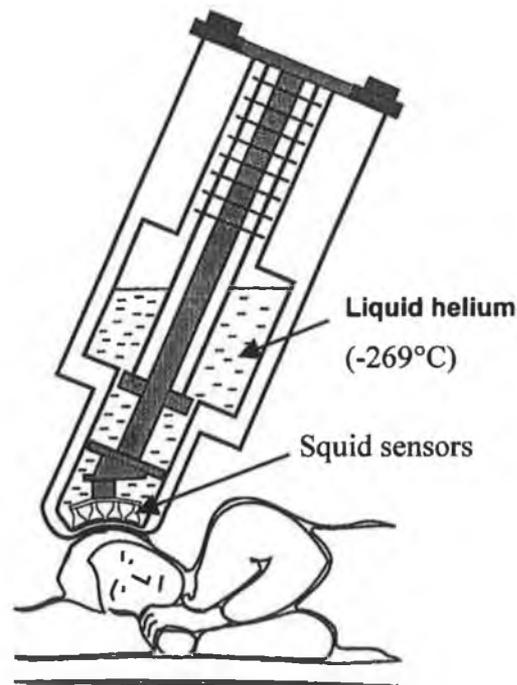
Figure 2.14 MEG measurement set-up. The magnetic fields produced by neuronal currents are detected by an array of superconducting sensors (Toga and Mazziota 2002).

2.5.5 Optical Imaging

It is often noticed in medicine that the functional state of tissue has a large influence on the optical properties of the tissue. This is evident from the colour of the skin, which may appear pale in cases of anaemia or yellow in cases of liver failure. By the same token, vascular changes can also affect the optical properties of tissue. An increase in blood flow causes more light to be absorbed, and changes in the oxygenation levels causes colour changes in blood. Light can be used as a tool to explore the nature of tissue. By monitoring vascular changes

30

in the brain optical imaging can be used as another indirect measure of brain function. This can be performed either invasively by shining light on an exposed brain or non-invasively shining light at the scalp surface. To identify metabolic changes extrinsic contrast agents may be used (e.g. calcium sensitive fluorescent dyes) or else natural indicators are used (e.g. colour changes between oxygenated and deoxygenated blood). Near-Infrared Spectroscopy (NIRS) is the optical imaging approach taken in this study, therefore the development of this approach is the main focus of this section.

Any optical imaging technology involves illuminating a part of the body with bright light and observing the transillumination pattern to reveal the tissue's optical properties. One of the first reports of optical imaging was in 1929 by Dr. Max Cutler who used transillumination of the female breast to diagnose tumours (Hebden and Delpy 1997). Using a bright light in a darkened room, he found that tumours tended to be more opaque, and attributed this to a greater blood concentration affecting the transparency. A high light intensity was required to attain an image and the "image" was perceived by the physician's eye. The technique was limited due to the blurred nature of the images and could not distinguish between benign and malignant tumours. The highly scattering nature of tissue causes the light to become diffuse and the images to be obscured. The high light intensity needed for these images caused overheating of the skin and the technique was temporarily abandoned in the 1940s. Not until the early nineties had optical imaging re-emerged as a serious contender for breast imaging, with improved light irradiation techniques and sensitive detection systems available to capture the images.

In the 1940's Millikan was one of the first to use optical techniques to develop an ear oximeter that could monitor the oxygen saturation of blood *in situ* (Millikan 1942). The system was based on the pulsatile light variation that was dependent on oxygen saturation. Using a wavelength of light that is absorbed equally by oxygenated and deoxygenated haemoglobin, and a second wavelength that is absorbed unequally by the two pigments allows the oxygen saturation to be expressed based on the fractional transmissions of the two detected light signals.

31

Monitoring compounds in tissue whose absorption of light is dependent on oxygenation status gives a useful indication of tissue functioning, and pulse oximeters are commonly attached to the earlobe or finger to monitor heart rate, blood pressure and oxygen saturation. The finger and earlobe present relatively small distances for light to pass through – the question is how deeply can light penetrate tissue in order to make such measurements. A great milestone in optical imaging occurred in the late seventies. Jobsis discovered an optical window in the NIR wavelength range that allows non-invasive imaging of the brain through the intact skull (Jobsis 1977). Near-infrared light is able to penetrate the skull as the refractive index of bone is of similar magnitude to the refractive index of tissue in the NIR wavelength range (Luo *et al.* 1996). Upon entering the epidermal layers of the head, light is subjected to multiple scattering events and follows diffusion-like patterns though the tissue. Hence the appellation diffuse optical tomography or topography (DOT) often serves to describe near-infrared modalities using arrays of light sources and detectors to image the body (Boas *et al.* 2001).

The fundamental phenomena making NIRS measurements possible are i) the existence of a NIR window of transparency in tissue and ii) the fact that there are oxygen dependent compounds in tissue.

Water constitutes a large proportion of biological tissue, approximately 80%. At wavelengths between 200nm and 900nm water has low absorption properties. Biological tissue has a relative transparency to light in this region. Another significant absorber in tissue is haemoglobin. Non-invasive spectroscopic measurements are typically carried out between 650nm and 900nm because haemoglobin has lower absorption properties in the NIR region compared to the visible spectrum and scattering decreases with increasing wavelength (Jobsis 1977) permitting near infrared photons to be transmitted farther than visible photons through tissue.

Light photons travelling though tissue are subject to multiple scattering and may also be absorbed. Changes in the optical properties of tissue affect the absorption of these photons. Therefore changes in the vascular response and

neuronal response within the brain affect the optical properties of tissue and modulate the attenuation of the photons. The detected light signal can be measured and used to monitor haemodynamic responses related to functional brain activity.

Initial NIRS studies predominantly involved infants, who are ideal candidates as the light penetrates more easily through thinner skulls and less myelinated neural tissue. NIR imaging is favorable for infant studies while other brain imaging systems have drawbacks in terms of safety, practicality, invasiveness and are thereby not feasible to implement. University College London has carried out various studies on neonates to monitor cerebral oxygenation in premature infants and also studies to investigate functional activation. Renowned work by Mark Cope involved the development of a NIR system for long-term monitoring of infants, used as a tool to investigate the cause of neurodevelopmental disorders (Cope and Delpy 1988; Cope 1991). These studies demonstrate the possibility of acquiring valuable information about the function of the normal brain, and about a variety of cerebral pathology such as hypoxic-ischemia. Currently there is no alternative method suitable for use in an intensive care environment to diagnose abnormality in cerebral oxygenation (Hebden 2003). The success of early NIRS studies in neonates has extended interests to studies in adults. While trans-cranial measurements are possible in infant heads, a reflectance approach is generally applied to the adult head.

Research in University College London led to collaboration with Hamamatsu that brought about the development of a commercial NIRS monitoring system (NIRO system) for measuring cerebral and muscle oxygenation. A number of NIR devices have emerged as the result of collaborations between university research groups and industry and have been implemented not only in a clinical environment for bedside monitoring but also in functional activation studies in children and adults. Among these collaborations are Shimadzu and Hokkaido University; ISS Inc. and University of Illinois (Rolfe 2000).

Given the relationship between cerebral vascular changes and functional brain activity, upon which imaging methods such as PET and fMRI are based, the

ability of NIR techniques to measure cerebral perfusion and haemodynamic responses makes it an ideal candidate for functional activation studies. The novelty of functional NIR brain imaging has attracted much interest by presenting new research challenges to improve accuracy and resolution through system optimization, signal processing and experimental approaches. Still in its infancy NIR brain imaging still remains largely research-orientated, but holds great potential for providing a low-cost accessible brain imaging system. Numerous studies have been carried out to date investigating brain activity due to motor, sensory, cognitive, visual and auditory functions (Benaron *et al.* 2000; Keenan *et al.* 2002). Although the depth of penetration in NIR studies is currently limited to the cerebral cortex this division of the brain, commonly called the "seat of intelligence", is the governor of most higher order cognitive tasks.

2.6 Physiological Signals for BCI Development

Given the variety of options for investigating brain function there are some techniques that are more practical than others for BCI development. Table 2.2 summarises the key aspects of each imaging modality, highlighting the suitability of some methods over others. Safety, accessibility and cost in addition to signal integrity are important criteria for BCI systems. Surface EEG has become the most widely used method for BCI development - given its good temporal and spatial resolution, non-invasive nature and relative accessibility. Implanted electrodes have also been used, although despite increasing signal to noise there are safety concerns in terms of infection and cell damage. MEG although closely related to EEG is currently not a practical option for BCI design as the equipment is bulky, costly and a magnetically shielded environment is required. In spite of this MEG has been demonstrated in an offline BCI system (Laitinen 2003). The same constraints limit the use of fMRI in BCI development, although a number of real-time fMRI-based BCIs have recently been demonstrated (Weiskopf *et al.* 2003; Yoo *et al.* 2004). PET and SPECT use radioactive tracers and are

therefore not a safe option for continual long-term use. Near-infrared functional imaging technology has the advantage of being non-invasive, portable, cost-effective, practical and safe for long-term use making it an ideal candidate for a BCI system. It is the aim of this thesis to demonstrate the feasibility of using optical imaging methods as an alternative basis for BCI development.

	Spatial Resolution	Temporal Resolution	Source of Signal	Restrictions on Subject	Invasive
Surface EEG	Approx. 1cm	ms	Post-Synaptic Potentials	Seated	No
EcoG	<1mm	ms	Post-Synaptic Potentials	Implantation of subdural electrodes	Yes
MEG	2-3mm	<1ms	Weak magnetic fields (10^{-14} Tesla) produced by brain activity	Complete rest seated/supine	No
NIR	Approx. 1cm	>1s ms	Hb/HbO changes (slow optical signal) Neuronal firing (fast optical signal)	Seated/supine slight movement allowed	No
fMRI	2mm	>1s	Paramagnetism of deoxy-haemoglobin	Complete rest supine	No
PET	4-6mm	>10s	Tracers in blood used to measure glucose/oxygen metabolism	Injection or inhalation of radioactive tracer	Yes

Table 2.2 Comparison of Brain Imaging Methodologies.

2.7 Summary

The brain is an intricate element of the body's nervous system that assimilates information from the five senses and initiates and controls all actions, both voluntary and involuntary. Brain activity can be measured directly as neuronal

activity in the form of electrical or magnetic signals, or else indirectly by measuring some consequence of cerebral metabolism e.g. glucose uptake or haemodynamic changes. Each imaging method gives complementary information, and each has its strengths and weaknesses. This makes some methods more suitable for BCI development than others. Although EEG remains largely the method of choice for BCI systems, NIRS shows great potential for BCI development because like EEG it is a non-invasive and accessible option. Since an optical BCI relies on a different type of physiological measure it calls for a whole new approach to BCI system design and presents a number of new and interesting challenges discussed in this thesis.

Chapter 3

Brain Computer Interfacing

"I often wonder about the effect of these one-way conversations on those at the other end of the line. I am overwhelmed by them. How dearly I would love to be able to respond with something other than silence to these tender calls."

(Jean Dominique Bauby, The Diving Bell and the Butterfly)

3.1   Introduction

Over the past decade interest in the field of BCI research has risen immensely. This is partly due to advances in medical treatment and technologies such as life support systems, which have improved the survival rate of "locked-in" patients. Another reason is that a better understanding of brain function has created an enhanced recognition of the needs and potential of people with disabilities. The evolution of computing and novel functional brain imaging methods has played a vital role, spurring on the development of new alternative communication devices for the severely disabled. In 1995 there were no more than 6 active BCI groups, in 1999 at the first international BCI meeting 22 research groups attended, while three years later the second international BCI convention hosted

researchers from 38 laboratories (Vaughan *et al.* 2003). In recent times BCI research has received much media attention (Weiss 2003; Philipkoski 2005). Escalating interest in the field has led to diversity in signal acquisition, processing and applications. This chapter reviews a number of BCI developments to date, most of which are based on electrical signals detected from the brain. While surface EEG is the most predominant signal acquisition methodology, there are numerous methods for analysing the EEG signal. Section 3.3 describes the different features of electrical activity used in some of the current BCIs. Section 3.4 and 3.5 discuss the possibility of using MEG and fMRI to control BCIs, an option that several groups have investigated recently. At the end of the chapter, table 3.1 illustrates the diversity and progress in the field of BCI research to date.

3.2 BCI Overview
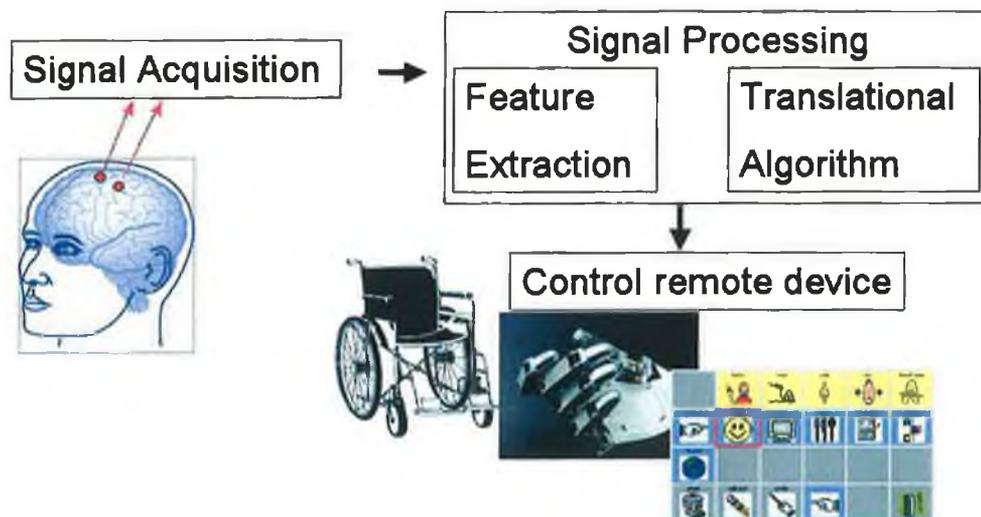
Figure 3.1 BCI Framework. Fundamental components of a BCI System include signal acquisition to record the physiological signal, signal processing involving feature classification and a translational algorithm to designate commands to an external device.

A BCI system comprises an input, process and output. Figure 3.1 outlines the main components of a BCI. The input acquired from the user is a physiological

signal relating to brain activity. It is then processed and translated to control an external output device e.g. a communication aid. The user must learn to control the input signal through some mental strategy. Electrical activity from the brain, detected using surface electroencephalography (EEG) has traditionally been used as a signal input in BCIs. The signal input may either be an evoked response where the signal results from sensory stimulation provided by the BCI, or spontaneous, where no external stimuli is needed for their generation. Once the signal is acquired it is amplified and digitised. The system can then process the information to extract features in the signal, decoding the user's commands. Classification algorithms are used to identify the features of the input signal either in the time or frequency domain. Once the features are established they can be translated to an output command. The output command is used to control an external device, e.g. cursor control, letter/icon selection.

3.3   EEG-based BCI

Electrical signals of the brain have a fast reactivity and co-variation with cognitive processes and therefore they are suitable candidates for BCI control (Kuebler *et al.* 2001). EEG-based BCI may rely on signals that are inherent responses due to sensory stimulation, e.g. potential shifts evoked due to a visual stimulus. Another mode of operation is to recognise potentials that occur due to operant conditioning and self-regulated training, e.g. learning to control sensorimotor rhythms or slow cortical potentials. The implementations of the different modes of BCI operation using EEG signals are discussed in the following sections.

3.3.1 Evoked potentials

Evoked potentials resulting from visual stimulation (VEP), oddball paradigms (P300) or preparation for movement (readiness potential) have been used in a

number of BCI applications. These signals are endogenous responses, which minimizes training periods. The implementations of these signals by various BCI research groups are discussed in the following sections.

3.3.1.1 *Visual Evoked Potentials*

A visual evoked potential is a response that has been elicited by a visual stimulus e.g. flashing light or checkerboard reversal pattern. BCIs using visual evoked potentials have been termed "dependent BCIs", as although they don't use the brain's normal output pathways to transmit a message, activity in these pathways is needed to generate the brain activity that does carry it (Wolpaw *et al.* 2000). Consequently, a major drawback of BCIs utilizing the VEP response is that control of extra-ocular muscle activity is usually required. If such control is present the BCI becomes somewhat superfluous, as it performs the same function as a system that determines gaze direction and an eye-tracking device would be a simpler approach. Nonetheless it is a valid demonstration of how brain activity can be harnessed to control an external device and was the basis of one of the first BCIs, demonstrated by Dr. Jacques Vidal in the 1970s. This study highlighted the distinction between communication systems that detected brain activity using EEG and other systems that detected muscular activity in the scalp or face using electromyography (EMG). Vidal's system operated by detecting VEPs and classifying the VEP events (Vidal 1977). VEPs are generally analysed off-line using averaging, on account of their magnitude, however the system used single-trial epochs of VEPs in real-time. Users were able to control a communication channel by choosing one of four fixations points presented on the screen relating to left, right, up and down. This control enabled users to direct a cursor though a two-dimensional maze.

Sutter also used visual evoked responses to create a "Brain Response Interface" (BRI) (Sutter 1992). An 8x8 matrix comprising of letters of the alphabet and most commonly used words was presented to users on a screen. Changing the colour or flashing each item within the matrix resulted in a particular spatiotemporal pattern in the EEG signal that was recorded at the visual cortex.

40

The system was tested with over 70 able-bodied subjects and 20 severely disabled people. Most able-bodied subjects achieved response times of 1-3sec following training of up to one hour. EMG artefacts were often a problem with severely disabled users. To overcome this four electrodes were implanted in an ALS patient between the skull and dura, boosting the signal amplitude up to ten times larger. By the end of the evaluation the patient was able to communicate at a rate of 10-12 words per minute.

An alternative signal acquisition approach to using single trial visual evoked potentials is to use the steady state visual evoked potential (SSVEP). The SSVEP is characterised as an increase in EEG activity at the same frequency as visual stimulation. Middendorf developed BCIs based on the SSVEP (Middendorf et al. 2000). Two approaches were reported. One study required users to control the amplitude of their SSVEP above or below a threshold, achieving binary control. Able-bodied participants who had previous SSVEP experience were able to achieve accuracies of 95.8% and selection took around 5s. Another study used naturally occurring SSVEPs to allow users to select one of two virtual buttons. Each button flashed at different frequencies, resulting in a SSVEP occurring at the frequency corresponding to the choice fixated by the user's gaze. No training trials were required and 92% accuracy was achieved with a selection time of 2.1s. The SSVEP approach has recently been applied to real-time gaming control. The subject focussed their gaze on one of two checkerboards patterns presented to the left or right on the screen and in so doing the user can control the balance of an animated character as it crosses a tight-rope (Lalor et al. 2004).

3.3.1.2   P300

BCIs using the P300 signal have the advantage that they require no prior learning. The P300 is a naturally occurring positive peak that happens approximately 300ms after the occurrence of an unusual stimulus and is most prominent in measurements taken above the parietal lobe (Picton 1992; Niedermeyer and Lopes da Silva 1999). When a subject is presented with a

series of stimuli, e.g. visual or auditory, the amplitude of the P300 is significantly larger in the event of a rare stimulus. The subject may be instructed to acknowledge the occurrence of the rare event by either press a button or taking a mental count. To apply this to a BCI scenario, the rare stimulus is the event that the user wishes to select. In this case the user is presented with a number of successive events, e.g. letters of the alphabet. The P300 response occurs when their desired target is shown, which can then be classified and selected by the BCI. A greater P300 amplitude is registered when the desired letter appears, while the P300 level is suppressed when an unwanted letter is displayed. In this way the P300 level operates as a binary switch allowing a user to toggle a choice. Farwell and Donchin have developed a communication aid based on the P300 signal using a 6x6 matrix of characters (Farwell and Donchin 1988). Each row and column is flashed successively, causing larger P300 amplitudes to occur when the target letter flashes. The initial system presented 12 events to the user, i.e. flashing each of the six rows and each of the six columns. By identifying the row and column with the highest P300 amplitudes the resultant letter from their intersection is chosen. Figure 3.2 demonstrates the presence of the P300 response that occurs when a desired choice is presented to the user. In a later study, a newer system investigating the response from each letter, i.e. 36 events, was found to improve the information transfer rate of the system (7.8 characters/min, 80% accuracy). The reported performance does not take into account the possibility of using spelling correction or prediction algorithms, which could be of benefit in improving speed and accuracy (Donchin *et al.* 2000). Polikoff has also carried investigated the use of the P300 response to provide cursor control (Polikoff *et al.* 1995). Targets were presented to the user in the form of compass positions (N,S,E,W). Each target was highlighted in random order. When the desired target was highlighted a P300 response was recorded. Data analysed off-line resulted in approximately 50% accuracy at an information transfer rate of 0.2bits/sec. A more recent study on P300 based BCI systems, that is based on work described by Farwell and Donchin, has achieved a communication rate of 5.45symbols/min (corresponding to a bit rate of 23.75bits/min) with an accuracy of 92.1% (Serby *et al.* 2005). This system also uses a 6x6 matrix of symbols containing the alphabet and other useful characters but takes a different signal processing approach based on independent component

analysis. The system performance may be improved further using spell check and word-completion software.
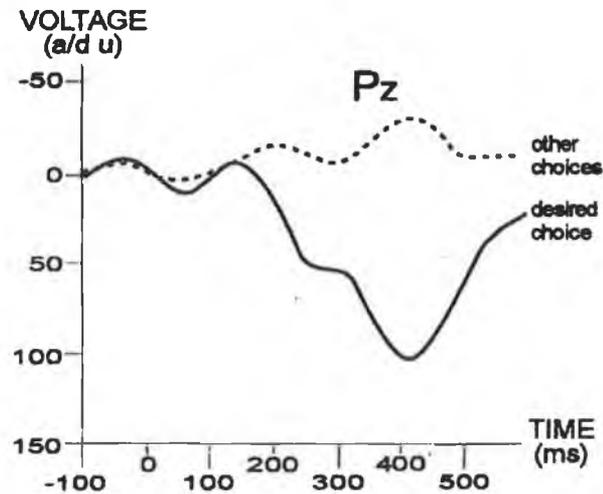
Figure 3.2. P300 Response. The user is presented with a number of choices on a screen that are flashed in succession. When a choice desired by the user is highlighted a large P300 potential is elicited. Reproduced from Wolpaw *et al.* (2002).

3.3.1.3   *Readiness Potential (RP)*

The readiness potential is an event related potential associated with movement (Krauledat *et al.* 2004). It manifests as a slow negative potential shift over the activated motor cortex within about one second prior to the onset of actual movement. The "Berlin Brain Computer Interface" (BBCI) identifies the RP feature and provides user feedback with a multimedia-based application e.g. a modified version of the well know arcade game Pacman (Namco®) (Krepki *et al.* 2003). User training takes 3-4 sessions, during which time the system adjusts its model parameters for the user, based on executed and imagined left and right finger movements. Data analysed offline suggests the system is capable of information transfer rates of up to 40bits/min.

Although most BCI research is geared to provide assisting technology to the severely disabled, the BBCI explores the possibility of applying BCI technology to multimedia devices, where the BBCI has potential to bypass the conduction

delays from brain to muscle which could lead to faster actions/reactions in an application such as a gaming environment.

3.3.2 Slow cortical potentials

SCPs measured concurrently with fMRI BOLD responses have shown cortical negativity in areas with increased metabolic activity and cortical positivity in areas with decreased activity. SCPs are slow voltage changes generated in the cortex, occurring over 0.5s to 10s. Dr. Neils Birbaumer and his team in the University of Tuebingen have developed a "Thought Translation Device" (TTD) that relies on self-regulation of these DC potential shifts (Birbaumer *et al.* 2000). Its principal emphasis is as a clinical application and having been tested extensively in people with late-stage ALS it has proved capable of supplying basic communication capability. In learning to use the TTD users are presented with a feedback cursor, the vertical position of which is controlled by the amplitude of the subject's SCP shift. Once users have gained sufficient control over their SCP shifts the responses can be applied to allow users to select presented icons on a computer screen. The typical time-course of the SCP response in selecting targets is shown in figure 3.3. Both healthy and severely paralysed patients have successfully used the TTD. Clinical trials have been carried out with eleven severely paralysed patients, nine of whom were diagnosed with end-stage amyotrophic lateral sclerosis. To achieve acceptable proficiency (75% accuracy) users generally takes several months of training (Birbaumer *et al.* 2000). After reaching such competency, users need about 2min for letter selection, i.e. 0.5 characters per min. The TTD was first developed as a spelling program, now a special internet browser has also been developed allowing patients to select links using their SCPs and navigate the world-wide-web (Hinterberger *et al.* 2004).
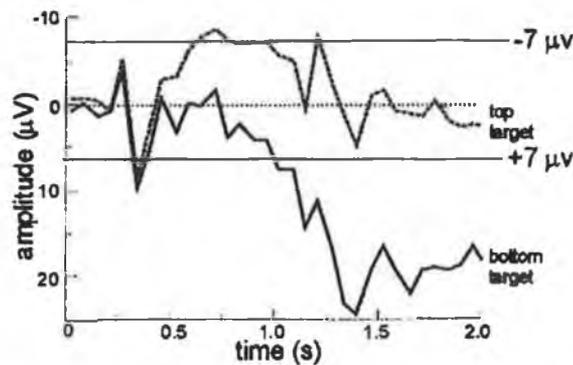
Figure 3.3 Slow Cortical Potentials. Users learn to control SCPs to move a cursor towards a target at the top or bottom of a screen. Positive potential shifts move the cursor towards the bottom of the screen while negative potential shifts move the cursor to the top of the screen. Reproduced from Wolpaw *et al.* (2000).

3.3.3 Sensorimotor rhythms

Mu waves and beta waves are EEG rhythms that are usually present over the primary sensory and motor cortex when they are not processing sensory input or directing motor output. Thoughts relating to movement, motor activity and tactile stimulation can block mu and beta rhythms. Attenuation of the amplitude of an EEG rhythm is known as event-related desynchronisation (ERD), while enhancement of an EEG band is known as event-related synchronisation (ERS) (Pfurtscheller *et al.* 1997). Figure 3.4 shows the effect of imagery of left hand movement on the EEG signal detected over the left and right cerebral hemisphere at electrode position C3 and C4. There is de-synchronization of the alpha band over the right hemisphere, while synchronous EEG activity is maintained at over the left hemisphere. In conjunction with the contralateral desynchronisation of the alpha band and/or beta components during motor tasks, an ipsilateral ERS of the beta rhythm has been observed in some subjects (Pfurtscheller *et al.* 1997b).

BCI research at the Wadsworth Center, New York State Department of Health, has focussed on the use of mu (8-12Hz) and beta (13-28Hz) rhythms associated with the sensorimotor cortex to provide one or two-dimensional control of a

cursor on a computer screen. Studies have been carried out on people with and without motor disabilities. Users learning to control their mu or beta rhythms are capable of achieving one-dimensional cursor control. Intensifying or diminishing the strength of the mu or beta rhythm can be used to move the vertical position of a cursor. Figure 3.4 shows the spectral analysis of a mu rhythm used to select a target presented at the top or bottom of a screen. In studies where users responded to spoken yes/no questions by moving the cursor, accuracies greater than 95% have been reported, with information transfer rates up to 20-25bits/min (Wolpaw 2003). In cases where users learned to control two different mu or beta channels two-dimensional cursor-control was achieved (Wolpaw 1994). A more recent study in the Wadsworth centre has demonstrated a non-invasive system capable of providing humans with multidimensional control of the same precision, accuracy and speed as reported by invasive BCI studies in monkeys (Wolpaw and McFarland 2004).

Another prominent BCI group, based in University of Technology in Graz, Austria, also use sensorimotor rhythms for BCI control. The system operates by characterizing two or more EEG rhythms associated with various motor imagery tasks i.e. mu or beta rhythms. The BCI architecture has served a number of applications in various projects (Pfurstscheller *et al.* 2003). In order to train users to gain control of their brain's oscillatory signals, the standard Graz BCI training involves a number of trials where the user is requested to shift a cursor in a designated direction. Each trial lasts 8s, including a 2s auditory/visual stimulus to indicate the onset of a task, followed by a visual cue to indicate the direction of cursor movement. During the last 4s of the trial the user performs a motor imagery task in an effort to move the cursor, which is displayed as continuous feedback during this period. This training takes from several weeks to several months. The mental imagery tasks involved in controlling specific EEG patterns along with the location of the EEG signal are highly subject-dependent (Obermaier *et al.* 2001). The system has been applied to hand-orthosis control in a tetraplegic patient. After five months of training the patient was able to independently pick up and eat an apple by using motor imagery of foot and right hand movements to control the device. Another application of the Graz-BCI is control of a virtual keyboard. A study was carried out on three able-

bodied subjects reported spelling rates ranging between 0.67 and 1.02 letters/min. Future plans to incorporate T9 technology (Tegic Communications 2005), as used on mobile phones, will improve spelling rates.
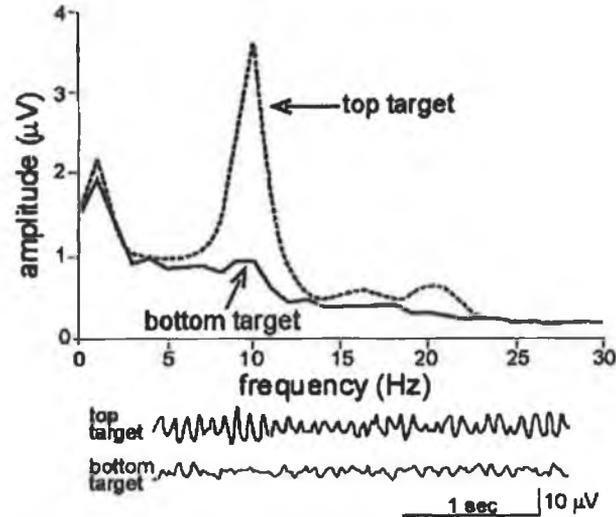
Figure 3.4 Control of sensorimotor rhythms. Users control the amplitude of a 8-12Hz mu rhythm to move a cursor to a target at the top or bottom of the screen. Reproduced from Wolpaw *et al.* (2000).
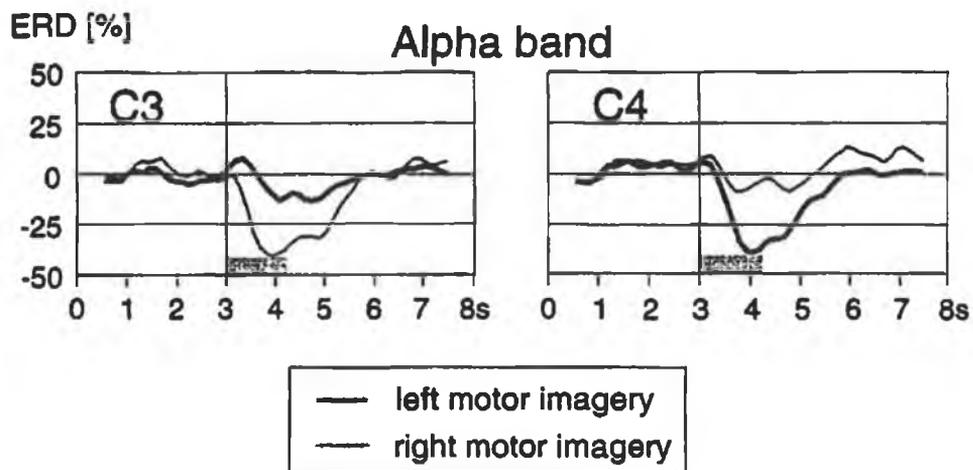
Figure 3.5 Event-related desynchronisation (ERD) due to motor imagery. Imagery of left hand movement leads to a de-synchronization of the alpha band over the right cerebral hemisphere at electrode position C4, while synchronous EEG activity is maintained at C3. Similarly for right motor imagery, de-synchronization is observed over the left cerebral hemisphere at C3. Reproduced from Pfurtscheller *et al.* (2000)

3.3.4 Implanted electrodes

Implanted electrodes allow direct measurement of neuronal activity from the cerebral cortex. The first such electrode to be approved by the Food and Drug Administration (FDA) for human use was developed by Neural Signals Inc. A research team led by Dr. Philip Kennedy, CEO Neural Signals Inc., have successfully demonstrated a brain computer interface that uses an electrode implanted into the motor cortex of the brain (Kennedy *et al.* 2000). The implant consists of a hollow glass cone that intercepts neural signals by making a direct connection to the neurons as they fire, shown in figure 3.6. Trophic factors are used to encourage the growth of neurons into the cone to make the connection. When a signal is transmitted electrical pulses are detected by two wires, amplified and transmitted to a nearby receiver, where the signals can then be processed, analysed and used to control a cursor. Controlling the cursor allows phrases to be selected and then synthesised or alternatively letters can be selected from a visual keyboard in order to communicate. The clinical outcome of trials in three patients has been reported (Mao *et al.* 1998) with one patient achieving a spelling rate of 3 letters per min after several months training.
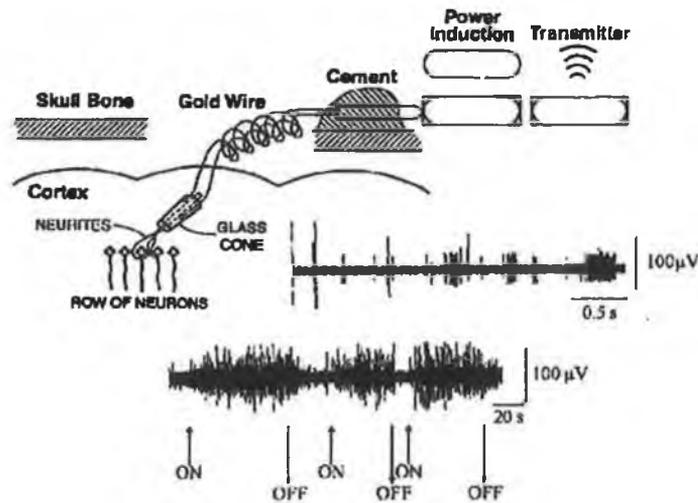
Figure 3.6 Invasive electrodes. Glass cone electrodes implanted into the motor cortex detect potentials of single cortical neurons. Users learn to control neuronal firing rates to control a cursor. Reproduced from Wolpaw *et al.* (2000).

Implantation of multi-electrode arrays into the cerebral cortex offers the possibility of increasing speed and performance. An image of an invasive electrode array developed by the University of Utah and Cyberkinetics Neurotechnology Systems Inc. (Rousche and Normann 1998) is shown in figure 3.7. A number of animal trials (Serruya *et al.* 2002); Wessberg *et al.* 2000; Taylor *et al.* 2002) have been carried out so far but the sensors have not yet been approved for human use.

Intracortical electrodes aim to capture the action potentials of many individual neurons, and also give the possibility of delivering microstimulation to sensory areas of the cortex, which could restore sensory input to those lacking intact somatic sensory pathways. The direct stimulation of the cortex would deliver signals indistinguishable from a natural stimulus. This has been successful in the implantation of electrodes in the cortical whisker areas of rats, used to provide a directional cue (Talwar *et al.* 2002) to control their movements, and has been used to restore sight to the visually impaired (Dobelle 2000). A combination of recording and stimulating intra-cortical electrodes could therefore provide the required elements for normal interaction. However, the disadvantage of this approach is that there are significant clinical risks associated with the implantation of electrodes, with a possibility of infection and brain tissue damage. The effectiveness of implanted electrodes for long-term use needs further investigation, as the extent of tissue damage is unclear and whether the signal will deteriorate significantly over time.

A slightly less invasive technology which may prove more effective is to record electrical activity from the surface of the cortex using electrocorticography (EcoG), providing a greater spatial resolution and frequency range than surface EEG, yet without the same level of technical difficulty and clinical risks associated with implanting electrodes into cortical tissue (Leuthardt *et al.* 2004). A BCI using sensorimotor rhythms detected using EcoG has been demonstrated in four subjects implanted with subdural electrodes. The subjects were able to achieve 1-D and 2-D cursor control by controlling features of the sensorimotor rhythms with reported accuracies ranging from 74% to 100%.
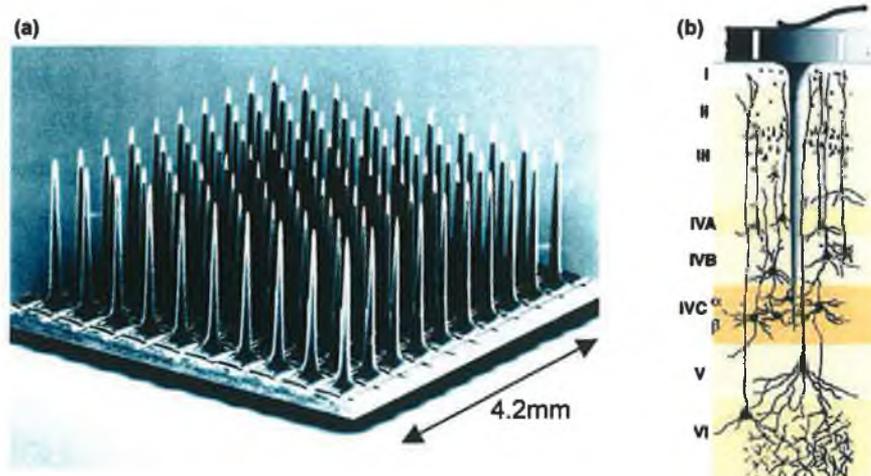
Figure 3.7 Invasive electrode arrays (a) Micro-electrode array containing 100 penetrating silicon microelectrodes designed to focally electrically stimulate or record neurons, manufactured by Cyberkinetics Neurotechnology Systems Inc. (b) residing in a single layer up to 1.5 mm beneath the surface of the cerebral cortex.

3.4 MEG-based BCI

As with EEG, MEG reflects activity directly related to neuronal firing (as opposed to the metabolic response) An advantage of using MEG is that the magnetic signals are not dispersed by the skull and scalp, whereas electric potential distributions are affected. The inverse problem for EEG suffers from non-uniqueness, i.e. there are multiple possibilities for the source of the EEG signal measured at a particular position on the head. The major disadvantage of MEG is the size and cost of the equipment involved at present.

Laitinen evaluates the use of MEG signals as an input to a BCI (Laitinen 2003). MEG signals were analysed as time frequency representations. The time frequency representations and spectra of the signals were used to classify features relating to motor tasks – both real and imagined. The classification was performed off-line. Classification results for real movements were good for all subjects – around 90%. Results for imagined movement were only above 50% in three out of five subjects, although this was put down to experimental design.

50

The study found that activation patterns between subjects differed, and an individual feature set needs to be created for each new user. Another study by the same research group has shown that neuromagnetic 10Hz and 20Hz rhythmic activity can be recorded over the sensorimotor cortex of tetraplegic patients. Features of the signals can be classified and potentially used for BCI control (Kauhanen *et al.* 2004).

3.5 fMRI-based BCI

Recently an on-line BCI based on fMRI has been demonstrated (Weiskopf *et al.* 2003). The system allows users to observe and control changes of their own blood oxygen level-dependent (BOLD) response. Local BOLD signals are continuously fed back to the subject in the magnetic resonance scanner with a delay of less than 2s from image acquisition. In the reported study, one healthy subject was trained to increase and decrease the BOLD signal of the anterior cingulate cortex (ACC). The ACC is located in the medial cortex of the frontal lobe and is made up of sub-divisions that are involved in cognitive, motor, and emotional processes. Self-regulation of the BOLD-response was performed using subjective feelings of emotional valence and arousal. The feedback sessions comprised of a number of activation blocks, each of 60s duration, preceded by baseline blocks of 60s duration. The subject had to increase the BOLD signals during activation blocks and decrease the BOLD signal, i.e., return the signal curves to the pre-task level, during the baseline blocks.

Another fMRI-based BCI has been demonstrated that allows subjects to navigate through a 2D maze (Yoo *et al.* 2004). Movement in each direction is classified by a response to one of four tasks. Vertical control is managed by mental calculation and mental speech generation while horizontal movement is determined by right and left hand motor imagery. The temporal resolution of the system is greater than 120s for command generation, largely due to the 111s scan time.

3.6 Comparison of BCI Methods

A summary of the main developments in BCI research is presented for comparison in the table below.

Author	Signal Acquisition	Feature	Application/performance
Vidal 1977	Surface EEG	Visual Evoked Potentials	Controlling cursor movement through 2-D maze
Sutter 1992	Surface EEG	Steady-State Visual Evoked Potentials	Word-processing program, 10-12 bits/min
Middendorf et al. 2000	Surface EEG	Steady-State Visual Evoked Potentials	Selection of one of two virtual buttons, selection time 2.1 sec, accuracy 92%
Lalor et al. 2004	Surface EEG	Steady-State Visual Evoked Potentials	Gaming environment Accuracy 76%-89%
Polikoff 1995	Surface EEG	P300 Evoked Potentials	Target detection(N,S,E,W) for cursor control 10.8 bits/min, 51.92% accuracy
Farwell and Donchin 1988	Surface EEG	P300 Evoked Potentials	Communication aid 12 bits, or 2.3 characters/min 95% accuracy
Donchin et al. 2000	Surface EEG	P300 Evoked Potentials	Communication aid 7.8 characters/min, 80% accuracy
Serby et al. 2005	Surface EEG	P300 Evoked Potentials	Communication aid 5.45 symbols/min, 92.1% accuracy
Krepki et al. 2003	Surface EEG	Readiness Potential (movement related cortical potential)	Computer game ("Brain Pacman") biofeedback 40bits/min (based on offline data)

Birbaumer *et* *al.* **2000**	Surface EEG	Slow Cortical Potentials	Thought Translation Device (TTD), Communication aid, 0.5 characters/min
Wolpaw *et al.* **2003**	Surface EEG	Sensorimotor Cortex Rhythms	Mu and beta rhythm to control 1-D and 2-D cursor movement, >95% Accuracy, 20-25 bits/min
Pfurtscheller *et al.* **2001**	Surface EEG	Sensorimotor Cortex Rhythms	Graz BCI - Hand orthosis, Communication aid >80% Accuracy, 17 bits/min
Kennedy *et al.* **2000**	Implanted electrodes	Action Potentials of Cortical Neurons	Communication aid, 3 letters/min after several months training
Leuhardt *et al.* **2004**	EcoG	Sensorimotor Cortex Rhythms	1-D Cursor control, 2-D Joystick control, 74%-100% Accuracy
Laitinen 2003	MEG	Neuromagnetic Sensorimotor Cortex Rhythms	Offline classification of MEG signals for use in BCI systems
Weiskopf *et al.* **2003**	fMRI	Blood-oxygen level-dependent (BOLD) response	Real-time fMRI analysis providing user feedback of BOLD signal of specific brain region
de Charms *et al.* **2004**	fMRI	Levels of Brain Activation in Target Regions of Interest	Time-course plots of region of interest activation presented as feedback to subjects
Yoo *et al.* **2004**	fMRI	Spatial Distribution of BOLD Response	Navigation through 2D maze Selection time >2min

Table 3.1 Review of current brain computer interface development.

3.7 Summary

The field of BCI research has grown rapidly in recent years, with a rising number of BCI research groups and a variety of techniques choosing different physiological measures of brain activity and various mental tasks. While the emphasis has been primarily routed towards non-invasive EEG-based systems, other methodologies are now under investigation. Speed, accuracy, ease of use and length of training period are the key criteria for BCI development. Currently no BCI performs well in all these aspects and there is scope for novel signal acquisition, signal processing and translation algorithms to accomplish this. There is currently a drive for invasive implanted electrodes in the hope that such systems will provide the speed and accuracy needed for neuro-prosthetic devices. MEG signals, which have strong correlates with EEG signals but with better signal to noise ratios, have been shown, using offline analysis, to be viable BCI control signals. MEG however is currently impractical due to hardware constraints. Another approach to BCI development has been shown using fMRI that is based on vascular changes, rather than detecting neuronal activity more directly as with EEG and MEG. While fMRI, like MEG, has the drawback of requiring a magnetically shielded environment and expensive equipment, the success of this approach, which measures the vascular response corroborates the optical BCI approach presented in this thesis.

Chapter 4

Basis of Near-Infrared Imaging

"These facts seem to us to indicate the existence of an automatic mechanism by which the blood supply of any part of the cerebral tissue is varied in accordance with the activity of the chemical changes which underlie the functional action of that part."

(Roy and Sherrington 1890)

4.1   Introduction

Roy and Sherrington (1890) carried out a series of experiments from which they deduced that an "automatic mechanism" exists relating variations in localised cerebral blood supply to variations in localised functional activity. Even before this, an Italian physiologist Angelo Mosso was interested in the pulsations of the brain (as normally observed in the fontanelles of infants) and made observations of a man who had defects in his skull above the frontal lobes (Martin 2000). Mosso observed an increase in the magnitude of the pulsations when the church bells rang at midday reminding the man to recite the Ave Maria. The blood flow to the brain appeared to give an indication of mental activity and changes in

blood flow to the brain occurred independently of any change in blood pressure or heart rate.

This relationship between localised cerebral haemodynamic changes and neural activity is the basis of optical functional brain imaging techniques and also various other functional imaging methodologies including PET and fMRI. Such techniques are considered indirect measures of neural activity as they examine vascular changes that accompany neural activity while other methods detect neural activity more directly, e.g. EEG and MEG detect electrical and magnetic correlates of neural activity. It is important to understand the origins of the signals arising from any indirect functional imaging methods in order to interpret them accurately. This chapter outlines the supply and flow of blood to the brain, discusses its relation to functional brain activity and describes how NIRS techniques can be used to detect vascular responses associated with such activation.

4.2   Cerebrovascular Coupling

Cerebrovascular or neurovascular coupling are terms commonly used to imply the mechanisms that occur in relating neural activity to cerebral blood flow and haemodynamics. Appreciating the link between cerebral vascular responses and neural stimulation is important in order to contend with optical imaging signals, or indeed with any of the indirect functional brain imaging signals. It is widely accepted that while the overall cerebral blood flow remains generally constant, regional cortical blood flow changes in association with regional neural activity (Berne and Levy 2000). However, the mechanisms governing cerebrovascular coupling in activated regions remain controversial. In particular there is a discrepancy between the cerebral metabolic rate of oxygen and cerebral blood flow. Studies by Fox and Raichle identified this inconsistency and noted large cerebral blood flow increases (29%) for small cerebral metabolic rate increase (5%). This occurrence was termed as "uncoupling" (Fox and Raichle 1986). A

further study reported an increase in glucose uptake and blood flow in excess of oxygen consumption (Fox 1988) which led them to the conclusion that aerobic metabolism reaches its maximum limit close to baseline conditions of brain activity and additional energy requirements are subsequently met through anaerobic glycolysis. Up until this time it had been assumed that activated brain tissue required more oxygen than those at rest, hence the findings reported by Fox and Raichle prompted further study into neurovascular coupling mechanisms. An optical imaging study carried out by Malonek and Grinvald (1996) revived the original theory that brain activity is aerobic. In this study blood oxygenation of the brain was measured by shining light through holes in the skulls of anaesthetized cats. The spectrum of the reflected light was then analysed. Given the different absorbtion spectra of oxygenated and deoxygenated haemoglobin, they were able to measure changes in blood oxygenation in the visual cortex during rest and activation. They reported an initial rise in deoxyhaemoblobin ("initial dip"), which is highly localised, within 200-400ms of the stimulus. This was followed by a large increase in oxy-haemoglobin and decrease in deoxyhaemoglobin due to a surge in blood flow within 3s, which occurred over a larger area (3-5mm away from the early response). This led them to believe that "aerobic metabolism took place immediately after sensory stimulation" (Malonek and Grinvald 1996). This fact is then somewhat masked by the effect of increased blood flow (Barinaga 1997).

In the case of fMRI BOLD contrast imaging, the following three main factors have been identified to influence the BOLD signal (Edvinsson and Krause 2002), and can be in turn related to optical imaging signals (Wolf *et al.* 2002).

> Cerebral blood volume (CBV)
> Cerebral blood flow (CBF)
> Cerebral metabolic rate of oxygen consumption ($CMRO_2$)

These three phenomena occur simultaneously and affect the concentrations of oxy-haemoglobin and deoxyhaemoglobin as shown in figure 4.1 and 4.2. An increase in cerebral blood volume increases both oxy-haemoglobin and deoxy-haemoglobin concentrations. An increase in cerebral blood flow velocity

57

increases oxy-haemoglobin concentrations and decreases deoxy-haemoglobin concentrations. An increase in oxygen consumption decreases oxy-haemoglobin and increases deoxy-haemoglobin concentrations.
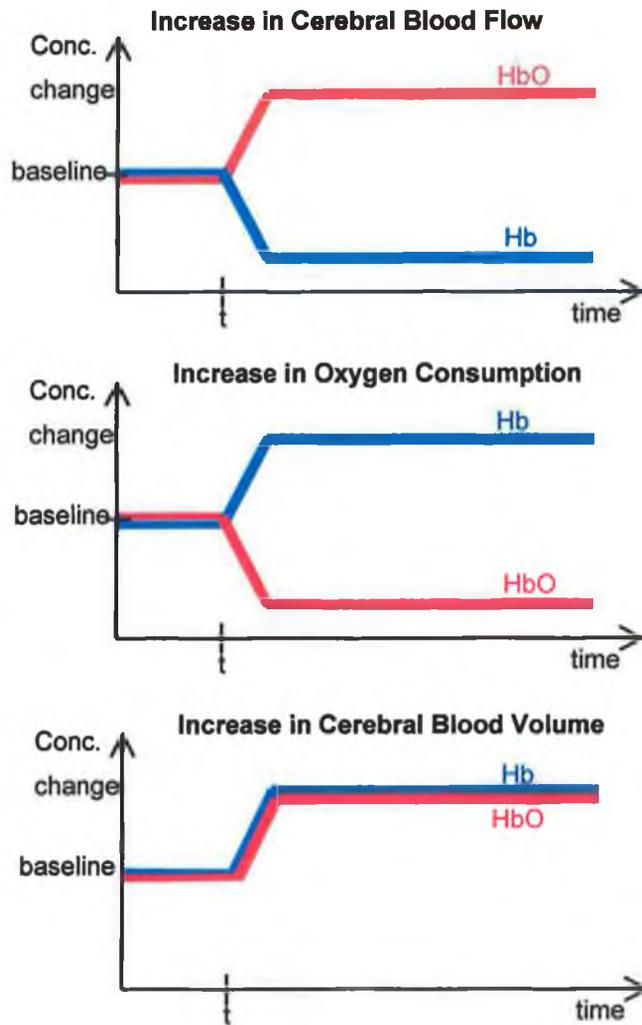
Figure 4.1 Schematic depicting the main phenomena affecting HbO and Hb concentrations. Each event occurs at time *t*.
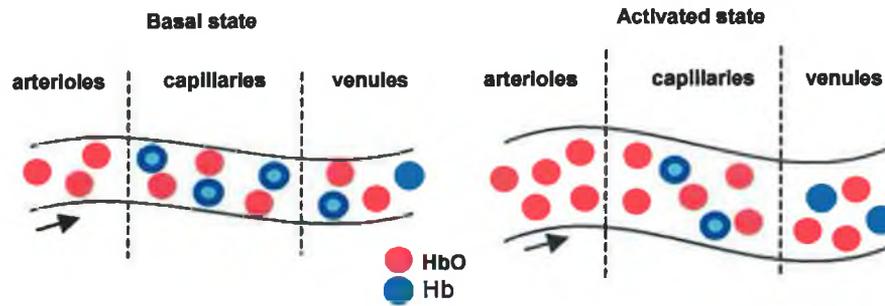
Figure 4.2 Overview of vascular changes from basal to activated state. Functional activation causes an increase in cerebral blood flow and cerebral blood volume. This has the effect of increasing HbO levels and decreasing Hb levels within the capillary bed.

During functional activation all of these events occur simultaneously and the BOLD signal or optical response is determined by the most dominant influencing factor. An overview of the vascular response is shown in figure 4.3. There are three main stages of the response illustrated.

(i)   According to the time-course of the vascular response due to neuronal activity, as reported by Malonek and Grinvald (1997), there is an initial increase in deoxyhaemoglobin. This indicates that oxygen consumption may be the governing factor. This feature, often referred to as the "initial dip", is somewhat controversial because it is not always observed. Its presence, or lack of, may be due to genuine variability of the physiological mechanisms between different trials, individuals and species (Buxton 2001).

(ii)   Subsequently blood flow velocity is the dominant factor; this causes a decrease of the BOLD signal. In the case of optical studies oxy-haemoglobin concentration increases are observed in addition to the de-oxyhaemoglobin concentration decrease. An analogy of "watering the entire garden for the sake of one thirsty flower" (Malonek and Grinvald 1996) has been used to portray

59

the excess supply of oxygen in response to oxygen deficiencies. While the analogy relays the importance of adequate cerebral perfusion, the reasons for such dramatic changes in blood flow in response to brain activity, first reported by Fox and Raichle, remain unknown.

(iii)   On cessation of a stimulus cerebral blood volume appears to be the most dominant factor, remaining transiently elevated while cerebral blood flow velocity and oxygen consumption return to baseline more swiftly (Edvinsson and Krause 2002).   This is observed as an overshoot in de-oxyhaemoglobin concentrations and consequently an undershoot in oxyhaemoglobin.

While the fMRI BOLD response is indicative of the deoxy-haemoglobin concentration levels NIRS can measure both deoxy-haemoglobin and oxy-haemoglobin levels.
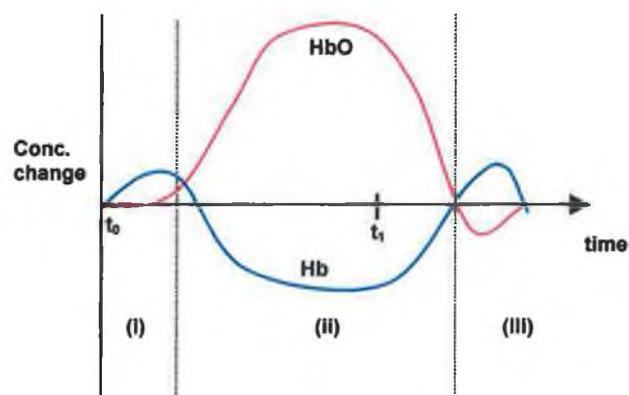
Figure 4.3 Schematic depiction of the typical haemodynamic response. Stimulus occurs at time
$t = t_0$ and ceases at $t=t_1$. There is (i) an initial increase in Hb, followed by (ii) decrease in Hb and increase in HbO. (iii) When the stimulus ends the Hb and HbO levels return to baseline.

60

4.3 Near-Infrared Spectroscopy

4.3.1 Principles of Near-Infrared Spectroscopy

"Soon it became evident that the much greater NIR translucency of skin and bone made it possible to reach brain and muscle tissue without surgical intervention"

(Franz Jobsis)

Jobsis(1977) discovered an optical window in the near-infrared spectrum allowing light, within this range, to usefully penetrate the intact cranium and reach sufficient depths to probe the surface of the cerebral cortex (Jobsis 1977). Such NIR studies can be performed either by trans-illumination methods or in reflectance mode. Trans-illumination is possible if the diameter of the object to be imaged is relatively small allowing light to enter in one side, traverse the sample and exit from the opposite surface e.g. a forearm. However in the case of larger samples, such as an adult head, reflectance mode must be used. Light entering the head at a particular point becomes diffuse as the photons undergo multiple scattering events. A number of photons are absorbed while others continue to be scattered following a random walk path movement through the medium. Some photons may be back-reflected from tissue and exit the surface up to several centimetres from the original point source location, as shown in figure 4.4. These back-reflected photons may be detected and analysis of the detected light signal over time can reveal optical properties of the tissue. Both experimental and theoretical studies have shown that the photons travel in an arc-shaped or "banana-shaped" path from source to detector (Okada *et al.* 1997). Changes in tissue oxygenation associated with brain activity modulate the absorption and scattering of these NIR photons and hence affect the detected light levels emerging from the tissue. Thus, through measurement of optical changes at various wavelengths in the NIR band, qualitative measures of brain activity can be obtained.
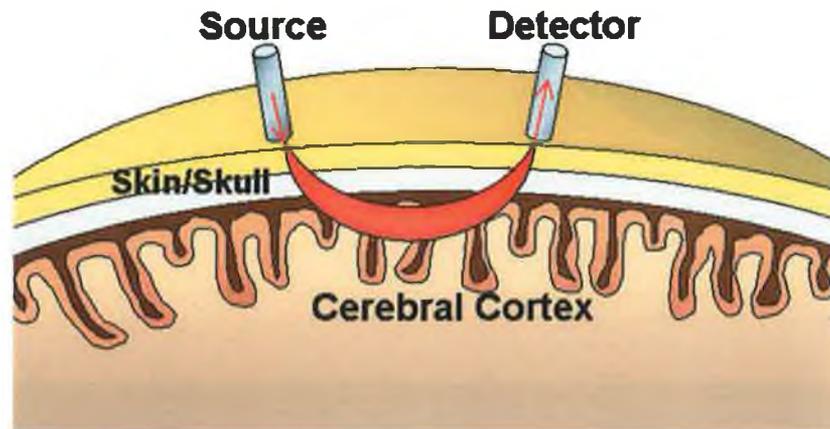
Figure 4.4 Propagation of NIR light in the head.

The NIR response in the brain encompasses two signals. A slow response (approx. 5-8sec) results from attenuation changes due to cerebral haemodynamic changes in blood volume and oxygenation. This signal is an indirect indicator of neuronal activity, related through neurovascular coupling, as discussed in Section 4.2. There is also a fast response, which occurs on the order of milliseconds and is thought to be due to changes in the scattering properties of the neuronal membranes during firing (Stepnoski 1991). This signal is more directly related to neural activity and may correlate with evoked potentials commonly used in EEG analysis. It has been termed the Event Related Optical Signal (Gratton and Fabiani 2001; Wolf *et al.* 2002). Given the two types of responses discernible in the NIR signal, the methodology has the capacity to examine both vascular and neuronal responses, making it a worthy approach for investigating neurovascular coupling phenomena. In order to interpret the optical signal it is helpful to first consider the nature of light propagation.

4.3.2 Propagation of Light- Absorption and Scattering Effects

Photons propagating through a medium can either a) pass through unperturbed, b) be absorbed or c) be scattered by molecules in the medium. Figure 4.5 outlines the propagation of photons though a scattering and absorbing medium.

From this diagram it is clear that scattering and absorption effects attenuate the detected light signal. The attenuation due to absorption effects can be described by a mathematical formulation known as the Beer Lambert Law (McNaught and Wilkinson 1997). Attenuation due to scattering effects is taken into account using a modified version of this law.
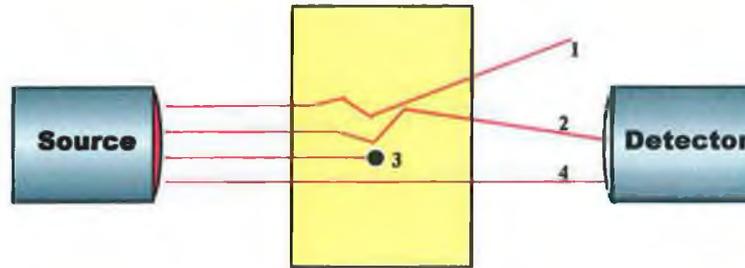
Figure 4.5 Light interaction with a scattering and absorbing medium. Photons 1 and 2 both undergo scattering events but only photon 2 arrives at the detector; Photon 3 is absorbed; Photon 4 is of ballistic nature, i.e. unaffected by scattering or absorption.

4.3.2.1   *Absorption of Light - Beer Lambert Law*

A law relating absorption to the thickness of a material was first derived by Bouguer in 1729, known as the Lambert-Bouguer law. It states that successive layers of material of thickness dl absorb the same fraction dl/I of the light I incident upon them i.e. $dl/I = \mu_a dl$ for a constant μ_a, usually called the absorption coefficient (Cope 1991). This leads to the expression

$$I = I_0 e^{-\mu_a d} \qquad\qquad 4.1$$

for an incident intensity I_0, transmitted intensity I and medium length d.

The absorbance of the medium can be expressed as a quotient of the incident and transmitted intensities as follows.

$$A = \ln\frac{I_o}{I} = \mu_a d \qquad\qquad 4.2$$

Where A is the absorbance, a dimensionless quantity, normally termed the optical density (OD).

Some time later in 1852, Beer derived a similar absorbance relationship dependent upon the number of absorbing molecules in a solution. It states that for an absorbing substance dissolved in a non-absorbing medium, the optical density is proportional to the concentration of the solution. Combining the two laws gives the following expression, known as the Beer-Lambert Law.

$$A = \ln \frac{I_o}{I} = \varepsilon c d \qquad 4.3$$

ε is known as the specific absorption coefficient for unit absorber concentration (units: $mol^{-1}m^{-1}$), it gives an indication of the probability of a photon being absorbed by a material; c is the concentration of the absorber (units: mol).

The law can also be expressed using base 10 logarithm instead of natural logarithm in which case α is the specific extinction coefficient for unit absorber concentration (units: $mol^{-1}m^{-1}$).

$$A = \log_{10} \frac{I_o}{I} = \alpha c d \qquad 4.4$$

The Beer-Lambert Law shows how light absorption is affected by the concentration of absorbing molecules in a material, and the thickness of the material. In a medium containing various quantities of different absorbers, the Beer-Lambert Law can be applied by considering the overall attenuation to be combined effect of all the absorbers present in the medium. The summation of the attenuation effects of n absorbers within a medium is expressed by equation 4.5.

$$A = \log_{10} \frac{I_o}{I} = \sum_{i=1}^{n} \alpha_i c_i d \qquad 4.5$$

This expression only takes absorption effects into account and does not account for scattering losses.

4.3.2.2   *Scattering of Light – Modified Beer-Lambert Law*

Light interaction with biological tissue is greatly affected by scattering events. Scattering is a result of mismatch between regions of different refractive indices. In tissue it occurs due to mismatch between intra-cellular and extra-cellular fluid, membrane boundaries, and also from particles such as mitochondria, ribosomes, fat globules and glycogen. Scattering of NIR photons is primarily due to elastic collisions, i.e. the photon changes direction but there is no energy lost during the collision (Elwell 1995). In a non-absorbing medium light attenuation due to scattering alone would be expressed by equation 4.6.

$$A = \ln\frac{I_o}{I} = \mu_s d \qquad\qquad 4.6$$

Where μ_s is the scattering coefficient of the medium.

The skull is a highly scattering tissue even though it has very low absorption properties. The photon's pathlength is increased as a result of scattering events. In the adult head the average photon pathlength is typically six times the distance between the light source and detector (Duncan *et al.* 1995). This extended pathlength also leads to scattering losses – the longer a photon remains in the tissue the higher chance it has of being absorbed. In order to accommodate these events the Beer-Lambert Law is modified by integrating a differential pathlength factor and a term to account for scattering losses. The term G is governed by the measurement geometry of the system.

$$A = \log_{10}\frac{I_o}{I} = \alpha c L B + G \qquad\qquad 4.7$$

Where is L is the distance between the source and detector, B is the differential pathlength factor and G is a term to account for scattering losses.

By combining the effects of scattering and absorption the propagation of light can be examined.

4.3.3 Light Transport in Tissue

Light propagating through tissue is subject to scattering and absorption events. Biological tissue is made up of multiple layers of various tissue types, each having different optical properties, which makes light interaction with tissue a complicated process. Figure 4.6 outlines the propagation of light through a homogeneous medium that is highly scattering. Biological tissue is a highly scattering medium and light travelling through tissue is therefore subjected to numerous scattering events and is also absorbed by various compounds within tissue. This section discusses the propagation of light through multiple layers of tissue in the head and the physiological factors affecting the optical properties of these layers of tissue.
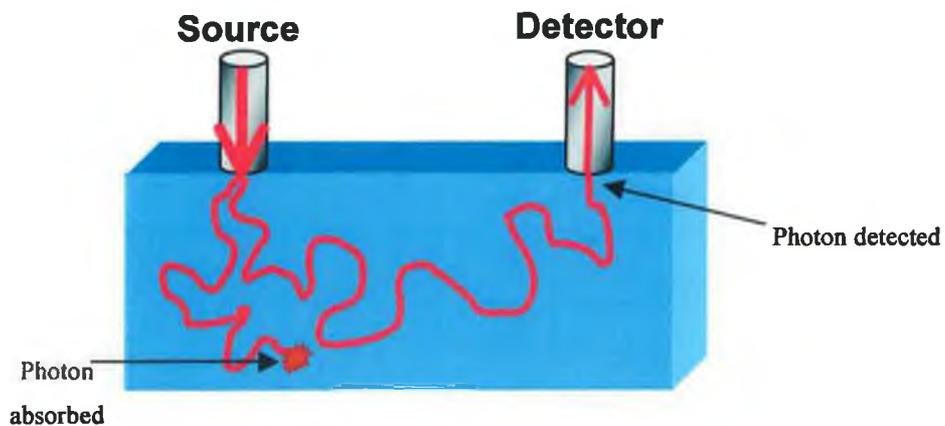
Figure 4.6 Random walk of photons through a homogeneous medium. There is multiple scattering with some photons being detected while others are absorbed.

4.3.3.1   Photon Propagation in the Adult Head

In the adult head, light must first penetrate skin, skull and cerebrospinal fluid before reaching the grey and white matter of the cerebral cortex. A number of studies, using both experimental and theoretical techniques, have investigated the nature of light propagation through tissue. This yields useful information for a number of optical diagnostic practices. A forward model of the propagation of light through the head is useful in solving the inverse problem in optical imaging studies, but also for determining irradiation doses in photodynamic therapy treatments.

Knowledge of the distribution of photon paths is the key to deciphering detected optical signals emerging from the surface of tissue. In near-infrared spectroscopic studies the photon path distribution is necessary for making quantitative measurements (Wyatt et al. 1990). The highly scattering nature of biological tissue means that photons travel a considerably greater distance than the direct source-detector path. This distance, known as the differential pathlength, is needed to quantify absorption and scattering coefficients and consequently chromophore concentrations.

The spatial sensitivity profile of the photon path is important to ascertain firstly the volume of tissue under interrogation and then to investigate which cells within that volume dominate the detected light signal. The relationship between penetration depth and source/detector spacing can be modelled. This is important for optode positioning and design of the optode geometry. Knowledge of the photon propagation is also important in determining light input and output powers. This is beneficial for choosing constituent components of an optical system, e.g. source power, and detector sensitivity.

Light transport in tissue is analysed using radiative transport theory or the diffusion approximation (Profio 1989). The Monte Carlo method has been widely used as a numerical solution of the radiative transport theory equation (Prahl *et al.* 1989) and it can be applied to an inhomogeneous medium of

complex geometry once a realistic model of the tissue sample has been developed. Monte Carlo simulations have been used to study the effect of the superficial tissue thickness, which differs between adult and neonates. It is also useful for investigating the effect of the cerebrospinal fluid, a layer with low scattering properties "sandwiched" between highly scattering tissue that has a significant effect on light propagation (Fukui et al. 2003; Okada and Delpy 2003). The optical properties of each layer of tissue are presented in table 4.1, according to previous studies (Fukui *et al.* 2003; Okada and Delpy 2003). The skin and scalp are highly scattering, as is the cerebral cortex. The CSF layer, which lies in between, has very low scattering properties and this has a significant effect on light propagation. It confines the penetration of light to the shallow region of the grey matter, with few photons probing the white matter. Spatial sensitivity profiles of adult head models, calculated from the accumulated trajectories of photons, show that for source detector spacings of 20-60mm, the intensely sensitive region is confined to the grey matter (Fukui *et al.* 2003; Okada and Delpy 2003). Increasing interoptode spacing does not allow absorption changes in the white matter to be calculated, but rather increases the volume of grey matter under investigation. The spatial sensitivity profiles of NIR light propagation in the adult head is shown in figure 4.7 for inter-optode spacings of 20mm and 50mm according to Monte-Carlo simulations carried out by (Fukui *et al.* 2003).

Tissue Type	Thickness (cm)	Transport Scattering Coefficient* μ_s' (mm^{-1})	Absorption Coefficient μ_a (mm^{-1})
Scalp	0.3-1	1.9	0.018
Skull	0.5-1	1.6	0.016
CSF	0.2	0.25	0.004
Grey matter	0.4	2.2	0.036
White matter	-	9.1	0.014

Table 4.1 Thickness and Optical properties (NIR range) of Tissue in Adult Head.

---

* $\mu_s' = \mu_s$ (1-g), where g is the scattering anisotropy factor, which is the mean cosine of the scattering angle, therefore g=-1 means totally back-scattering; g=0 means isotropic scattering and g=1 means complete forward scattering.
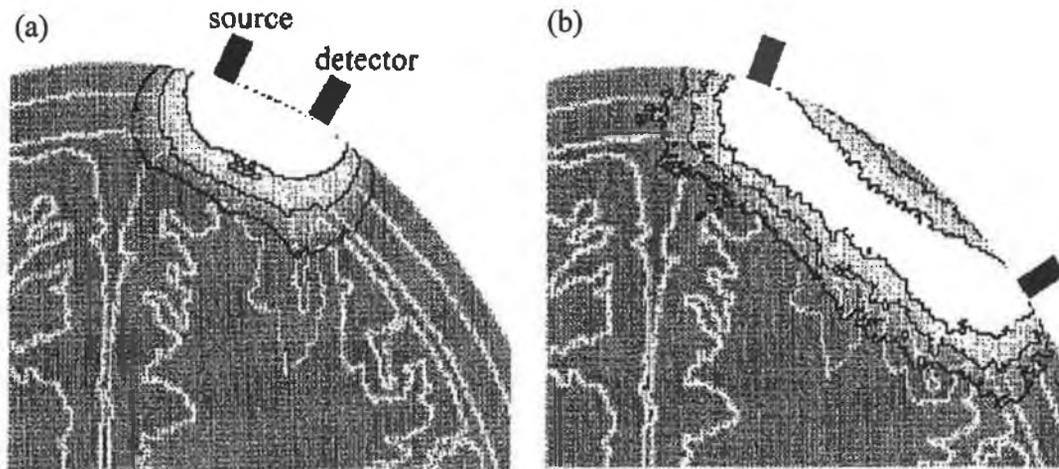
Figure 4.7 Spatial sensitivity profile in the adult head model for a source–detector of (a) 20 mm, (b) 50 mm, reproduced from Fukui *et al.* (2003).

4.3.3.2 Chromophores in Biological Tissue

A compound which absorbs light in the spectral region of interest is known as a *chromophore*. The main absorbers or chromophores in tissue include water, lipids, melanin, haemoglobin and a respiratory enzyme cytochrome-c-oxidase. Each chromophore has its own particular absorption spectrum that describes the level of absorption at each wavelength. The level of absorption is described by an absorption coefficient or specific extinction coefficient, as stated in equations 3.3 and 3.4. Changes in the amount of chromophores in tissue cause changes in the optical signal. Some of the chromophores can be thought of as "constant absorbers" i.e. their effect is an overall static attenuation of the signal throughout an experiment. The properties of the main chromophores in tissue are as follows:

i) Water

Water constitutes approximately 80% of adult brain tissue (Woodard and White 1986). Its absorption properties are shown in figure 4.8. It has relatively low absorption properties between 200nm and 900nm providing a window of transparency within this range. Beyond 900nm its absorption properties increase with wavelength limiting the thickness of tissue to be interrogated by optical

measures. The concentration of water in tissue is assumed to remain constant throughout typical experimental procedure.
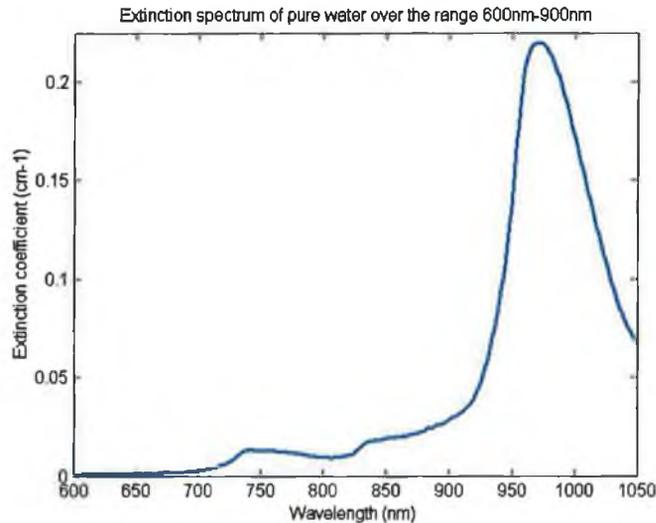
Figure 4.8 Extinction spectrum for pure water over the range 650-1050nm. (Data from Biomedical Optics Research Group at University College London.)

ii) Lipids

The absorption properties of lipids are similar to water in the near-infrared range. It is relatively transparent as it contains few absorbers and has low scattering effects. The distribution of lipid in tissue is dependent upon tissue type comprising 10-40% of tissue. It can be considered a constant absorber during clinical measurements.

ii) Melanin

Melanin is a pigment in the epidermis layer of skin. It is a highly effective absorber of light particularly in the ultraviolet range, which protects the skin from damage from the sun. When melanin absorbs UV light it darkens, causing the skin to tan to protect against further damage from the sun. Melanin is considered to be a constant absorber, however its concentration will directly affect the reflectance of light from the skin and therefore the transmission of light into the tissue below.

iv) Haemoglobin

The most important chromophores in NIRS measurements are the haemoglobin group. Haemoglobin, either in its oxidised or reduced state is the principal chromophore affecting the optical signal in accordance with the vascular response of the tissue. These two compounds have different absorption spectra, as shown in figure 4.9. There is an isobestic point, where the absorption coefficients of both compounds are equal, around 800nm. Measurements of haemoglobin concentration, independent of oxygen saturation, can be carried out at this wavelength. The use of multiple wavelengths of light allows for spectroscopic separation of these chromophore concentrations.
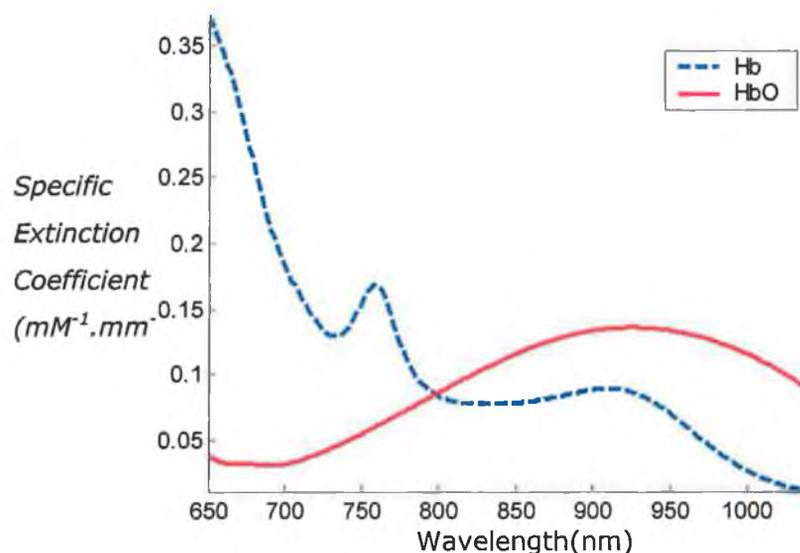
Figure 4.9 Absorption spectra for oxy-haemoglobin(HbO) and deoxy-haemoglobin(HbO). Values taken from Cope (1991).

v) Cytochrome-c-oxidase

Cytochrome-c-oxidase is an enzyme involved in the respiratory chain, located in the mitochondrial membranes. In its oxidised form it has a high extinction coefficient around 830nm, but this absorption band disappears when the enzyme is reduced. Total cytochrome-c-oxidase concentration in tissue does not alter, therefore NIRS measures the change in redox state. To do this the difference spectrum between the oxidised and reduced forms of the enzyme is used, shown in figure 4.10. The redox state of the enzyme gives an indication of the

71

metabolic processes occurring within tissue, although this is the subject of much debate. The absorbance of NIR light by cytochrome-c-oxidase may be used as an indicator of oxygen availability at a cellular level and ultimately of cell metabolism. While its absorption spectrum is of similar levels to haemoglobin the concentration of cytochrome-c-oxidase tends to be an order of magnitude less than haemoglobin quantities (Sato *et al.* 1976). This makes it a more challenging chromophore to quantitate accurately.
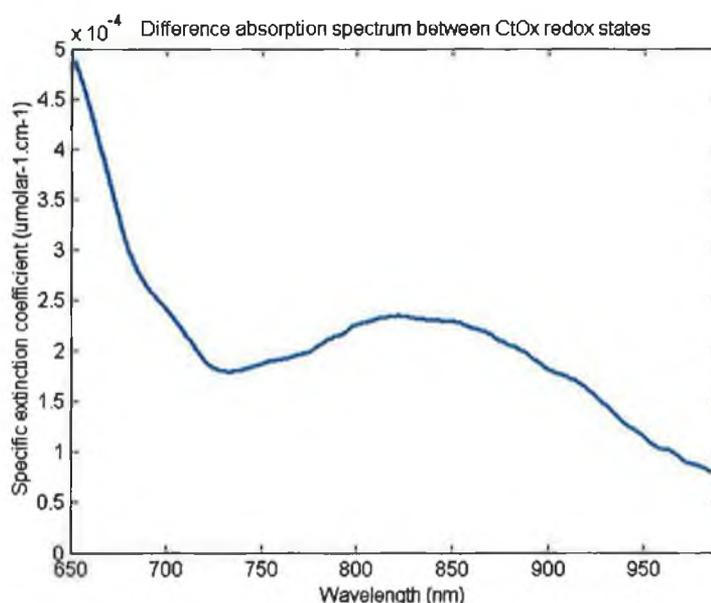
Figure 4.10 Difference absorption spectrum between the reduced and oxidised (redox) forms of cytochrome-c-oxidase. (Data taken from Biomedical Optics Research Group at University College London).

4.3.3.3   Calculation of Haemoglobin Concentrations Changes

The algorithm implemented by the optical BCI to calculate changes in haemoglobin levels is based on an algorithm described by Cope (1991) that relies on the Modified Beer-Lambert Law. The algorithm can be applied to multiple wavelengths of light; in this case two are used. The two NIR light sources, at 760nm and 880nm, are chosen to be on either side of the isobestic point. They are used to evaluate the two chromophores of interest i.e. Hb and HbO.

According to equation 4.5 and 4.7 the attenuation due to oxygenated haemoglobin (HbO), and deoxygenated haemoglobin (Hb) can be expressed by

$$A = (\alpha_{HbO}c_{HbO} + \alpha_{Hb}c_{Hb})LB + G \qquad\qquad 4.8$$

Where α_{HbO} and α_{Hb} are the specific extinction coefficients of oxy-haemoglobin and deoxy-haemoglobin respectively; c_{HbO} and c_{Hb} are the concentrations of oxy-haemoglobin and deoxy-haemoglobin respectively; L is the source-detector distance; B is the differential pathlength factor and G is a term to account for scattering losses.

For small time intervals the scattering term G can be assumed to remain constant, therefore by differentiation:

$$\Delta A = (\alpha_{HbO}\Delta c_{HbO} + \alpha_{Hb}\Delta c_{Hb})BL \qquad\qquad 4.9$$

Using measured and a priori data the concentration changes of Hb and HbO can be calculated by equation 4.9. Changes in light attenuation (ΔA) can be measured as can the inter-optode distance L. The absorption coefficients have been measured for a range of wavelengths and tabulated (Cope 1991). An approximation can be made for B based on previous studies that have been carried out on various tissue types in adults and neonates (Duncan *et al.* 1995; Duncan *et al.* 1996; Kohl *et al.* 1998). Alternatively B can be measured using time-resolved or frequency domain NIR techniques, which are discussed in more detail in Section 4.3.

The detected light signals at the two wavelengths of light used are expressed by equations 4.10 and 4.11.

$$\frac{\Delta A_{760nm}}{B \cdot L} = \alpha_{760nm,Hb}\Delta c_{Hb} + \alpha_{760nm,HbO}\Delta c_{HbO} \qquad\qquad 4.10$$

$$\frac{\Delta A_{880nm}}{B \cdot L} = \alpha_{880nm,Hb}\Delta c_{Hb} + \alpha_{880nm,HbO}\Delta c_{HbO} \qquad 4.11$$

Where $\alpha_{760nm,Hb}$ is the specific extinction coefficient of Hb at 760nm and $\alpha_{760nm,HbO}$ is the specific extinction coefficient of HbO at 760nm, similarly for $\alpha_{880nm,Hb}$ and $\alpha_{880nm,HbO}$.

In matrix form this can be represented by equation 4.12

$$A/BL = \alpha C \qquad 4.12$$

Where

$$A = \begin{pmatrix} \Delta A_{760nm} \\ \Delta A_{880nm} \end{pmatrix}, \quad \alpha = \begin{pmatrix} \alpha_{760nm,Hb} & \alpha_{760nm,HbO} \\ \alpha_{880nm,Hb} & \alpha_{880nm,HbO} \end{pmatrix} \text{ and } C = \begin{pmatrix} \Delta c_{Hb} & \Delta c_{HbO} \end{pmatrix}$$

The solution for C is shown by equation 4.13.

$$C = \alpha^{-1} A / (B \cdot L) \qquad 4.13$$

Where α^{-1} is inverse of α.

ΔA_{700nm} and ΔA_{880nm} can be found by the measured changes in each optical signal at each sample point with respect to an initial baseline, and then scaled accordingly by the wavelength dependent differential pathlength (B·L).

The differential pathlength factor is wavelength dependent and has also been shown to be age dependent (Cope 1991).

$$B_{780} = 5.13 + 0.07A_y^{0.81} \qquad 4.14$$

Where B_{780} is the differential pathlength factor at 780nm, to which the differential pathlength factors at other wavelengths can be normalised to by a

factor B_N. Table 4.2, shows this factor for the wavelengths used in this application. A_y is the age of the subject in years.

Applying this algorithm to find changes in Hb and HbO concentrations comes down to a simple multiplication of a 2x2 matrix of the inverse of the specific extinction coefficients by the measured and scaled data set. The data required for this calculation is given in table 4.2.

Wavelength (nm)	HbO - Extinction Co-efficient $(mM^{-1}cm^{-1})$	Hb - Extinction Co-efficient $(mM^{-1}cm^{-1})$	B_N
760	0.6096	1.6745	1.12
880	1.2846	0.3199	0.84

Table 4.2 Wavelength dependent optical parameters. Based on measurements in (Cope 1991) and (van der Zee 1993).

The implemented algorithm is subject to some error as there is an assumption that the light source is only at the wavelengths stated when in fact the LEDs have a broader spectral bandwidth. This can be overcome by using appropriate filters or lasers. There is also cross-talk between the resulting chromophore concentrations, due to inaccuracy in the differential pathlength factors (Strangman *et al.* 2003) that should ideally be measured for each subject.

4.3.4 Near-Infrared Spectroscopy Instrumentation Principles

While the underlying principle of NIR techniques remains the same throughout, each NIR research group has taken its own approach in developing NIR imaging systems in accordance to its desired applications. There are three approaches to NIRS instrumentation – Continuous Wave, Time-Resolved Spectroscopy and Frequency Domain or Phase-resolved Techniques.

4.3.4.1   Continuous Wave

The simplest method of NIRS to implement is continuous wave. In this mode the light source is switched on constantly and magnitude changes in the detected light signal are used to evaluate tissue attenuation. Systems using light sources modulated at low frequencies (a few kilohertz) are also considered to be continuous wave. The light source is typically a laser or LED but halogen lamps have also been used. The attenuation of light is the only parameter measured by this method. Light detectors used for this purpose include sensitive photodiodes, avalanche photodiodes (APDs), photomultiplier tubes (PMTs) or charge coupled devices (CCD). The continuous wave approach can be implemented easily on account of its simplicity and flexibility, however it cannot make accurate quantitative measurements of chromophore concentrations. This is because a direct measurement of photon pathlengths cannot be made, and therefore the differential pathlength factor must be estimated based on previous studies (Duncan *et al.* 1995). Quantitative measurements rely on the differential pathlength factor being measured using either time resolved spectroscopy or frequency domain methods (Arridge *et al.* 1992).

4.3.4.2   Time-Resolved Spectroscopy

Time resolved spectroscopy measures the time taken for photons to traverse a medium termed time of flight. This type of formulation has been used in the past to determine the thickness of clouds (Weinman and Shipley 1972). Laser pulses broaden after propagation though thick clouds due to multiple scattering events. The temporal response of a detector to a delta function shaped laser pulse propagating through a cloud can be used to determine the thickness of the cloud. This theory can be applied to measurements in tissue using a simple time of flight approximation to calculate the differential pathlength, i.e. total distance traveled through the tissue, given by equation 4.15.

$$\beta \approx c \cdot t \qquad\qquad 4.15$$

β is the differential pathlength, t is the time taken for an optical pulse to be transmitted through a medium, and c is the speed of light within the medium
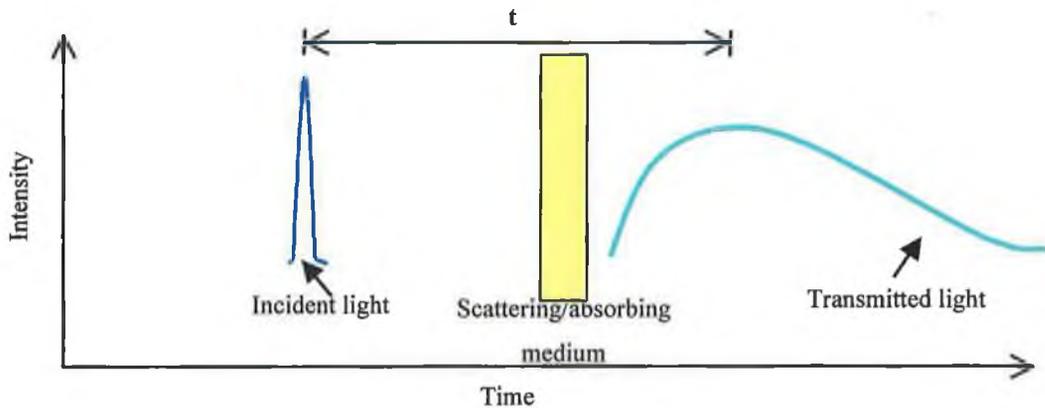
Figure 4.11 Time-resolved spectroscopy. A short pulse of incident light is broadened and attenuated by the medium.

In order to measure the time of flight, t, time-domain systems employ a light source capable of emitting short picosecond pulses of light and a photodetector that can capture the distribution of photon arrival times, e.g. a streak camera. The temporal distribution of the detected signal provides information about the optical interaction with tissue, i.e. scattering and absorption effects (Patterson *et al.* 1989). Figure 4.11 shows the temporal spread of the transmitted light signal.

4.3.4.3   *Frequency Domain Measurements*

By Fourier theory, the same information attained using a time-domain approach can also be calculated by using a frequency domain approach. In this case the light source is modulated at very high frequency (hundreds of megahertz). Light migrating through tissue undergoes both amplitude and phase shifts as shown in figure 4.12. The transmitted optical signal is detected at the same modulation frequency but with a phase shift that can be measured using phase sensitive detection techniques (Chance *et al.* 1998). The phase delay is related to the average time of flight of the photons. The differential pathlength in this case is given by equation 4.16.

$$\beta = \frac{\phi \cdot c}{2\pi \cdot f} \qquad\qquad 4.16$$

Where ϕ is the phase shift, c is the speed of light within the medium and f is the modulation frequency of the light source.
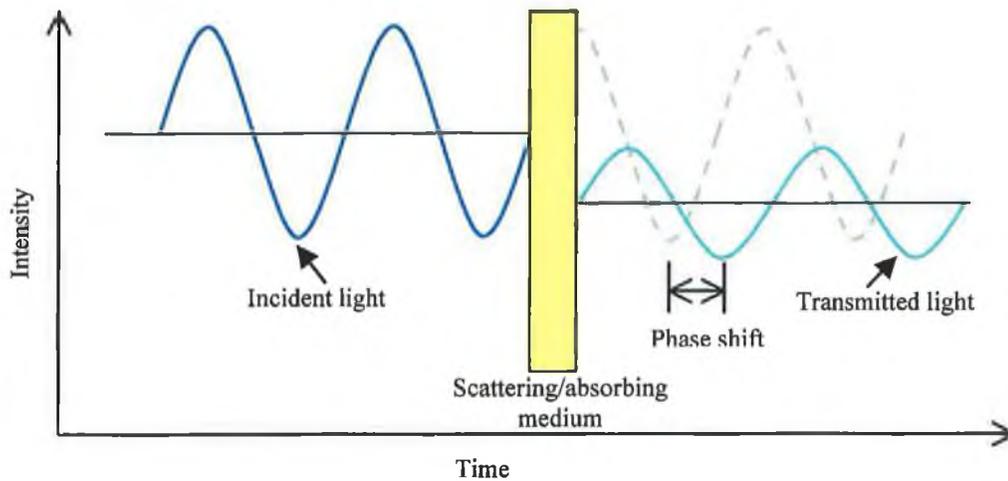
Figure 4.12 Frequency domain measurements. Incident light modulated at high frequency (MHz) undergoes phase shifts and amplitude decay.

Measurements of tissue absorption and scattering coefficients can also be determined using frequency domain techniques using methods based on a solution of the diffusion equation for highly scattering mediums (Rolfe 2000). A comprehensive review of frequency domain systems given by (Chance *et al.* 1998) discusses the equipment required, compares different approaches and considers the applications of such measurements in medical science.

4.4 Summary

This chapter outlines the underlying physiological activities affecting cerebral blood flow and metabolism and how these affect the propagation of light through tissue. The relationship between neural activity and cerebral blood flow is termed cerebrovascular coupling, and forms the basis for NIRS measurement and

other indirect functional imaging methods such as fMRI and PET. Vascular changes within the cerebral cortex, relating to brain activity, cause changes in the optical parameters of tissue. Although there are a number of absorbers in tissue, not all of them are responsible for modulating the detected light signal. Some absorbers maintain a constant concentration level and therefore contribute to an overall attenuation of light. Other absorber concentrations vary with time. Of specific interest, the absorption properties of haemoglobin are oxygen dependent and spectroscopic analysis can be used for oximetric measurements. There are three methods of implementing NIRS systems: Continuous Wave, Time-Resolved Spectroscopy and Frequency Domain techniques. A continuous wave system is more easily implemented and has therefore been assembled for the optical BCI. The disadvantage of this approach is that it does not allow for the photon pathlength to be calculated. This is needed in order to apply the modified Beer-Lambert law algorithm used to detect changes in haemoglobin levels. Tabulated data is used which means that accurate quantitative measurements of chromophore concentrations are not possible. However qualitative measures of haemoglobin changes are sufficient to investigate the occurrence of functional brain activity. Given its accessibility a continuous wave system is ideal for the purpose of the optical BCI. The details of instrumentation design will follow in Chapter 5.

Chapter 5

NIRS System Design

"Everything should be made as simple as possible, but not simpler."

(Albert Einstein)

5.1 Introduction

The fundamental components of any NIR system are the light source and detector. To complete the system driving electronics, amplification and data acquisition methods are carefully chosen according to the demands of the relevant application. As discussed in Chapter 4 there are three ways of performing NIR measurements – Continuous Wave, Time Resolved Spectroscopy and Frequency domain methods. The system design will depend largely on the application in question. The system configuration depends on the kind of spatial resolution needed, the size of the area to be imaged, whether qualitative measurements are sufficient and how many channels are to be used (Strangman *et al.* 2002). These requirements will govern the choice of sources, detectors and subsequently associated electronics. Continuous wave systems are sufficient for monitoring brain activity over time where qualitative measurements are sufficient for noting functional activation changes and therefore appropriate

for BCI studies. The added simplicity of this approach makes implementation and development of the system more straightforward than time domain or frequency domain systems.

This chapter outlines the main considerations in designing a NIRS system for the BCI's signal acquisition system. The typical configuration of a continuous wave NIR system, as developed for the BCI application, is shown in figure 5.1. Light sources, LEDs, are modulated at low reference frequencies (kHz range) and phase sensitive detection techniques are used to recover the light signals at the reference frequencies. The issues to be addressed in choosing a light source and detector are presented in Section 5.2 and 5.3. These sections also discuss the necessary driving electronics, amplification and acquisition hardware to accompany the chosen light source and detector.
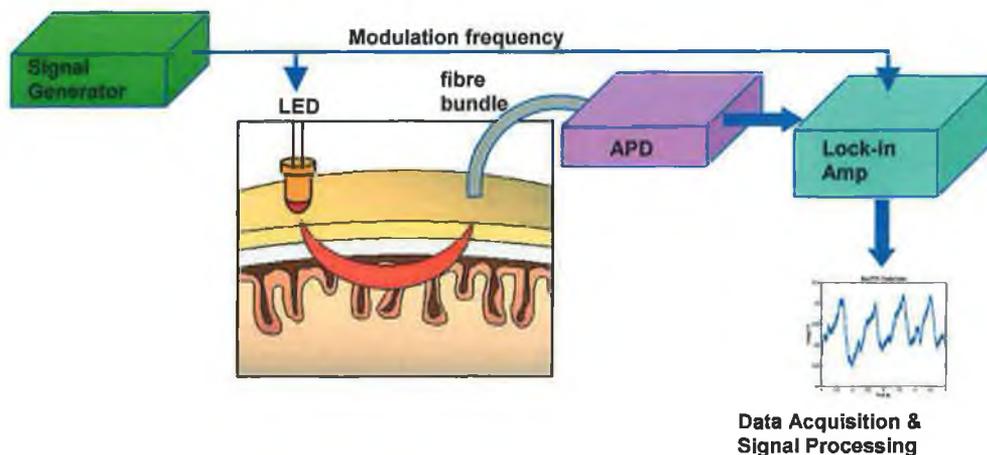
Figure 5.1 Components of a continuous wave NIR system.

In addition to giving careful attention to the choice of light source and detector, careful design must be applied to the mechanics of coupling light from the optical sources and detectors (optodes) to and from the subject's head. This is an important factor regardless of the NIRS instrumentation approach taken, i.e. time-domain, frequency-domain or continuous wave systems. The procedure involved in connecting optodes to the head is often trivialised, but has a great bearing on the system performance and presents many interesting and novel challenges with regard to sensor placement, depth of penetration, signal intensity,

artefact reduction and robustness of measurement. Section 5.4 discusses the requirements and factors involved in optode design and placement. The various mechanisms used to couple light into the head that have evolved throughout the study are also discussed.

5.2   Light source

The main considerations involved in choosing a light source are adequate power and the need for discrete wavelengths. There is inevitably a trade-off between these two parameters. Light emitting diodes (LEDs) and laser diodes are typically used although some studies have utilized white light, e.g. a tungsten lamp, in conjunction with NIR filters (Rolfe 2000; Strangman *et al.* 2002). Recent developments in semiconductor technology have resulted in high power NIR LEDs suitable for NIRS studies, presenting an inexpensive and safe option. The light source must also be suitable for the adopted imaging approach, i.e. time resolved, frequency domain or continuous wave. For example, a source capable of delivering picosecond pulses of light is necessary for time resolved spectroscopy, while frequency domain systems require a source that can be modulated in the megahertz range (Rolfe 2000). For a continuous wave system a light source that can be modulated from DC up to several kilohertz is required. A NIR LED can fulfil this requirement and can be easily integrated into any physiological measurement system.

5.2.1 Near Infrared Light Emitting Diodes

Near-infrared LEDs were chosen as light sources for a number of reasons. Their compact form makes them suitable for attachment directly to the head, while laser diodes typically require optical fibres to couple light to the head. They are also an inexpensive solution and easy to implement. However, the prime advantage of LEDs is safety. Laser sources, which are coherent light sources of

much greater radiance, present higher risks of biological damage, particularly retinal injury. Considering the highly scattering nature of the biological tissue to be interrogated in this study, a coherent light source is not essential, as multiple scattering effects occur in the first few millimetres of tissue causing any beam to become diffuse.

LEDs can transmit a range of radiation patterns. An important parameter of the light output is the beam angle which is the off-axis angle where the output power drops to 50% of the peak value. LEDs with a narrow beam angle should be used in order to maximise the amount of light entering the head. The relative effectiveness of light penetrating the epidermis varies according to, approximately, the cosine of the angle of incidence. Therefore light incident on the skin at grazing angles is less likely to be transmitted through the epidermis (Sliney and Wolbarscht 1980). In order to maximise light delivery the LED should have a narrow beam width and the beam should be positioned perpendicular to the scalp.

The algorithm to calculate oxy-haemoglobin and deoxy-haemoglobin concentration changes is implemented based on the transport of light at discrete wavelengths. LEDs have a spectral bandwidth, which peaks at a particular operating frequency. In order to avoid cross-talk in the chromophore concentration calculation algorithm, it is important to ensure that the spectral bandwidths of the various LEDs utilised do not overlap. Therefore it is advisable to use the smallest spectral bandwidth possible and use wavelengths adequately separated from each other within the spectrum, in order to minimise error.

The LEDs used in this study were manufactured by Opto-Diode (APT-0010, OD-880F). The LEDs have peak wavelengths of 760nm and 880nm, have a narrow beam angle of 8° and a spectral bandwidth at 50% of 30nm and 80nm respectively. The maximum output powers of the LEDs are up to 17mW.

As light is attenuated by 7-9 orders of magnitude in tissue, it is beneficial to supply the maximum amount of power possible while still adhering to the safety

guidelines for optical radiation. LEDs are generally regarded as safe because they are of limited radiance. There is a lack of safety regulations underpinning their use, however with recent developments in higher power LEDs there has been an effort to develop LED safety standards. (Horak 1999; O'Hagan 2003) Safety issues are discussed in more detail in the next section.

5.2.1.1   *Safety guidelines*

Near-infrared light is non-ionising, therefore the main safety concern is heating effects. The majority of the NIR energy (>95%) (Strangman *et al.* 2002) affects the skin layer in the vicinity of the light source. There are maximum safe exposure duration limitations specified by organisations such as the International Commission on Non-Ionizing Radiation Protection (ICNIRP) and the International Electrotechnical Commission (IEC) (British Standards 1994; ICNIRP Guidelines 2000).

The optical radiation of LEDs differs from laser sources placing them between incoherent broadband and coherent laser sources (ICNIRP Guidelines 1997). The ICNIRP recommends that the safety evaluations and related measurements of LEDs should adhere to the guidelines for incoherent sources. However the IEC includes LEDs in its safety guidelines for laser products (British Standards 1994). However there is a need for LED specific safety standards, as the measurement conditions used to assess laser beams are not necessarily realistic for LED applications (O'Hagan 2003).

According to the IEC safety standards (British Standards 1994), a coherent light source in the 700nm to 1400nm range has the following Maximum Permissible Exposure (MPE) of skin, for an exposure time t where 10^3 s < t < 3×10^4 s

$$MPE = 2000 \cdot 10^{0.002(\lambda - 700)} \quad \left[W/m^2\right] \qquad 5.1$$

Therefore a laser operating at 880nm under these conditions has a MPE of 4.6mW/mm^2.

Two LEDs at different wavelengths are required at each point source. One LED with a spectral peak at 760nm, the other at 880nm. These LEDs have typical output powers of 10mW and 17mW respectively and are housed in a TO-46 packaging. Connecting the LEDs directly to the scalp delivers light to a surface area of approximately 20mm^2. Thus when the 760nm and 880nm LEDs are on continuously they provide irradiance of 0.5mW/mm^2 and 0.866mW/mm^2 respectively, when both LEDs are switched on simultaneously the combined light output still remains well below the MPE for coherent light in this wavelength range. If the LEDs are modulated with a duty cycle of 50% the irradiance is halved. A useful comparison to put these figures into perspective is to consider the irradiance of sunlight on the earth's surface, which is approximately 1mW/mm^2 (Ito *et al.* 2000) and is more efficiently absorbed than near-infrared light (Sliney and Wolbarscht 1980). A study examining the heating effects in skin during near-infrared spectroscopic measurements showed that the maximum temperature rise in the human forearm was 7.93×10^{-6} $^\circ\text{C/mW/mm}^2$ at 0.5mm below the skin's surface and even smaller temperature increments occurred at greater depths (Ito *et al.* 2000). The light output powers typically used in NIRS studies considered to be safe given that skin temperature is normally around 31°C, and tissue damage occurs above 41°C (Ito *et al.* 2000).

5.2.1.2   LED Driver

LEDs are current driven devices. The light output of a LED is proportional to the current through the LED. Therefore a stable current source is needed to drive the LED. Modulating the current at a particular frequency therefore modulates the light output of the LED at the same frequency. By modulating each light source at a different frequency the detector arrangement can identify individual light signals by using phase sensitive detection techniques, which is discussed in more detail in Section 5.3.3. Using phase sensitive detection or "lock-in"

detection allows each source to be identified but also reduces noise due to ambient light. A signal generator can provide the reference signal used to modulate an LED, as shown in figure 5.2 It is important to ensure that the various LEDs are modulated at frequencies that avoid harmonic cross-talk. The LEDs are biased and modulated so as to produce a sine wave signal from the detector. Square wave modulation of the LEDs adds harmonic noise to the signal and runs the risk of cross talk between channels e.g. modulation of an LED at 1kHz with a square wave produces a sizeable contaminant signal at 3kHz and 5kHz.

Figure 5.2 Modulation of LED.

Figure 5.2 shows a signal generator supplying a sine wave with amplitude of 1Vp-p and frequency of 4.1kHz. Appropriate gain is applied to the signal to provide adequate optical output. A voltage to current converter is then used to provide one LED with a stable modulating current at 4.1kHz. A similar circuit is used to drive a second LED modulated at 5.23kHz.

5.3 Light Detection

5.3.1 Photodetector

The light detector must suit the nature of the chosen light source and the imaging approach taken e.g. a streak camera or photon counting system is needed for time resolved spectroscopy. High sensitivity of the detector in the NIR wavelength

range is a critical factor as the light transmitted through tissue is greatly attenuated (typically 7-9 orders of magnitude through a few centimetres of tissue). The types of photodetectors typically used in NIR studies include silicon photodiodes (SiPDs), avalanche photodiodes (APDs), photo-multiplier tubes (PMTs) and charge-coupled devices (CCDs) (Strangman *et al.* 2002). Each photodetector has advantages and disadvantages associated with it. Although PMTs have very high sensitivity they are the least straightforward or portable option to use. They require high voltage supplies, protection from excessive current to prevent them from damage and they require cooling because their quantum efficiency is highly temperature dependent. CCDs can be used to detect many wavelengths of light simultaneously and are typically used in conjunction with white light sources. Separation of the various wavelengths can be achieved by using prisms to disperse the emerging light across the surface of the CCD. Semiconductor detectors such as SiPDs and APDs are easy to integrate into a portable system. While SiPDs have a lower sensitivity compared to APDs they can be placed in direct contact with the scalp. Due to the associated circuitry, APDs cannot be placed directly in contact with the scalp easily and therefore it is more practical to incorporate fibre optics when coupling APDs to the head. This does cause losses, however APDs are more sensitive and have much higher quantum efficiency than SiPDs due to an avalanche multiplication process that occurs when a high electric field is applied to the internal depletion layer.

The photodetector chosen for the BCI application was a highly sensitive, high speed APD module developed by Hamamatsu (C5460-01). The module has a high-speed current-to-voltage amplifier and a temperature-compensating bias circuit as shown in figure 5.3. A high bias voltage is needed to exceed the avalanche breakdown threshold of the diode. Temperature compensation is needed to ensure a constant APD gain.

The detector has a minimum detection limit of 0.005nW and saturates at 0.06μW. Taking the average combined power of two LEDs to be 13.5mW, and allowing attenuation of 10^7 the light reaching the detector is approximately 1.35nW, which falls within the detector's range.

HIGH VOLTAGE GENERATOR
+200 V ← +12 V

±12 V

VOLTAGE CONTROLLER

BNC CONNECTOR

TEMPERATURE MONITOR

LOW-NOISE CURRENT-TO-VOLTAGE AMPLIFIER CIRCUIT

APD

THERMOSENSOR
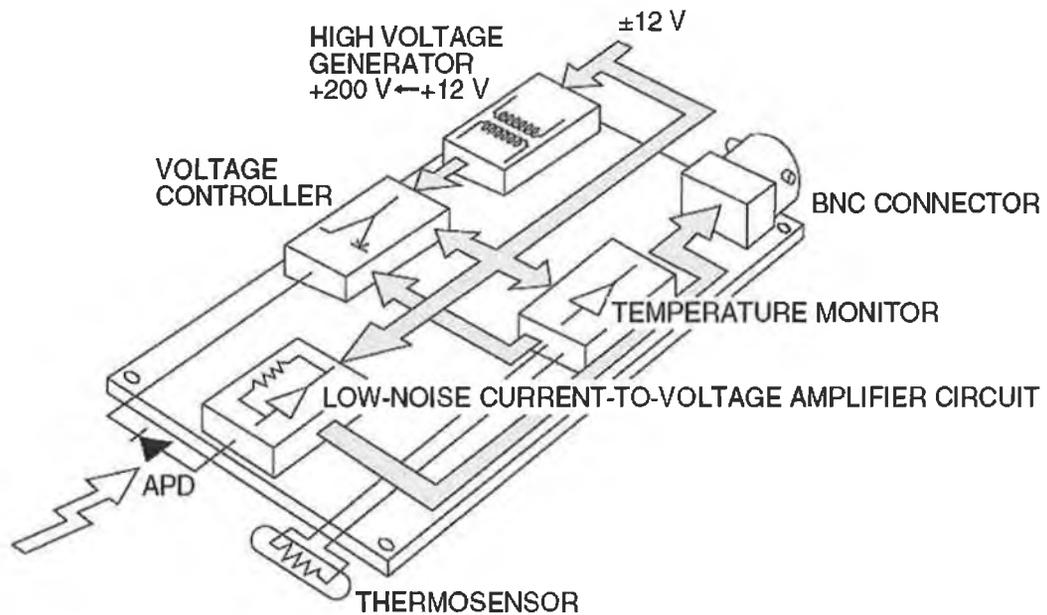
Figure 5.3 Block diagram of APD module.

Given the extremely low light levels exiting the head, it is desirable to use a detector with a relatively large active area in order to maximise the detected signal level. Very small point sources may be required if arrays of sources and detectors are used to image an area of the brain requiring accurate spatial resolution, however in the case of single optode pair arrangements achieving a higher SNR is more important. Although detecting light from the largest possible surface area would yield the largest signal, practicality must ensue. The APD has an active area of 3mm diameter, and a fibre optic bundle of similar diameter is used to transport the light collected from the surface of the head to the detector. This diameter deems sufficient, it is not too large with respect to the curvature of the head, and is not too narrow that would cause a hair follicle lying directly beneath it to obstruct the path of light. The APD output is composed of signals of both source colours and also noise from ambient light. In order to distinguish signals of each wavelength, synchronous (lock-in) detection techniques are employed.

5.3.2 Fibre Optic Bundle

Fibre optic probes can be useful elements in many biomedical optical imaging devices as they provide a flexible solution for interfacing between spectroscopic devices and the tissue to be examined (Utzinger and Richards-Kortum 2003). A fibre optical bundle is used to transmit light exiting the surface of the head to the APD. Robust coupling must be applied at each end of the fibre optic bundle to prevent loss of signal. Unless a focussing lens is applied the APD active area and fibre bundle diameter should be the same to ensure maximum coupling efficiency. A fibre with good transmission in the NIR wavelength, and large acceptance angle is required. The collection efficiency of a detector is proportional to the product of its active area and the square of its numerical aperture (NA) (Cope 1991). NA is a measure of the light gathering power of a detector and is defined by equation 5.2.

$$NA = n \sin \theta \qquad\qquad 5.2$$

Where n is the refractive index of the medium and θ is the angle that a ray of light makes with the optical axis lying perpendicular to the detector surface. The fibre bundle used in this work has a numerical aperture of 0.66 and an acceptance angle of 82°. Approximately 70% of light enters the fibre bundle, with 6% loss every 30cm.

The fibre bundles have a diameter of 0.3mm and are 90cm in length. The end of the light guides are ground and fitted with stainless steel ferrules as shown in figure 5.4.

The APD is housed in a metal box, protected from ambient light. To couple the optical fibre to the APD there is an aperture to insert the fibre bundle where it is aligned with the APD's active area and held securely in place. The connection at the opposite end of the light guide must also be coupled securely to the head's surface. This is discussed in detail in Section 5.4.

Figure 5.4 Fibre optic bundle with metal ferrule at each end is used to deliver light detected from the head to the APD's active area.

5.3.3 Lock-in amplifier

The output from the detector is sent to a lock-in amplifier, which is a useful instrument for retrieving a small AC signal that is obscured by noise of significantly greater magnitude. A lock-in amplifier employs phase sensitive detection techniques to single out a component of a signal at a specific reference frequency and phase. Noise signals that are not at the reference frequency are rejected.   In the experimental environment the optical noise sources include computer monitors (60/72Hz), room lights (100Hz) and daylight (DC).

Lock-in amplifiers can be divided into four stages – an input gain stage, a reference circuit, a demodulator and a low pass filter, as shown in figure 5.5.
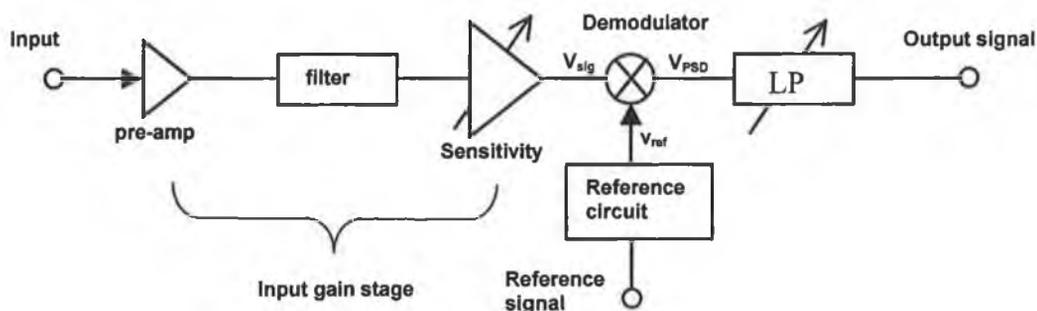
Figure 5.5 Basic lock-in amplifier architecture.

The input gain stage pre-processes the signal by amplifying it to a level suitable for the demodulator. The demodulator multiplies the input signal (v_{sig}) and the reference signal (v_{ref}), given in equations 5.3 and 5.4. The reference signal is at the same frequency as the AC signal being sought. Multiplying the two

waveforms yields a signal made up of the sum and difference frequencies as shown by equation 5.5.

$$v_{ref} = v_R \sin(\omega_R t + \theta_{ref})$$ 5.3

$$v_{sig} = v_S \sin(\omega_S t + \theta_{sig})$$ 5.4

Where ω_R and ω_S are the frequencies of the reference and desired signals respectively, θ_{ref} and θ_{sig} indicate the phase of the signals and v_R and v_S are the amplitudes.

$$\begin{aligned} v_{PSD} &= v_R \sin(\omega_R t + \theta_{ref}) \cdot v_S \sin(\omega_S t + \theta_{sig}) \\ &= 0.5 v_R v_S \cos(\omega_R - \omega_S)t + \theta_{ref} - \theta_{sig}) \\ &\quad - 0.5 v_R v_S \cos(\omega_R + \omega_S)t + \theta_{ref} + \theta_{sig}) \end{aligned}$$ 5.5

As the desired signal and reference signal are at the same frequency, the difference frequency is zero. The demodulator output has an AC component at the sum frequency and a DC component $0.5 v_R v_S \cos(\theta_{ref} - \theta_{sig})$. By adjusting the phase of the reference signal using the reference circuit, the phase difference between the input signal and the reference can be brought to zero and hence the DC output level from the multiplier is proportional to the desired signal. The output of the demodulator is then low-pass filtered, removing any AC signals that are present due to noise in the input signal. The time constant of this filter significantly reduces the bandwidth of the detected signal and hence the noise level, but also limits the rate at which the desired signal intensity changes can be detected (Siegel 1999).

The lock-in amplifier used in this study was an Ametek Model 7265, which has the advantage of having a dual reference mode. This means that it effectively performs the tasks of two lock-in amplifiers by making simultaneous measurements at two different reference frequencies. The modulation frequencies of the LEDs, being in the low kilohertz range, are well within the specifications of the amplifier, which operates at reference frequencies from 1mHz up to 250kHz.

Once the sensitivity, time constant and phase have been established to give the best signal achievable, the data can be acquired for further processing.

5.3.4 Data acquisition

An analog to digital converter is used to sample the signals generated by the lock-in amplifiers either for real-time or off-line analysis. A data acquisition card with 16-bit resolution samples the signals at rates of up to 100kHz (Keithley PCMCIA-16AI). The card can be controlled by a number of application programming environments – this study used Visual C++ to control the device. This environment allows for the Beer-Lambert algorithm to be applied to the NIR light signals and feedback relayed regarding based on the calculated haemodynamic changes. Using this information, applications can be developed to serve as control channels for the user.

5.4 Optode design

This section outlines the main considerations in connecting the source and detector to the head and reveals various mechanisms used throughout this study to perform this task.

5.4.1 Design Brief

Careful design must be applied to the mechanics of coupling light from the optical sources and detectors (optodes) to and from the subject's head, whether the system is time-resolved, frequency domain or continuous wave. Although this may seem a minor issue it has a huge bearing on the signal quality and must be considered as part of the system design. In recent years considerable effort

has been devoted to optimum optical/electrical component design in order to improve system accuracy and resolution. However, the fundamental method of connecting optodes to a subject's head is often trivialised even though this seems to have the greatest bearing on the system performance as it has great influence on signal quality. A means of ensuring good optical contact between the optodes and the head has yet to be perfected and there is a lack of literature regarding the topic.

Stable connection between the optodes and scalp is vital to ensure the pathlength of the photons does not change and also to prevent ambient light saturating the detector. Such effects create spurious motion artifacts affecting the validity of the detected NIR signals. Motion artifacts cause slight movements of the optodes on the scalp instigating large changes in the optical signal, due to variations in optical path. It is therefore important to ensure robust coupling of optodes to the subject's head. The challenge is to ensure rigid optode positioning while still allowing for subject comfort. Solutions to date include modified cycle helmets, thermoplastic moulded to the contours of each subject's head, spring-loaded fibres attached to semi-rigid plastic forms and fibres embedded in rubber forms (Strangman *et al.* 2002). Rubber patches are often used to hold a pair of optodes, being kept in place using straps or bandages; while this is an adequate solution for single point measurements, it proves unsuitable for multiple point tomographic imaging.

Different research groups have developed distinct optodes for particular application and target populations. An interesting concept of using fibre hairbrushes, to overcome the problem of hair absorption has been presented (Luo *et al.* 1996). Single fibres can be set in between hair strands. The dilemma is holding them securely in place without bending or moving the "bristles". Other groups have investigated holding the fibres away from the scalp, which reduces any risk of tissue damage due to excessive pressure and also reduces motion artefacts as the light is covering a larger surface area (Hillman 2002). Thermoplastic can be moulded to a person's head, and allows for precise repositioning in subsequent studies, however wearing it for a long time is

uncomfortable. Taking a cast solely of a region of interest can be used to overcome this drawback (Montcel *et al.* 2004).

There are a number of factors to consider when designing the apparatus used to couple light to and from the head. Consideration must be given to the practical implementation and general safety precautions while at the same time trying to optimise the detected light signal and minimise noise effects. Some of the factors to be considered are outlined as follows:

Secure support for optodes: Sources and detectors can be placed directly in contact with the head if they are small and light enough e.g. LEDs and photodiodes, but is not always practical depending on their dimensions. Fibre optic probes are often used in biomedical optical imaging devices as they provide a flexible solution for interfacing between spectroscopic devices and the tissue to be examined (Utzinger and Richards-Kortum 2003). They are useful in coupling laser diodes, avalanche photodiodes and photomultiplier tubes to the head. Fibre optic bundles can be quite heavy and need adequate support at the skin surface.

Hair: The presence of hair is a key issue affecting the coupling of light to the head. Dark hair absorbs more NIR light than fair hair, however this does not exclude dark-haired subjects from NIR studies providing adequate care is taken during optode placement. While strands of hair affect the absorption of light, movement of hair may cause instability of the signal. In addition, hair follicles strongly absorb near-infrared wavelengths. Therefore in any NIR brain interrogation study carried out on a part of the head covered by hair, e.g. motor cortex, visual cortex, attention must be given to securing the hair in place to prevent its movement, and also ensuring that hair is pushed aside directly beneath the optode positions. Styling-gel and hair-pins are useful to fasten hair at this stage.

Optode positioning related to associated brain function: The placement of the optodes is crucial, as the photon propagation path must traverse an area activated by the experimental task. Movement of the optodes even a small distance from the region of interest can result in a huge reduction in the desired response. The

conventional electrode 10-20 system is typically used as a basis for optode positioning in NIR brain functional investigation studies. The midpoint between source and detector is the point of maximum penetration depth; where photons reach the cortical grey matter, and the optodes should be positioned in a way that their midpoint lays at the required 10-20 electrode position e.g. C3 for hand movement. In the case of diffuse optical imaging systems with multiple optodes there is further complexity if each detector can "see" more than one source. The actual arrangement of sources and detectors has been shown to influence spatial resolution. Arrangements with overlapping measurements of either a rectangular or hexagonal geometry provide better spatial resolution (Boas *et al.* 2004). In addition, a means of decoding respective sources is needed, e.g. time multiplexing or frequency encoding in an imaging situation.

Interoptode distance: The distance between source and detector must be large enough to achieve sufficient penetration depths but not so great that signal is attenuated excessively. A wider source-detector distance increases the photon path length and absorption, and therefore decreases the signal strength at the detector. Inter-optode distances of 2-7cm are typically used, based on experimental and theoretical studies (Okada *et al.* 1997; Fukui *et al.* 2003).

Optode angle of incidence: The angle at which the source and detector are arranged with respect to the head's surface is important so as to maximise the amount of light being coupled to and from the head. The optodes should be placed perpendicular to the surface of the scalp (Sliney and Wolbarscht 1980). Using an LED with a narrow beam width helps to ensure that the majority of light enters the head. The active area of the detector in contact with the head should also be perpendicular to the surface to maximise coupling efficiency. In the case of fibre bundles, prisms can be used to deflect the light at the end of the bundle by 90° (Elwell 1995). This allows fibres to run parallel to the head, taking the strain from the weight of fibre bundles, and can help to reduce motion artefacts.

Shielding light: It is advisable to reduce the amount of ambient light in the room to ensure maximum detector efficiency. In addition to minimising the effects of

stray light entering the head, it is essential to block light from passing directly from source to detector. If this does not have the effect of saturating the detector it affects the validity of any analysis that assumes that light has travelled in the classic banana-shaped path through the head. To avoid cross-talk the source and detector must be shielded from one another using a material that will absorb NIR light as shown in figure 5.6. Compressible black foam can be used, which also serves as a cushioning textile. Black PVC foam commonly used as a sealing strip and black polyurethane foam used for sound insulation are good solutions that can be easily integrated within the coupling mechanism. The foam should be tested for its efficiency in absorbing NIR light, as although an object appears black to the eye not all black dyes are fully absorbing in the NIR spectrum.
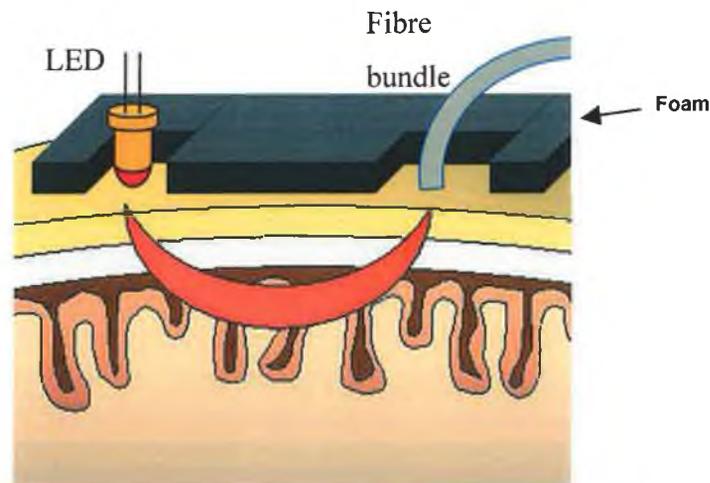
Figure 5.6 Shielding the detector from stray light using black PVC foam.

Safety and Comfort: The subject's wellbeing and safety is central to the experimental procedure. The subject should be at ease throughout experimental procedures as stressful situations activate the autonomic nervous system which, among other physiological functions, affects cerebral blood flow (Coyle *et al.* 2003c). Fastenings should not be too tight, and the head should be supported if the subject assumes a supine position. Optodes should make good contact with the skin, without applying undue pressure. For safety purposes the subject should be able to release themselves from the experimental apparatus easily and quickly should the need arise.

Most of the current BCIs using surface EEG integrate electrodes into caps that secure them tightly to the head. This is quite effective as the electrodes themselves are light and are attached to thin wires. However the EEG cap does not suffice for most NIRS systems that use fibre optics to deliver light to and from the head. Fibre optic cables are quite heavy and need to be anchored appropriately at the skin surface. Therefore a reliable means of coupling optodes to the head during optical imaging is needed to provide adequate support for the weight of the fibre bundles and wires. There are essentially two ways of dealing with this problem. One option is to use a fixed structure to hold the optodes. The subject's head must remain motionless within the structure, thus preventing the scalp pulling away from the optodes. This has the advantage of providing adequate support for the weight of the optode connections however locking the subject's head into a fixed position for any length of time is an uncomfortable solution. Alternatively, the optodes are securely fastened to the subject, and the subject is allowed limited motion. In this case the optodes and head move collectively and thus maintain optical contact. This method still requires a light rigid structure to support the weight of the optodes, the strain of which can cause optodes to pull away from the head. While this method is more flexible in terms of subject movement, ensuring stable optode connections to the head can require tight restrictive straps, which can cause discomfort for the subject.

5.4.2 Design Process

Throughout the study various renditions of optode holding devices have evolved. Initially the use of a helmet was the thought to be the most logical solution. However, the problem with helmets is that they do not conform to the shape of every subject's head. Ideally an optode mounting system that is adaptable for multiple users is required, or at least a few versions to suit similar sized heads. The main advantage of helmets is also ironically their disadvantage. While helmets, especially motorcycle helmets, block out light from the surroundings, they also impede the placement of optodes, in terms of measuring positions for optode alignment and also for shifting hair from beneath the optode position. Unless a large area is removed from the helmet over a section of the cortex to be

97

examined there is little flexibility for optode positioning, and also accessibility to placement. A mechanism is needed whereby the optode position can first be identified, hair combed aside, and then the optodes placed carefully in their designated setting without displacing the hair significantly. Rubber patches holding individual or pairs of optodes can be positioned and subsequently held in place using straps or bandages. Mounting of the optodes in this way was found more effective than rigid structures such as modified hats and helmets as the rubber patch makes it easier to comb hair out of the way of the optode. Embedded in the rubber patches were small brass tubes with a collar, which provide mechanical support for the LED and fibre optic cable. The source and detector connect to the metal holdings that are made to fit the source and detector dimensions. Two detector metal supports were embedded 3cm and 4 cm from the source support allowing options for the interoptode distance. Separate rubber pads could be manufactured for each source and detector in order to have more manipulation of the interoptode distance. On the underside of the rubber patches, black foam was used to shield the source and detector. Velcro was embedded on the upper side of the rubber patches with which to attach headbands to hold the rubber patches and optodes in place, as shown in figure 5.7.

This arrangement proved to be quite convenient for studies on the frontal lobes, with the optodes placed on the forehead, and the occipital cortex, as it was straightforward to secure the straps around the head. However for the motor cortex, the strap configuration needed to be rearranged. A chinstrap and a fastening around the back of the head were incorporated to accommodate the contours of the head, shown in figure 5.8. This arrangement was less comfortable due to the movement restrictions of the chinstrap.

Figure 5.7 Rubber patches held in place by strap configuration for positioning optodes.
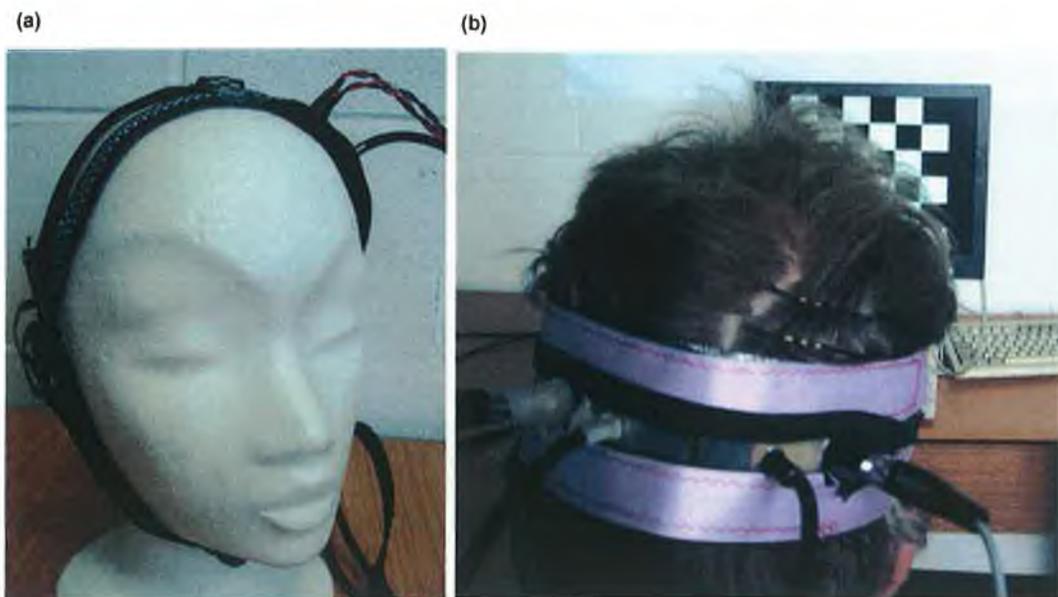
Figure 5.8 a) optode arrangement for motor function studies b) optode arrangement for visual function investigations.

5.4.3 Mechanical Mounting System

While the rubber patches attached by various strap configuration can yield satisfactory results, to improve the robustness of the signal, there was a need for a more stable structure to support the optical fibre bundles and LEDs, and improve the subject's comfort level by taking away strain from tight restrictive straps. The mechanical mounting system allows the person to sit comfortably, while a supporting structure is positioned about the person to hold the optodes in place. Mechanical supports for the optodes are connected to a seat with an adjustable back incline. This provides the option of conducting studies where the subject is supine, reducing certain physiological noise effects such as the Mayer wave (Tachtsidis *et al.* 2004). This was shown for measurements taken from the same subject assuming different postural positions. Spectral characteristics of the responses measured at various postural positions are shown in figure 5.15. The original headrest of the seat was replaced by a mechanical framework to cradle the head and also support and position the optodes, as shown in figure 5.9. The position of the supporting structure can be altered by varying the height and also within the horizontal plane to allow for varying spinal curvations, i.e. a subject's head sits more forward if there is a large curvature of their back. The framework allows optodes to be positioned over areas of the head that are generally of interest in functional brain imaging studies e.g. visual and motor association areas. The framework consists of semicircular rails onto which optode holders can be attached and removed. The optode holders can slide along these rails and be secured into a required position. One of the semicircular rails curves above the left and right sensorimotor cortices, which provides good optode placement for investigating motor imagery. This is of particular interest to our application, as characterisation of the brain's response to motor imagery forms the basis of the optical BCI (Coyle *et al.* 2004b; Coyle *et al.* 2003e). The mechanical framework allows for measurement above the left and right motor cortices and also the occipital cortices, as shown in figure 5.14. For cognitive studies involving the frontal cortices there is a semicircular rail that passes across the forehead that can be attached to the framework. However this makes the entire structure quite restrictive and is not imperative for visual or motor studies.

The optode holder, illustrated in figure 5.12, is a cuboid structure with a cylindrical hollow (of 2cm diameter) to support an optical studies fibre bundle or LED arrangement. Three LEDs of different wavelength, to allow spectroscopic measurements to be performed, are soldered to the receptacle of a miniature microphone connector and encased in brass tubing that can be held within the optode holder, illustrated in figure 5.10. A cylinder, of the same diameter as the LED's encasement, holds the fibre optic bundle off-centre to allow greater adjustment of positon, as shown in figure 5.11. The conformity of the LED and optical fibre mounts means that the optode holders are standardised for both light sources and detectors. A cylinder is hollowed to accommodate the fibre bundle ferrule and a grub screw used to secure placement. The proximity of the light sources and detectors to the head's surface may be controlled by sliding the LEDs or fibre bundles, within their encasements, through the optode holder and fixing their position using a grub screw.
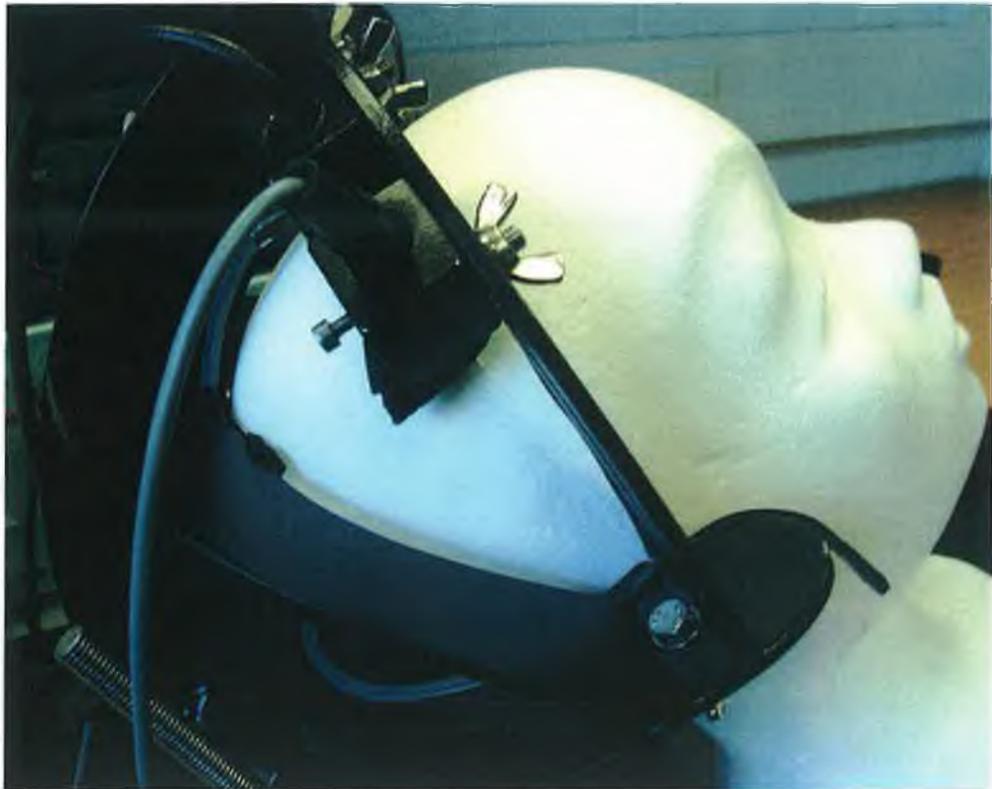
Figure 5.9 Mechanical Mounting System is connected to a seat with an adjustable back incline
The framework cradling the subject's head consists of semicircular rails onto which optode holders can be attached.
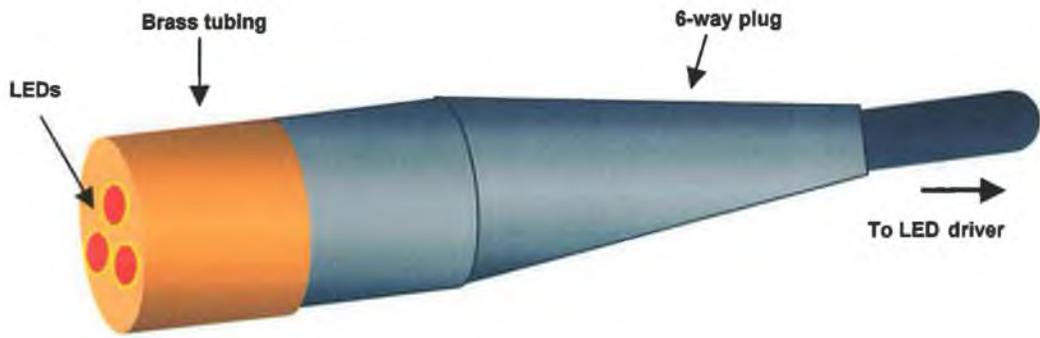
Figure 5.10 LED connector - Three LEDs of different wavelength are soldered to the receptacle of a miniature microphone connector and encased in brass tubing.
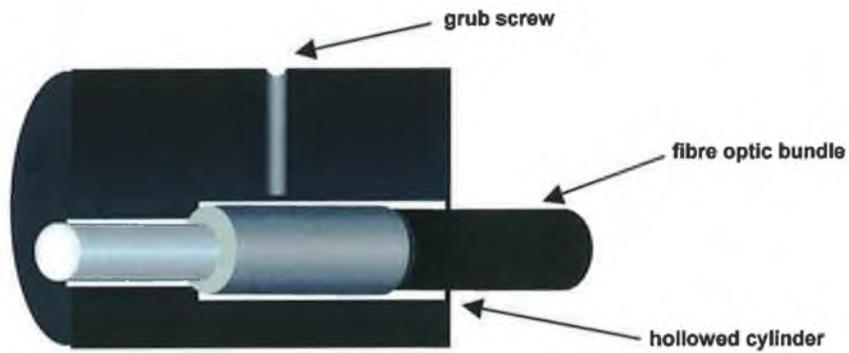
Figure 5.11 Fibre bundle connector, a brass cylinder holds the fibre optic bundle off-centre
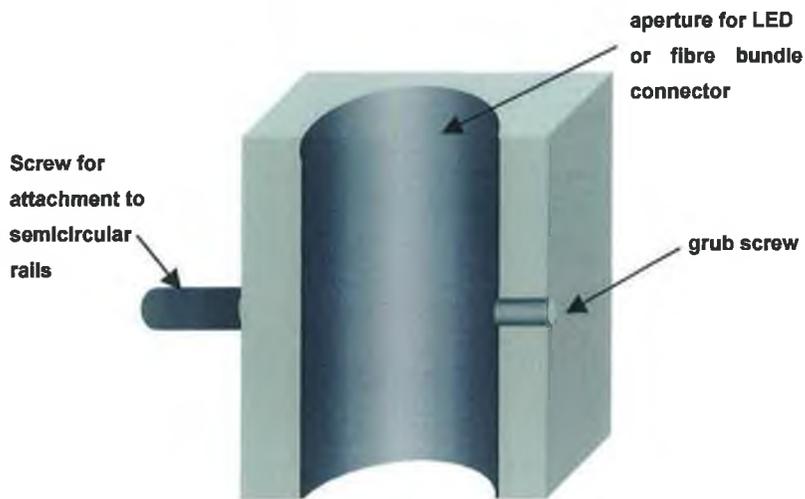
Figure 5.12 Optode holder, used to support and position light source or detector, the optode holders are standardised to fit the LED and fibre optic bundle attachments
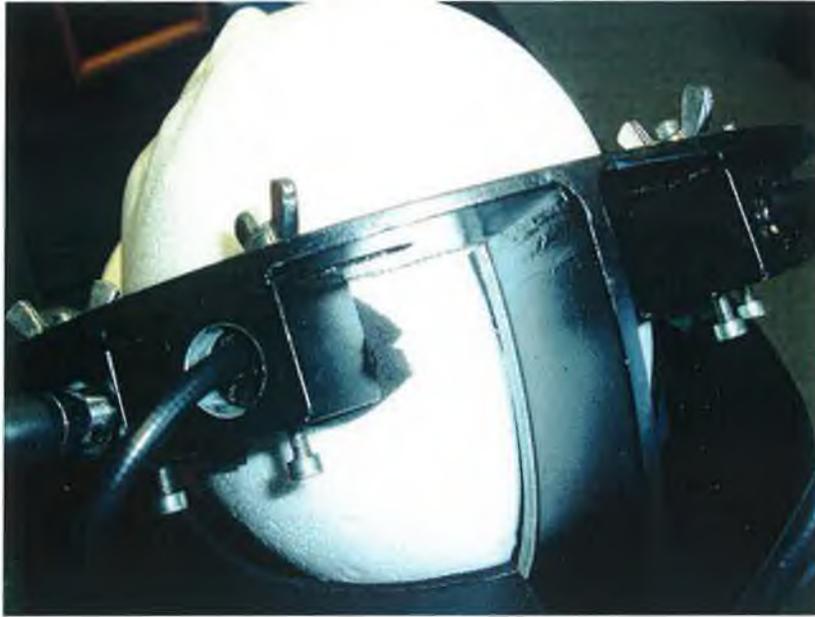
Figure 5.13 Optode arrangement for motor function investigations. The optode holders can slide along the semicircular rails allowing the optode to be placed at various positions for signal acquisition.
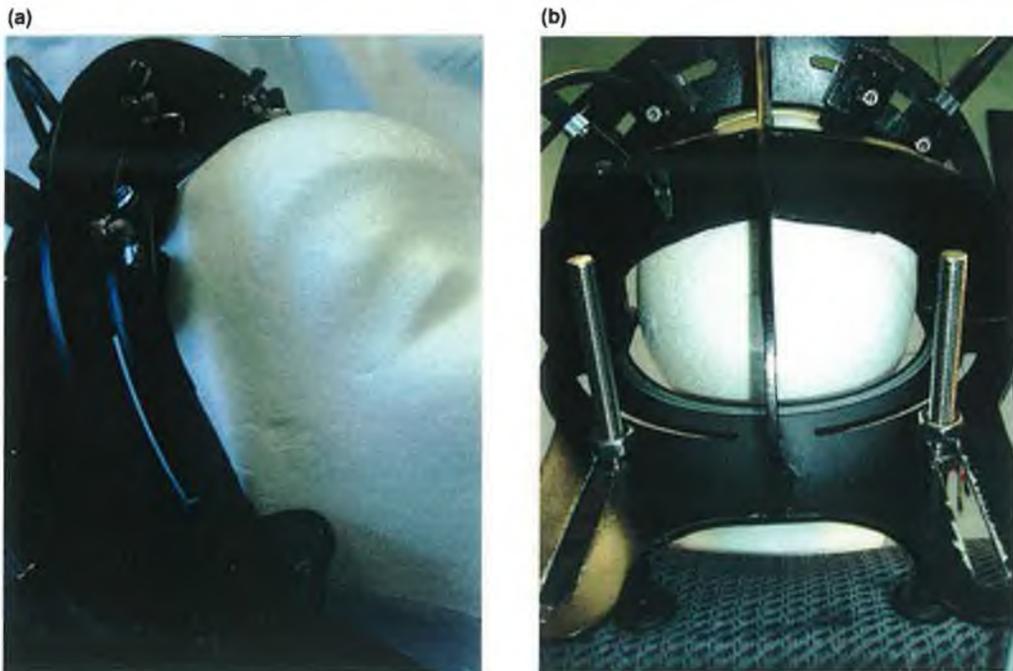
Figure 5.14 (a,b) The mechanical structure replaces the seat head-rest, cradling and providing support to the head. Detector fibre and LED light sources are positioned over the left and right motor cortices.
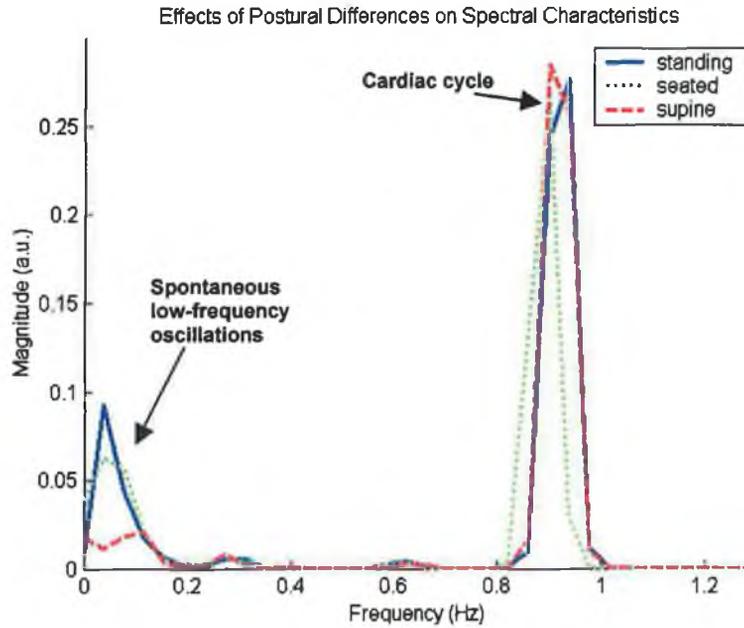
Figure 5.15 Effect of Postural Differences on Spectral Characteristics of the Optical Response. The mechanical mounting system allows the subject to remain supine throughout the experiment, which reduces some physiological noise effects occurring at low frequencies around 0.1Hz. The spectral characteristics of the near infrared signals are compared for three postural arrangements – standing, seated and supine.

The mechanical mounting system allows secure placement of optodes during BCI experimental trials. The seat and cradling mechanism is ideal for subject comfort, which is important during long experimental trials. Keeping the subject in a supine position has a relaxing effect and also helps to reduce postural-dependent spontaneous oscillations. Such oscillations are typically centred around 0.1Hz and have similar temporal dynamics to the characteristic vascular response, as shown in figure 5.15.

5.4.4 Optical Placement Scheme

While there is a need to enhance optode coupling mechanisms, there is also a need for a standardised placement scheme, in order to be able to reproduce measurements from the same subjects and also to ensure consistency between studies. A well-defined method of performing physical measurements needs to be defined. This is especially important in the absence of fMRI information,

where anatomical and functional details are available. Electroencephalography has a standardised electrode placement system described by the 10-20 system. Optical measurements are typically taken based on these measurements. However this system is too vague for optical techniques, which involve the placement of two components, source and detector for each measurement site. Therefore there is a need for a standardised optical placement system as exists for EEG measurements. A possibility is to describe the optode positions using a type of polar coordinate system in terms of the 10-20 positions, where the optode distance and angle with respect to an EEG 10-20 position is defined e.g. positions of a source (S1) and detector (D1) placed 4cm apart, lying 2cm directly above and below C3 respectively, can be described by C3:2($\pi/2$) and C3:2($3\pi/2$), as shown in figure 5.17. This is the convention used throughout this thesis. The vertex, i.e. Cz, should be used as a reference point where the orientation of polar coordinates at all other positions consider Cz to be at an angle of $\pi/2$. Therefore optodes placed on the forehead for frontal lobe investigations could be positioned at Fp2:1.5(0) and Fp2:1.5(π),on either side of position Fp2, with an interoptode distance of 3cm, as shown for a source (S2) and detector (D2) in figure 5.17.

A standardised placement scheme is important for concurrent measurements with other imaging technologies such as EEG and fMRI and an optode mounting system to accommodate such measurements needs to be considered jointly. Optical imaging is ideal for multi-modal imaging and BCI development as the optical signals do not interfere with electrical or magnetic fields. To use NIR with EEG the source and detector need to be positioned on either side of an EEG electrode. To use with fMRI the optode holders/mounting system must be made from plastic or other suitable non-metallic material, and the light transported to and from the subject via fibre optics.
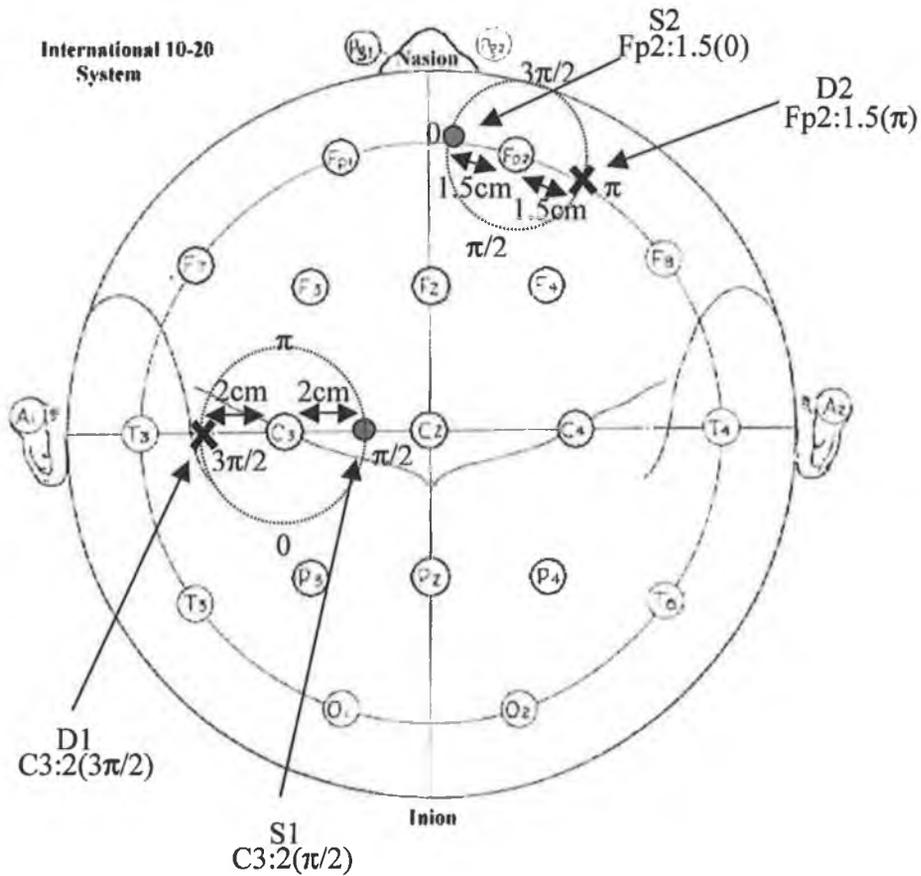
Figure 5.17 Proposed Optode Placement System based on the conventional EEG 10-20 system.

5.5 Summary

The essential components of any optical imaging system are a light source and detector. These must be chosen to meet the relevant application. To detect the event of brain activation, a continuous wave approach is suitable. Although it cannot provide quantitative measurements, it is a straightforward system to implement. In choosing system components the light signal must be of sufficient intensity to penetrate to the depth of the cerebral cortex and be detectable a few centimetres from its entry point. Like any transmission system the source power, attenuation and detector sensitivity must be designed accordingly, while taking safety and physical constraints into account. Once the components are chosen and their associated driving circuits designed, there still remains a vital element

of the system configuration to be decided: the optode coupling arrangement. Although this may seem like a minor issue it has a huge bearing on the system performance and therefore robust coupling between the optodes and the subject's head is required to ensure optimum signal quality. Placement of the optodes is critical and a mechanical mounting system providing adequate support for the optodes has been developed for the application. It has the advantage of providing rigid support while also allowing for subject comfort during functional activation studies.

Chapter 6

Mental strategy for BCI control

" It's a poor sort of memory that only works backwards. "

(Lewis Carroll)

6.1   Introduction

The mental task involved in controlling a BCI must be straightforward and preferably related to natural intent. This eases the learning curve and makes the device user-friendly. A significant problem of many current BCIs is the lengthy training periods involved in learning to control the interface. This can often lead to frustration and anxiety for the user (Spinney 2003). Mental tasks used to control BCIs can include imagery tasks or inherent reactions such as visual evoked responses or P300 oddball responses, while some BCIs call for an entirely new thought process to be learnt (Wolpaw *et al.* 2000).   In order to develop an optical BCI, the functions that can be detected using optical methods must first be established.

With current instrumentation NIRS studies are confined to the cerebral cortex. At this level a range of investigations have successfully detected brain activity

resulting from a number of functions governed by the cerebral cortex. These studies have measured optical responses relating to visual function in the occipital cortex, motor functions in the motor cortex, auditory functions in temporal and parietal areas, language and problem solving in the frontal lobes (Rolfe 2000). Of these attainable responses motor imagery is a well-established method of achieving BCI control. This chapter presents the concept of motor imagery and demonstrates that NIRS can be used to detect neural activity in the motor cortex due to motor imagery tasks. The experimental results of the NIRS motor imagery investigations are reported in Section 6.3. Alternative mental tasks for OBCI control, such as optical correlates of VEPs and the P300 that have been used in EEG-based BCIs are discussed in Section 6.4. Section 6.5 examines the characteristics of the optical response due to functional activation, identifies noise components in the optical signals and presents some signal processing approaches.

6.2 Motor Function

"A part of the convexity of the hemisphere of the brain of a dog is motor... another part is not motor. The motor part, in general, is more in front, the non-motor part more behind. By electrical stimulation of the motor part, one obtains combined muscular contractions of the opposite side of the body."

(Fritsch and Hitzig 1870)

In the 1860's Eduard Hitzig, a German doctor working at a military hospital, was treating patients who had pieces of their skulls blown away in battle. He took this an opportunity to conduct some experiments investigating brain function. He stimulated exposed brains with wires connected to a battery and discovered that weak electric shocks, when applied to areas at the back of the brain, caused the patients' eyes to move. This led to further experiments with another physician, Gustav Fritsch. By stimulating the brains of live dogs they found that

they could cause crude movements of the dogs' bodies and discovered that specific areas of the brain controlled specific movements (Fritsch and Hitzig 1870). Years later in the 1940's Wilder Penfield, a pioneering brain surgeon, applied mild electric currents to specific brain areas while operating on epileptic patients in order to find problem areas (Martin 1997). Since the patients were awake during the operations, they could tell Penfield what they were experiencing. Throughout the procedure Penfield watched for any movement of the patients' bodies and from this information he was able to map the motor cortex. The localisation of function within the motor cortex can be seen in figure 6.1. While it may seem as though disproportionate amounts of cortical area are devoted to movements of the fingers and muscles used for speech, these are the parts of the body that perform the finest and most complex movements. Areas of the motor cortex are responsible for initiating movements but also partake in preparation of movement or imagination of movement, i.e. motor imagery.
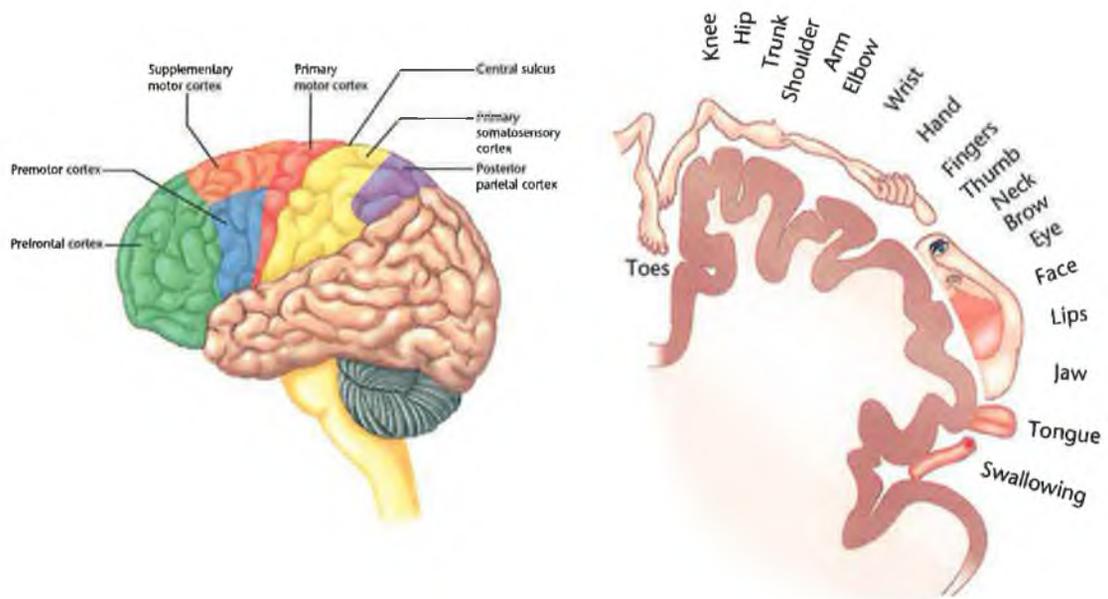
Figure 6.1 (a) Location of the motor cortex and motor association areas on the cerebral cortex (b) map of the motor cortex.

6.2.1 Motor Imagery

Motor imagery is the mental rehearsal of a motor act. Motor imagery is a cognitive state that can be experienced with minimal training. It involves a kinaesthetic representation of an action where the person feels that he or she is executing the action. This can transpire from the imagination of a motor representation but also from observation of another person's actions with the desire to imitate the same tasks (Jeannerod 1995). On account of such neural correlations, motor imagery is often used by athletes to improve performance. Mental practice of movements has been shown to improve sports performance, particularly when skills that follow a pre-planned complex motor sequence are required e.g. gymnastics, diving and athletics (Decety and Ingvar 1990). Mental imagery, either as an internal process or as an observation of actions, activates the motor pathways associated with the simulated action. Hence, by enhancing the neural pathways through "mental practice" the muscles are trained to move in a more skilful manner during actual performance of the action. It has also been postulated that the neural correlates between overt motor tasks and associated imagery may prove to be an effective attribute in motor rehabilitation in patients that have suffered central nervous system trauma, such as spinal cord injury or stroke (Lacourse *et al.* 2004).

A wide range of studies, adopting both a psychological methodology and physiological approach, support the view that motor imagery and execution involve activation of similar cerebral structures. Motor imagery studies adopting a cognitive approach, i.e. from a psychological perspective, have shown that the time taken to perform a mental movement is similar to the duration of the executed movement and that mental reaction time increases with the difficulty of the task. These studies support Fitts Law (MacKenzie 1991), which models psychomotor behaviour in terms of time, distance and precision, e.g. the time taken to imagine walking along a thin beam would be greater than the time taken to imagine walking through flat open space. Studies also show that imagined movements are subject to the same physical laws and physiological limitations that apply to executed motions, e.g. one can not imagine playing a piano faster

than one's fingers can actually move (Crammond 1997). Motor imagery can also be investigated by analysing various physiological phenomena during imagery tasks (Jeannerod 1995). In particular physiological studies of motor imagery have investigated a) electromyographic (EMG) activity, b) spinal excitability, c) autonomic nervous system activation, d) functional brain activity .

(a) EMG activity is often present in muscles involved in the simulated movement, which supports the view that an excitatory motor output occurs, as produced for execution of an action. This excitatory output is then counterbalanced by a parallel inhibitory output to prevent the overt movement, although the origin of the inhibitory output has not yet been identified (Jeannerod and Decety 1995).

(b) Spinal excitability studies have shown that motoneuron excitability increases during mental simulation and that the magnitude of the response is correlated with simulated effort (Jeannerod 1995).

(c) The autonomic nervous system exhibits increased activity during motor imagery, just as it would for movement preparation in anticipation of forthcoming metabolic demands. Heart rate and respiration have been shown to increase during mental simulation of motor tasks in proportion to the amount of simulated exercise (Decety *et al.* 1993).

(d) Initial studies analysing brain activation during motor imagery utilised PET imaging techniques (Roland and Friberg 1985). Since then fMRI and EEG studies have been carried out (Mao *et al.* 1998; Lotze *et al.* 1999; Pfurtscheller and Neuper 1997). These functional brain mapping techniques have identified certain key areas associated with motor imagery phenomena; the prefrontal cortex, supplementary motor area, cerebellum and basal ganglia. The role of the primary motor cortex during motor imagery remains controversial. Many studies have reported that activation of the primary motor cortex only occurs during executed movements and not during imagery although EEG studies have shown changes in DC potentials generated in or close to primary sensorimotor

areas during executed and imagined movements (Beisteiner *et al.* 1995; Pfurtscheller and Neuper 1997). In these studies patterns of EEG desynchronisation were similar to the pattern during planning of voluntary movements. In preparation and imagination of movements the mu and beta rhythms are desynchronised over the contralateral primary sensorimotor area (Pfurtscheller *et al.* 1997; Schloegl *et al.* 1997). These findings have formed the basis for a number of EEG-based brain computer interfaces, where EEG signal changes are recorded and classification of during different types of motor imagery. A recent fMRI study has reported a transient BOLD signal increase in the primary motor cortex at the onset of motor imagery (Dechent *et al.* 2004). The response was observed in four out of six subjects with an average duration of 4s at a delay of 4s after stimulus onset. The patterns of brain activation are influenced by the nature of the imagined task (Jeannerod and Decety 1995), e.g. repetitive movements or rotational tasks provide different responses. Based on the results of these different studies NIRS should also be able to detect a response during motor imagery tasks.

6.3   Motor Imagery Responses using NIRS

"Think left and think right and think low and think high. Oh the thinks you can think if only you try"

(Theodor Giesel)

Motor imagery has become a well-established protocol for BCI control. A number of NIRS studies have focussed on optical responses due to the performance of motor tasks such as fist clenching and finger opposition tasks (Maki *et al.* 1995; Maki *et al.* 1996; Toronov *et al.* 2000; Wolf *et al.* 2002; Franceschini *et al.* 2003; Leung *et al.* 2003). Typically a peak response occurs at 5-8s after the onset of movement (Benaron *et al.* 2000; Boas *et al.* 2002), as shown in figure 6.2. This is due to a slow vascular response causing an increase

in oxy-haemoglobin occurs and a decrease in deoxy-haemoglobin. On completion of the task the concentration levels return to baseline values.

Since it has been known for some time that motor imagery activates similar areas of the cerebral cortex as real executed movements, it would seem logical that the optical response due to motor imagery would be similar to that during executed movement. This is one of the principal hypotheses of this thesis. While motor imagery has been investigated using other functional imaging techniques (Pfurtscheller and Neuper 1997; Mao *et al.* 1998; Lotze *et al.* 1999), no study had been carried out using NIRS technology up until now. From the findings of other imaging modalities one would expect the NIR signals due to motor imagery and motor execution to be similar although definitive conclusions on this idea would be naïve without appropriate scientific investigation. Experiments to verify the hypothesis were carried out (Coyle *et al.* 2003b), the results of which are presented in this section.
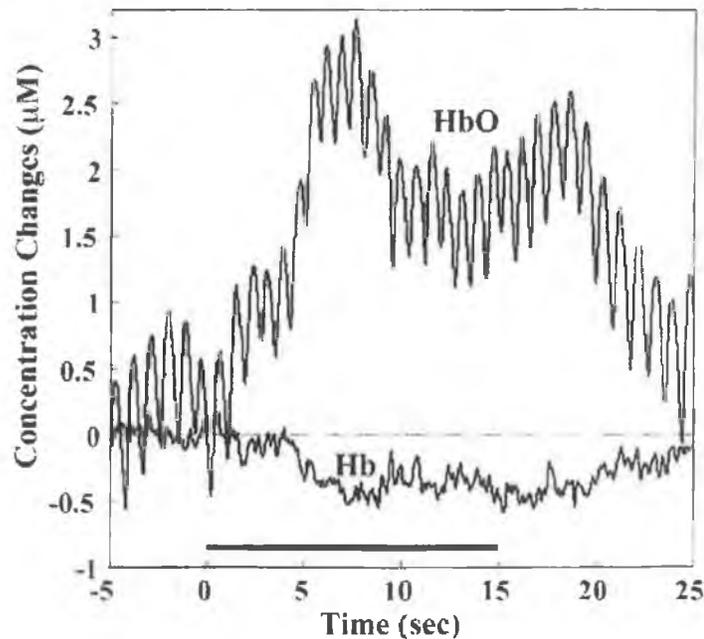
Figure 6.2 Time-course of the haemodynamic response recorded at the motor cortex during hand movement (Boas *et al.* 2002).

6.3.1 Experiment 1 - Cerebral Blood Volume Changes Related to Motor Tasks

6.3.1.1   Introduction

Initial experiments investigating motor imagery recorded blood volume changes (Coyle *et al.* 2003b). This was carried out using a single wavelength of NIR light. Changes in the detected light level are inversely proportional to blood volume changes. The detected light signal therefore gives an indication of neural activation. Four subjects participated in this experiment, all right-handed.

6.3.1.2   Methods

A single NIR LED (peak wavelength 880nm, radiant output power 5mW, modulated at 6kHz) was placed in direct contact with the head. The detection system was as described in Chapter 5. The light source and detector were separated by 4cm and held in place using rubber patches and straps as shown in figure 5.7. The optode holder was centered either over position C3 or C4 above the cerebral hemisphere contralateral to hand movement. Evidence suggests that this position is above the cortical area related to the hand (Homan *et al.* 1987).

Subjects resided in an upright, seated position throughout the experiment. The procedure was carried out in a dimly lit room. Five minutes rest was allowed at the start of the experiment in order to establish a baseline condition. The subject was then asked to perform three actual hand movement tasks, fist clenching or finger opposition tasks for a duration of 30s. Between each task was a rest period of 30s. Following real executed hand movement tasks, imagined hand movement was performed. The subject was asked to imagine clenching their hand for 30s, using the mental image of clenching a tennis ball. The visualisation task was also followed by a rest period.

6.3.1.3   Results

The detected signal was linearly detrended and low-pass filtered using a fourth order Butterworth filter with a cut-off frequency of 0.5Hz to reduce the effects of the cardiac pulse. Forward and reverse filtering was applied in order to prevent phase distortion. This was performed in Matlab® as follows:

```
nir=detrend(nir);
[b a] = butter(4,0.5/50);   %100Hz sampling rate
nirf=filtfilt(b,a,nir);
```

The mean detected light intensity was calculated for each epoch of rest and motor tasks. Results for each subject are shown below. The optical response found is an indication of blood volume changes in the region of motor cortex associated with the hand. The results show that the optical response due to real executed hand movements and imagined hand movements is similar.

6.3.1.4   Discussion

The bar-charts shown in figure 6.3 clearly show a decrease in detected light intensity during motor tasks – both real and imagined. As a single wavelength of light was used in this study, the signal here is essentially photoplethysmographic in nature. The blood volume changes are proportional to total haemoglobin concentration changes HbT, where HbT = Hb + HbO. Oxy-haemoglobin and deoxy-haemoglobin concentration changes has been shown to give a clearer indication of brain activity than total haemoglobin changes (Villringer *et al.* 1993). This differentiation can be achieved by using a second wavelength of light. The reason for this is evident in figure 6.2 – The increase in HbO during functional activation is greater than the increase in HbT due to a reduction of Hb. In order to develop a BCI using optical techniques a dual-wavelength system would be preferable in order to measure these subtle haemodynamic changes.
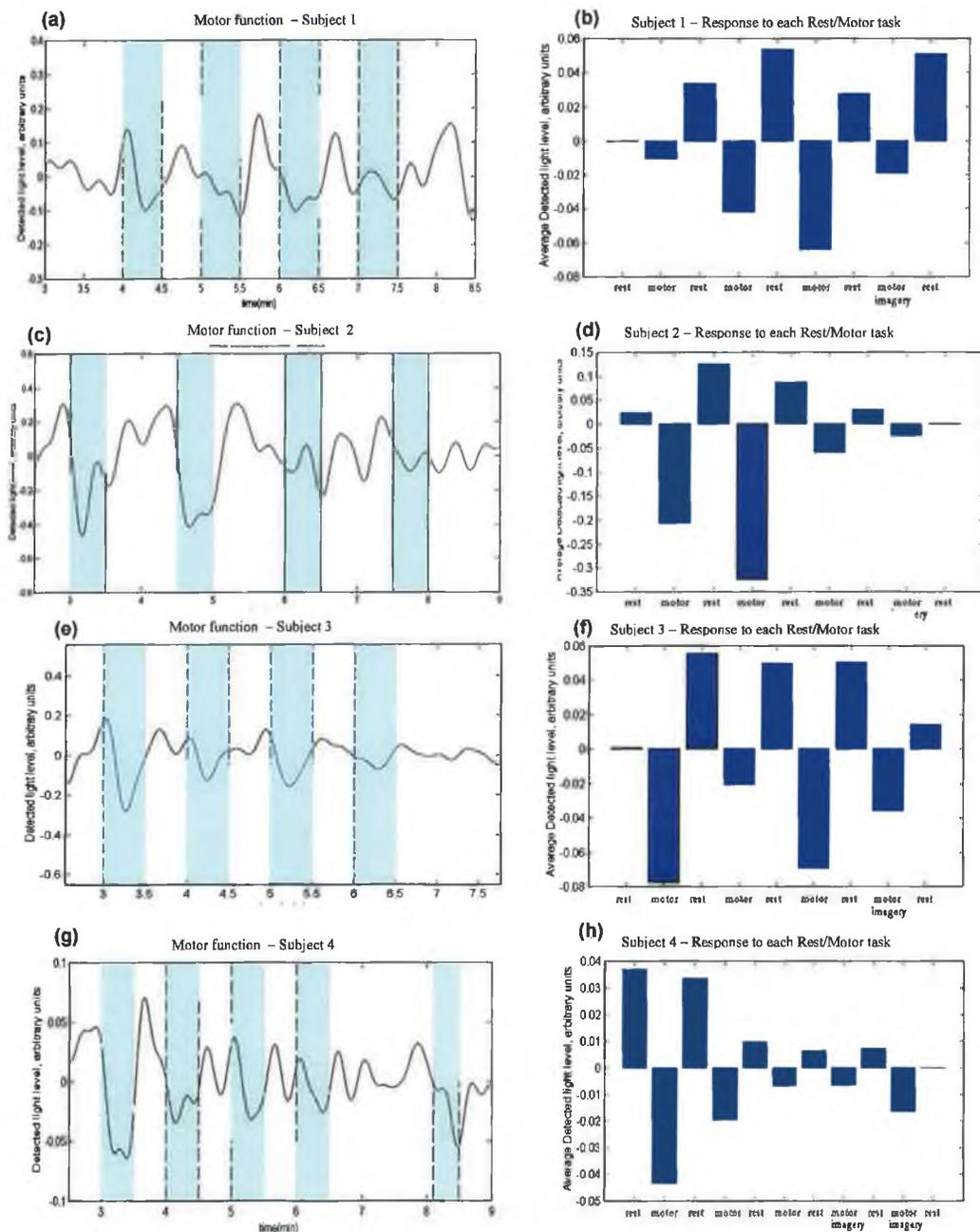
Figure 6.3 (a,c,e,g) Detrended and filtered optical response during motor and rest sequences. The first three shaded regions indicate periods of actual hand movement. Subsequent shaded regions indicate visualisation of hand movement, i.e. motor imagery. (b,d,f,h) The average of each rest and motor activity epoch, the bar-charts show a decrease in detected light intensity during motor tasks – real and imagined.

6.3.2 Experiment 2 - Cerebral Blood Oxygenation Changes Relating to Motor Tasks, using single site measurements.

6.3.2.1   Introduction

By using a second wavelength of light, the optical response yields information about oxygenation changes of the blood. Studies were carried out to investigate the haemodynamic response due to motor function during hand movement/imagery. The first trials involved recording responses from the motor cortex contralateral to hand movement, while later investigations recorded the response at the ipsilateral motor cortex. The results of the two experiments are discussed in the following sections.

6.3.2.2   Methods

This experiment involved a single source-detector configuration, investigating the optical response at one position of the head. The experiment was carried out on a right-handed subject and involved both left and right hand movement and imagery. The experiment was carried out in a dimly lit room and the subject remained seated during the procedure. Instructions for motor tasks involving fist clenching execution or imagery were given verbally to the subject. Eight right hand movement trials were performed (five motor execution, three motor imagery) and seven left hand movement trials were performed (four motor execution, three motor imagery). Hand movement, and imagined hand movement initiate neural activity within the motor cortex of the contra-lateral hemisphere. The optical response was measured over the left motor cortex at position C3. The response was measured for ipsilateral hand movement (left hand) as a control measure to ensure signal changes were not a result of motion artifacts or global cerebral haemodynamic changes.

6.3.2.3   Results

For right hand movement trials, an increase in oxy-haemoglobin occurs and a decrease in deoxy-haemoglobin occurs after the onset of movement execution or imagery. On completion of the task the concentration levels return to baseline values. The overall response is the result of combined changes in localized cerebral metabolism, blood flow and blood volume. The increase in oxyhaemoglobin and decrease in deoxyhaemoglobin in response to the stimulus is due to a localized increase in blood flow that far exceeds the cerebral metabolic rate of oxygen. When the concentrations return to baseline there are slight overshoots due to transient focal uncoupling within the autoregulatory mechanism (Edvinsson and Krause 2002). Figure 6.4 shows the average response of 6 trials due to right and left motor functions. The detected light signals were linearly de-trended and low-pass filtered using a fourth order Butterworth filter with a cut-off frequency of 0.5Hz as in Experiment 1. The Beer-Lambert law algorithm (as described in Section 4.3.3) was then applied using the two detected light signals in order to calculate haemoglobin concentration changes. The haemoglobin calculation algorithm is performed by Hbcalculate.m given in Appendix C.
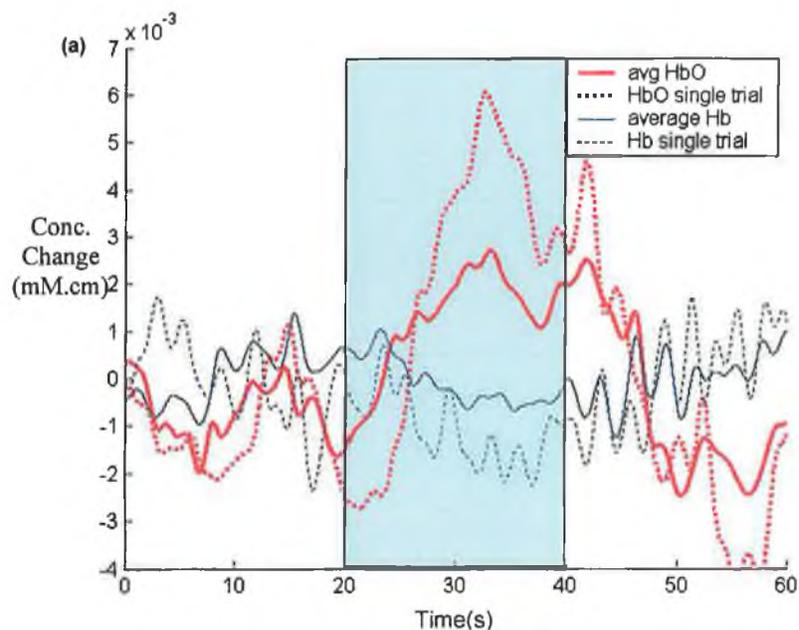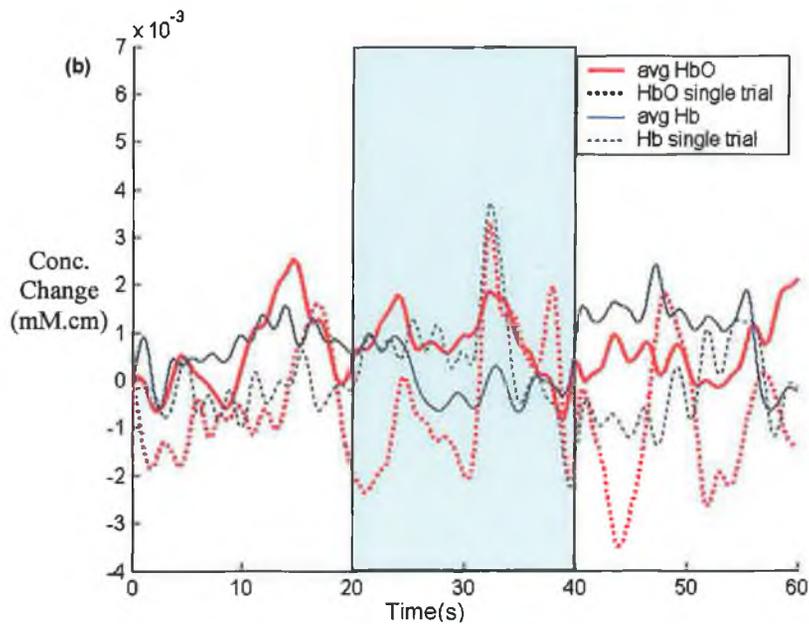
Figure 6.4 Haemodynamic response measured at the left motor cortex during left and right motor imagery/execution. a) Solid lines indicate average HbO and Hb changes for 6 right motor task trials (4 motor execution, 2 motor imagery). Dotted lines indicate a single motor execution trial. b) Solid lines indicate average HbO and Hb changes for 6 left motor task trials (4 motor execution, 2 motor imagery). Dotted lines indicate a single motor execution trial.

In order to verify that the signals were due to motor tasks and not occurring by chance significance test was applied. The sign test (Kanji 2000) was used to identify the significance of signal changes between rest and stimulus epochs. The averages of the oxy-haemoglobin and deoxy-haemoglobin signals during each rest and stimulus interval were found were calculated and compared and the tests were carried out for both left and right motor execution/imagery.

The purpose of the significance test is to indicate whether the change in signal is small enough to have occurred by chance, or if other possible mechanisms of causality exist. If the null hypothesis were true the probability of a change being positive would be equal to the probability of a change being negative, ($p=0.5$)

The probability of a number of positive or negative signal changes (r) is based on the binomial, e.g. if there are 8 trials, the probability of getting 0 negative differences is given by equation 6.1.

$$\frac{n!}{r!(n-r)!}p^r(1-p)^{(n-r)} = 0.0039 \qquad\qquad 6.1$$

Where r=0, n=8 and p=0.5. The probability of getting 8 negatives (opposite extreme, as far from expected value as possible) is also 0.0039.

Right Hand Movement Trials						
HbO changes						
	Rest 1	Stimulus	Rest 2	Stimulus - Rest 1	sign of difference	Rest 2 - Stimulus	sign of difference
execution	24	135	-39	111	+	-174	-
execution	-164	-98	-207	66	+	-109	-
execution	24	138	-3	114	+	-141	-
imagery	74	84	58	10	+	-26	-
imagery	-14	11	-66	25	+	-77	-
execution	-34	-10	-76	24	+	-66	-
execution	-144	-102	-142	42	+	-40	-
imagery	-22	32	-114	54	+	-146	-
Probability of observed changes				0.78%		0.78%	
Hb changes						
	Rest 1	Stimulus	Rest 2	Stimulus - Rest 1	sign of difference	Rest 2 - Stimulus	sign of difference
execution	-36	-56	3	-20	-	59	+
execution	20	2	33	-18	-	31	+
execution	6	-44	13	-50	-	57	+
imagery	57	49	37	-8	-	-12	-
imagery	-13	-16	-54	-3	-	-38	-
execution	19	-77	58	-96	-	135	+
execution	-105	-86	-76	19	+	10	+
imagery	20	-2	39	-22	-	41	+
Probability of observed changes				7.04%		27.92%	

Table 6.1 Average HbO and Hb signals during rest and stimulation epochs (right hand imagery/execution). The sign test is used to identify the significance of signal changes between rest and stimulus epochs.

Left Hand Movement Trials							
HbO changes							
	Rest 1	Stimulus	Rest 2	Stimulus - Rest 1	sign of difference	Rest 2 - Stimulus	Sign of difference
execution	-111	-122	-161	-11	-	-39	-
execution	-209	-162	-199	47	+	-37	-
execution	-1	18	75	19	+	57	+
imagery	-56	-48	-22	8	+	26	+
imagery	-68	-98	-117	-30	-	-19	-
execution	35	48	2	13	+	-46	-
imagery	-137	-146	-150	-9	-	-4	-
Probability of observed changes					**55%**		**33%**
Hb changes							
	Rest 1	Stimulus	Rest 2	Stimulus - Rest 1	sign of difference	Rest 2 - Stimulus	Sign of difference
execution	40	-10	-4	-50	-	6	+
execution	72	53	49	-19	-	-4	-
execution	6	3	62	-3	-	59	+
imagery	-8	22	5	30	+	-17	-
imagery	-35	-61	-44	-26	-	17	+
execution	45	41	20	-4	-	-21	-
imagery	22	-38	-31	-60	-	7	+
Probability of observed changes					**12.50%**		**54.68%**

Table 6.2 Average HbO and Hb signals during rest and stimulation epochs (left hand imagery/execution). The sign test is used to identify the significance of signal changes between rest and stimulus epochs.

If the probability of the detected events is very low it suggests that the data is not consistent with the null hypothesis, i.e. changes in the optical signals are quite likely due to an increase in neural activity.

6.3.2.4   Discussion

From the results presented in table 6.1 it would seem that there is a high probability that right hand movement and imagery cause increases in HbO and decreases in Hb within the left motor cortex. The probability of the null hypothesis being true is 0.78% and 7.04% respectively for these events. Left hand movement and imagery trials yield probabilities of 55% and 12.5%. In comparison to right hand movement and imagery trials this suggests that such actions do not significantly affect neural activity in the left motor cortex. Further investigation to examine the response over the right motor cortex concurrently

and to examine if a contralateral response is present during left hand movement. A more rigorous analysis also needs to be implemented on a larger dataset, e.g. using t-tests.

6.3.3 Experiment 3 - Cerebral Blood Oxygenation Changes Relating to Motor Tasks, using dual site measurements.

6.3.3.1   Introduction

The third experiment used a dual source-detector configuration, allowing optical response to be measured at two positions on the head.   This allowed measurement of the optical response at the motor cortices of both the contralateral and ipsilateral hemispheres.   The experiment was carried out on four subjects (three right-handed, one left-handed).   The trials involved both left and right hand imagery.

6.3.3.2   Methods

The mechanical mounting system described in Chapter 5 was used to connect optodes to the head for this study and concurrent investigations. This allowed subjects to assume a supine posture throughout the investigation, thus reducing Mayer wave effects. Subjects kept their hands relaxed by their sides on armrests throughout the experimental procedure.   Keeping the hands in a position that is compatible with the imagery tasks to be performed makes visualisation easier and enhances the cortical response (Vargas *et al.* 2004).   The optical response was measured over the left motor cortex with source 1 at $C3:2(\pi/2)$; detector 1 at $C3:2(-\pi/2)$; over the right motor cortex with source 2 at position $C4:2(\pi/2)$, and detector 2 at $C4:2(-\pi/2)$.   Before the imagery tasks were carried out subjects were instructed to perform actual hand movements, to ensure that the optodes were placed over motor association areas related to the hand.   Instructions were

projected onto a screen approximately 2m in front of the subject. Left or right arrows were presented indicating when left or right motor tasks were to be performed. During rest intervals a '+' symbol was displayed.

6.3.3.3   Results

The temporal responses of cerebral haemodynamic changes observed in each subject during motor imagery tasks are presented in Figures 6.5-6.8. The graphs display the average response (thick trace) and also a typical single-event response (thinner trace). Solid lines denote HbO concentration changes while dashed lines denote Hb concentration changes. Shaded regions indicate the duration of imagery tasks.

6.3.3.4   Discussion

As observed during Experiment 2, a pronounced response tended to occur when imagery tasks were performed involving the hand contralateral to the cortex. On observation of the results for Subject 1 shown in figure 6.5 the characteristic haemodynamic response occurs at the right motor cortex due to left hand imagery. In addition to the contralateral response a notable ipsilateral response is also observed at the left motor cortex due to left hand imagery. While this occurrence was not observed during Experiment 2, a bilateral cortical responses have been shown to occur during motor tasks in previous fMRI (Dassonville *et al.* 1997; Baraldi *et al.* 1999; Porro *et al.* 2000) and PET (Decety *et al.* 1994) studies. Activity in the ipsilateral motor cortex during motor imagery and execution may be due to a neural population that is activated during movements of either hand (Porro *et al.* 2000; Baraldi *et al.* 1999). The ipsilateral response is also seen in the right motor cortex during right hand movements, as shown in figure 6.5 for Subject 1. The extent of the bilateral response has been shown to relate to the degree of handedness, with activation in the motor cortex tending to be more lateralized with increasing degrees of handedness in both left and right-handed subjects (Dassonville *et al.* 1997). This may explain why an ipsilateral

response was not evident in the signals acquired from the subject who participated in Experiment 1.

The signals measured from the four subjects give an indication of cerebral activity in response to a stimulus as shown in figures 6.5 – 6.8. The responses show a clear inter-subject variability, which aside from functional and anatomical individuality may be partly due to the level of handedness, position of optodes, concentration levels and the ease at which motor imagery was performed. Subject 1 is right-handed and there is a significant response on both the left and right cortex due to left-hand imagery. Right hand imagery initiates a similar but smaller response. Subject 2 is left-handed and left hand imagery causes the most significant signal change, in the left motor cortex ipsilateral to imagery. Subject 3 is right-handed and the most significant response is due to right hand imagery, at the contralateral left motor cortex. Subject 4 is right-handed and right hand imagery is the most significant response. Interestingly for this subject, the response at the right motor cortex is opposite to the expected characteristic, i.e. HbO decreases and Hb increases, which has been observed in ipsilateral response in some cases in a previous NIRS study (Franceschini *et al.* 2003). Table 6.2 shows the results of a significance test of the responses recorded at both motor cortices. The values given are the results of signed rank tests, which investigate the significance of a signal changes from zero. This test takes into account more information about the signal by assigning a rank number to each trial. The most significant responses are highlighted in bold for each subject. The data used in the significance tests, i.e. the average signal changes between rest and stimulus for every trial performed by each subject is listed in Appendix A.
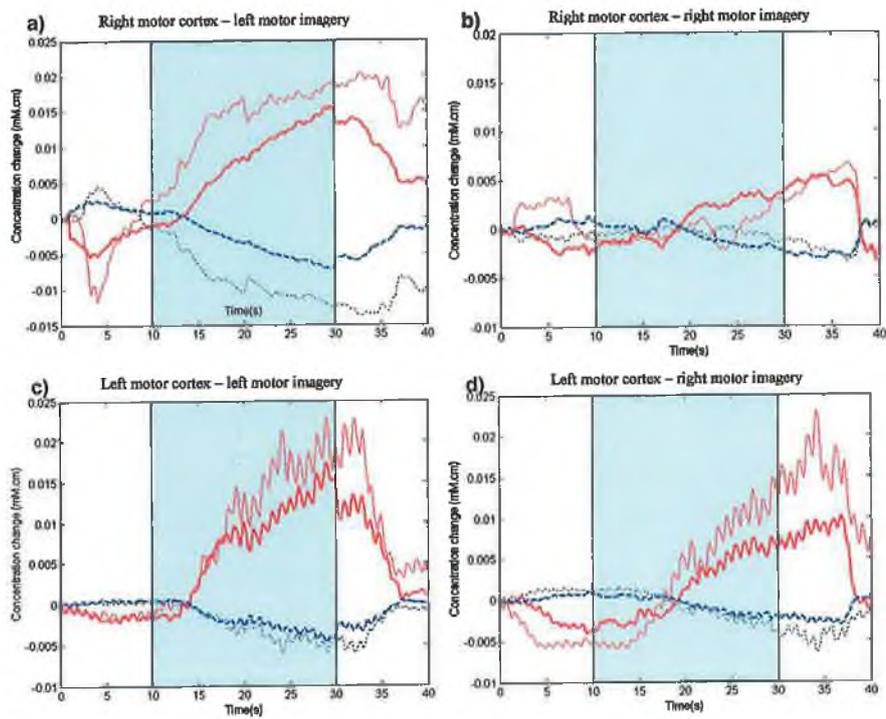
Figure 6.5 Haemodynamic responses for Subject 1 for the right motor cortex during a)left and b)right motor imagery and the left motor cortex due to c)left and d)right motor imagery.
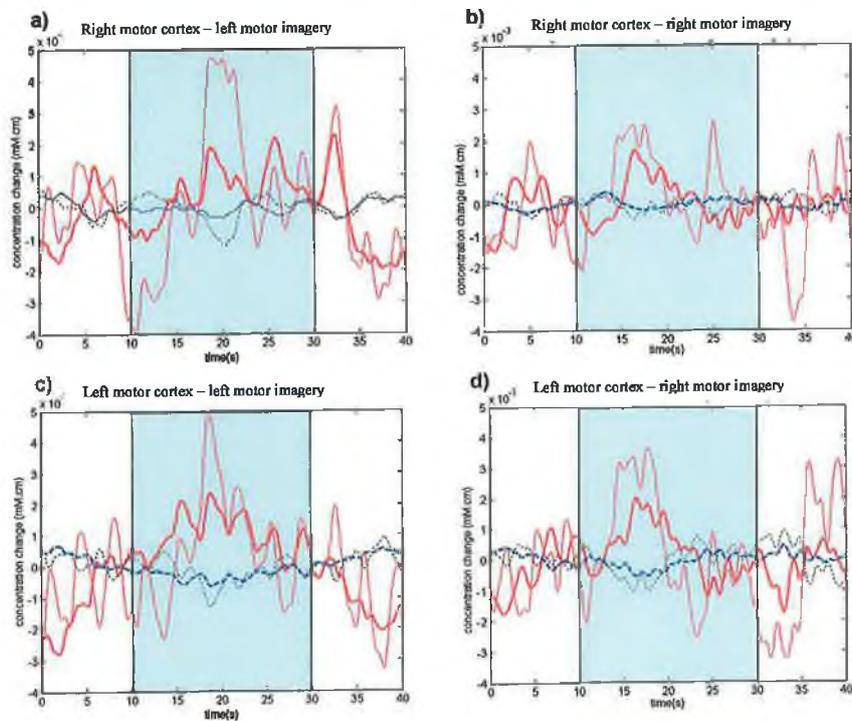
Figure 6.6 Haemodynamic responses for Subject 2 for the right motor cortex during a)left and b)right motor imagery and the left motor cortex due to c)left and d)right motor imagery.

126
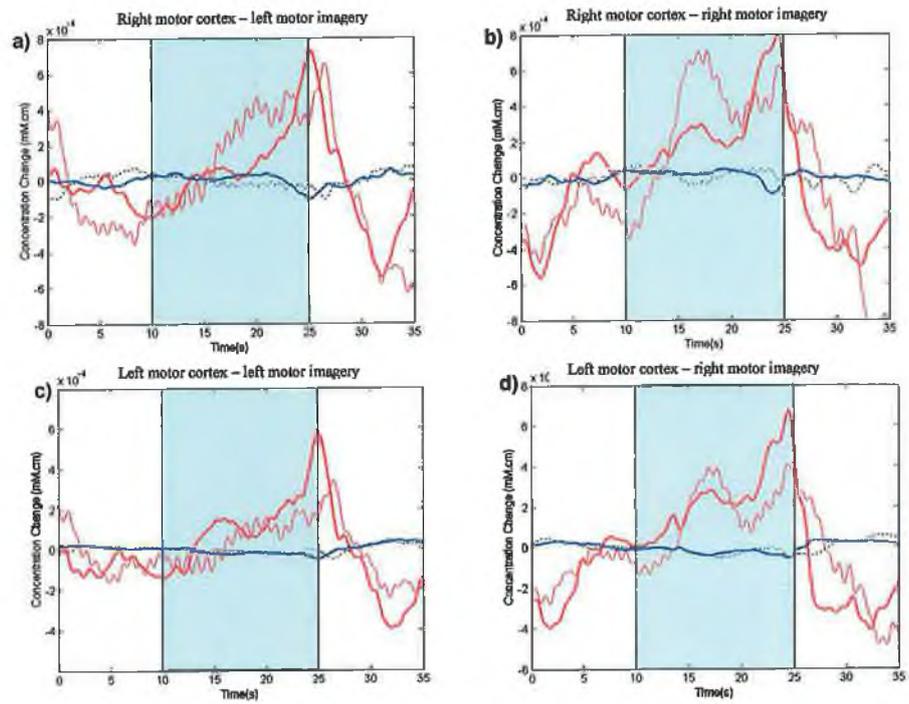
Figure 6.7 Haemodynamic responses for Subject 3 for the right motor cortex during to a) left and b)right motor imagery and the left motor cortex due to c)left and b)right motor imagery.
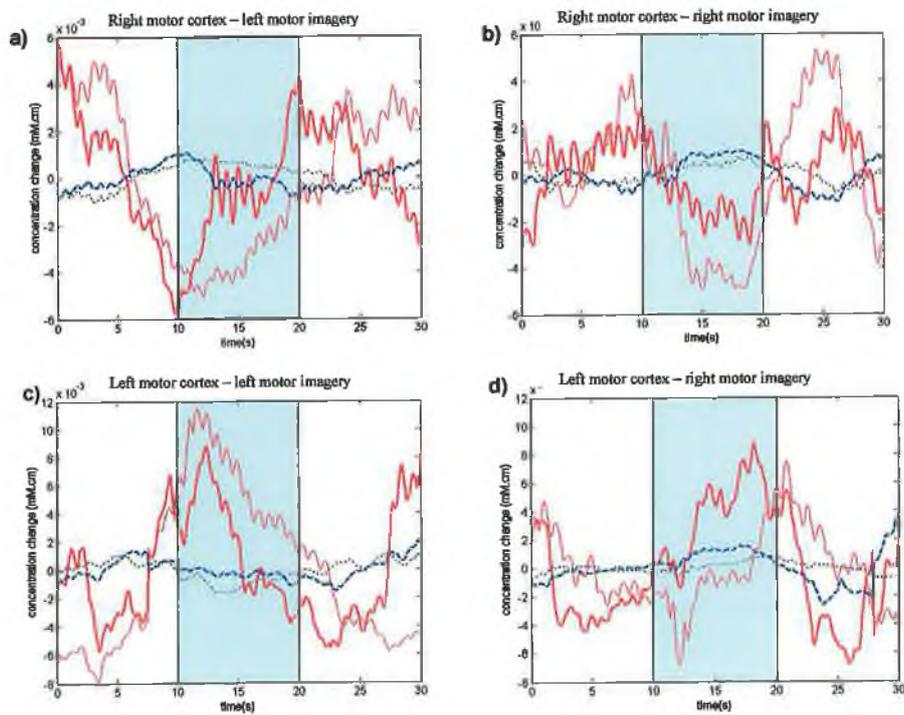
Figure 6.8 Haemodynamic responses for Subject 4 for the right motor cortex during a) left and b) right motor imagery and the left motor cortex due to c)left and d)right motor imagery.

	Left motor Imagery				Right motor imagery			
	Left motor cortex		Right motor cortex		Left motor cortex		Right motor cortex	
	HbO	Hb	HbO	Hb	HbO	Hb	HbO	Hb
Subject 1	0.0625	0.0625	**0.0625**	**0.1250**	0.3125	0.3125	0.4375	0.8125
Subject 2	**0.0006**	**0.0006**	0.0215	0.3575	0.107	0.38940	0.7197	0.8469
Subject 3	0.57	0.23	0.84	0.85	**0.26**	**0.27**	0.62	0.26
Subject 4	0.8457	0.4316	1	0.625	1	0.375	**0.2188**	**0.2188**

Table 6.3 Results of the signed rank test for haemodynamic signal changes that during left and right motor imagery tasks. Full results of each trial are presented in Appendix A. This test is used to identify the significance of signal changes between rest and stimulus epochs. The probability that the signal changes have occurred by chance has been calculated for responses of the left and right motor cortices. The most significant responses (lowest probability) for each subject are highlighted in bold.

Given the variability between subjects it is important to identify the most significant response on an individual basis when seeking a mental imagery task for BCI control. Due to a bilateral response of the left and right motor cortices observed in some subjects mental tasks other than motor imagery may be necessary for harnessing multiple control channels for input to a BCI.

6.4 Alternative Mental Tasks for OBCI control

While motor imagery has become a widely accepted method for BCI control there are various other cognitive tasks that can also be acquired, as discussed in Chapter 3. Many of the signals currently utilized in BCI systems have the potential to be implemented using their optical counterparts, e.g. evoked potentials. In addition to motor function, NIRS functional activation studies to date have investigated a number of cognitive tasks that could be used for BCI control.

6.4.1 Cognitive tasks

An fMRI based BCI has been demonstrated using mental calculation and mental speech generation tasks in addition to motor imagery to control the BCI output (Yoo *et al.* 2004). Areas within the frontal lobe became active during mental calculation and mental speech generation tasks. Similar mental activities have been assessed using NIRS techniques engaging tasks involving working memory (Izzetoglu *et al.* 2003; Hoshi *et al.* 2000), mental arithmetic (Hoshi and Tamura 1993), verbal fluency (Herrmann *et al.* 2003) and language translation (Quaresima *et al.* 2002). These studies have been carried out with optode placement on the left side of the forehead or in the case of language switching on the left side of the head covering Broca's area. Tasks involving creative imagination and visuo-spatial abilities such as the design fluency task have been shown to activate right frontal areas (Elfgren and Risberg 1998). The verbal fluency test activates the left frontal areas involves citing as many nouns as possible given a particular letter. The design fluency test is a non-verbal parallel where as many different abstract forms as possible must be visualised.

Mental calculation has been shown using NIRS to activate the left frontal lobes, by placing the optodes on the left side of the forehead (Hoshi and Tamura 1993). This was investigated in this work by placing optodes around Fp1, with the source and detector at positions Fp1:2(0) and Fp1:2(π). The subject remained in a seated position throughout the experimental procedure. Verbal commands instructed the subject when to start or stop mental calculations. The tasks were performed for epochs of 10s with rest periods of 30s in between. The longer rest period allowed a control measure to be compared to the response during the cognitive task. The responses measured during mental calculation and rest are shown in figure 6.9 for one subject. The thick lines show the average response (n=6) while the thinner lines represent single trials. The response observed during the cognitive task shows signal characteristics that could be rendered by a BCI translational algorithm, however further investigation is needed with a larger subject population.
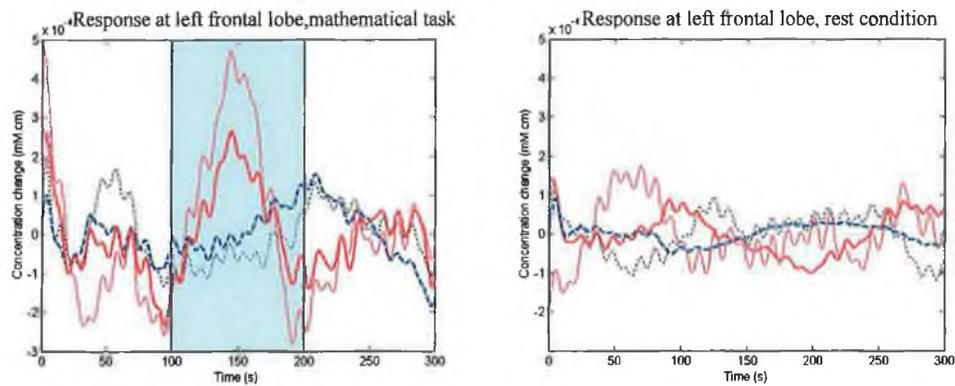
Figure 6.9 Haemodynamic responses recorded at the left frontal lobe during mental calculation tasks. Solid lines indicate HbO, dashed lines Hb. The thick lines show the average response (n=6) while the thinner lines represent single trials.

6.4.2 Visual functions

Activity in the occipital cortex can be measured in response to visual stimulation using NIRS. While the temporal response due to visual stimulation has been observed to have a different time evolution compared to motor function (Wolf *et al.* 2002), the characteristic increase in HbO and decrease in Hb has been observed. The average response (n=20) measured at the left and right occipital cortex in response to a checkerboard reversal pattern is shown in figure 6.10. Optodes were placed at the back of the head at positions O1:2(π) (source 1); O1:2(0) (detector 1); O2:2(0) (source 2) and O2:2(π) (detector 2). Details of the experimental protocol are given in (Lebid *et al.* 2005).

While the analysis of the cerebral haemodynamic response to visual function may be of interest in clinical examinations it may not be practical for BCI control as it may require control of extra-ocular activity. Nevertheless, EEG-based BCIs making use of visual function have proven useful (Wolpaw *et al.* 2000) and therefore the optical response relating to visual stimulation is worth consideration. Recent studies have reported fast optical signals that may correlate with the VEPs detected by EEG. The optical counterpart of the EP has been termed the Event Related Optical Signal (EROS) (Gratton and Fabiani

130

2001). Using frequency domain NIRS methods the EROS is recorded as phase changes in the detected light waveform. The signal maintains a time course that is consistent with the expected latency of the neural activity, as shown in figure 6.11. However, currently the EROS is difficult to measure (Syré *et al.* 2000) and a reliable means of attaining the signal must first be determined before it can be applied to BCI use.
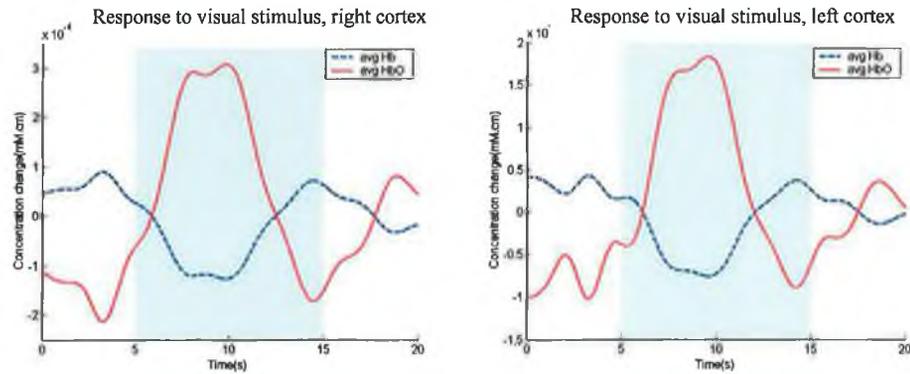
Figure 6.10 Average haemodynamic response at the a)right and b)left occipital cortices. Shaded region indicates visual stimulation (flashing checkerboard).
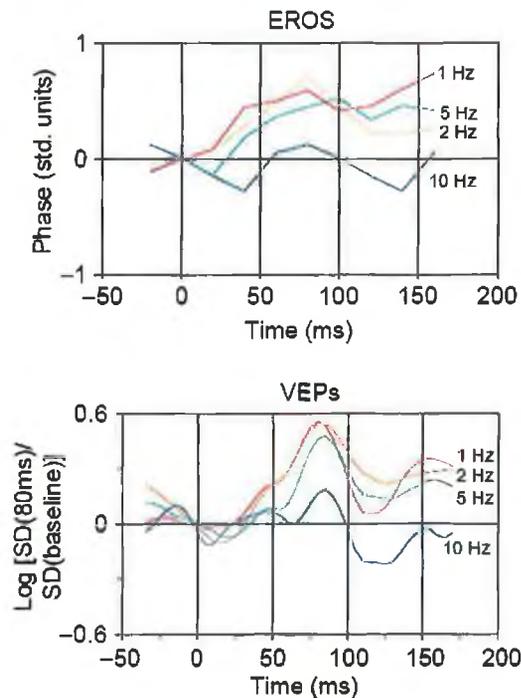
Figure 6.11 Event related Optical Signal (EROS) recorded over the occipital cortex due to visual stimulation shows a similar time-course to EEG VEP signal (Gratton and Fabiani 2001). Different traces indicate different frequencies of visual stimulation (grid reversal paradigm).

6.4.3 P300

The P300 signal has the advantage that it is a naïve response that does not require user training. Being able to reliably detect this response optically would be a useful channel for BCI control. (Keenan *et al.* 2002) have reported the hemodynamic responses associated with an "oddball" auditory stimulus that corresponds to the electrical P300 signal. The change in total haemoglobin in response to oddball tones is significantly greater than the response due to frequent tones as shown in figure 6.12. The time-course of the haemodynamic signal is much greater than the electrical P300 response, with a peak response occurring 6s after the stimulus.
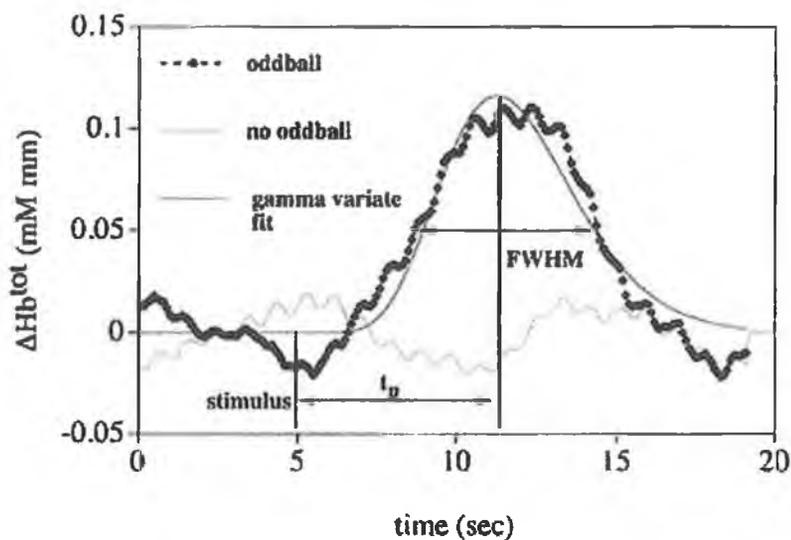
Figure 6.12 Single subject averaged time-courses of total haemoglobin for auditory oddball response, taken from Keenan *et al.* (2002).

A similar study using a visual oddball stimulus has been carried out recently (Izzetoglu *et al.* 2003). Measurements were taken from the forehead, based on a theory that the P300 response also activates cortical areas involved in working memory tasks. Infrequent targets presented to subjects throughout the study produced a comparatively higher response than the frequent targets.

Further study is needed however to investigate the consistency of the optical oddball response. Both the slow haemodynamic signal and the fast EROS ned to be investigated (Rinne *et al.* 1997). It would also be beneficial to examine the possibility of characterising single trial events.

6.5 Signal Processing

In order to determine the event of a stimulus in the optical response, it is essential to first characterise components of the signal. The feature of interest in the optical signal is due to the haemodynamic response. This is observed as negative peaks in the detected light intensity 5-8s following the onset of a stimulus e.g. response of motor cortex due to hand movement as shown in figure 6.3. (Gratton *et al.* 2003). This 'slow' response causes changes in transmitted light intensity of approximately 1%. Recent studies investigating the EROS which is more directly related to neuronal firings, have reported signal changes of 0.01-0.1% (Gratton *et al.* 2003). In order to identify features of the signal for translation to a BCI output it is vital to then optimise the signal to noise ratio, especially as single trial event detection is desirable for optimum speed. In comparison to electrical or magnetic technologies, it is quite easy to reduce the effects of environmental noise using optical techniques. One of the great benefits of optical methods is the lack of mains-induced electrical interference – the dreaded mains "hum". Chapter 5 has discussed the efforts undertaken to reduce the effects of system and environmental noise i.e. modulation of LEDs, shielding of light and reliable coupling of light to the head. Physiological effects tend to be the greatest sources of noise, namely cardiac pulses, respiratory effects and cerebral vasomotion, a spontaneous low frequency oscillation. A good description of the constituent oscillations in cerebral haemodynamics is given in (Elwell *et al.* 1999) where the characteristics of physiological noise have been investigated using near-infrared techniques. This section looks at the typical noise sources present in optical responses and the signal processing approaches developed to overcome such noise.

6.5.1 Spectral characteristics of the optical response

Analysis of the spectrum of optical signals helps to identify the quasi-periodic noise sources present. Spectral analysis of the optical signal acquired from a single subject is shown in figure 6.13. Cardiac signals are typically centered around 0.5-2Hz, respiration between 0.2-0.4Hz and the Mayer wave around 0.1Hz. The results are consistent with the study reported in (Elwell *et al.* 1999).
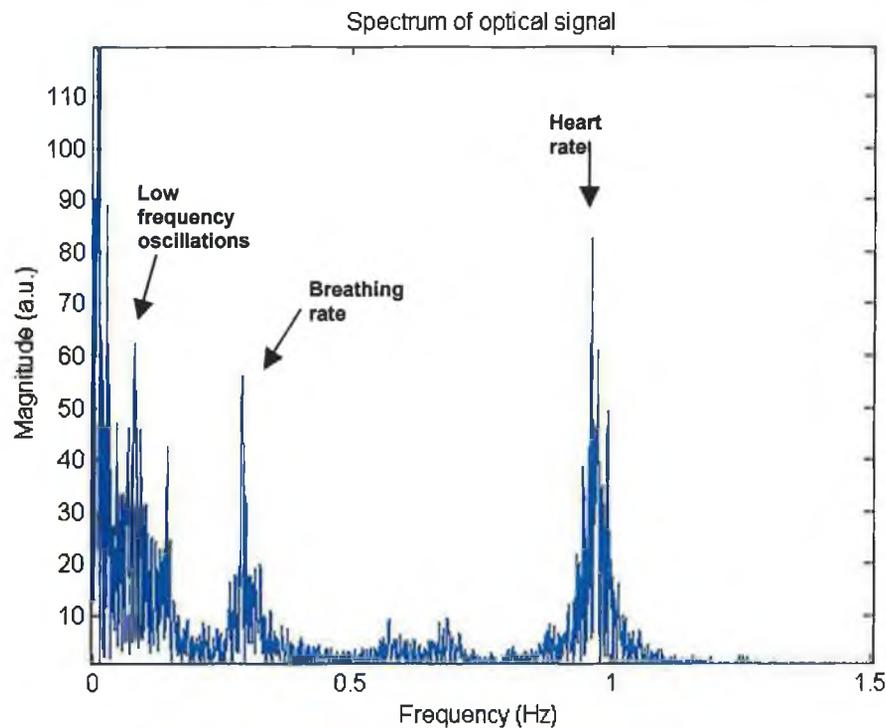
Figure 6.13 Power spectrum of the near-infrared signal. The cardiac signal is centered around 0.95 Hz, respiration around 0.3Hz and spontaneous low frequency oscillations around 0.1Hz.

6.5.2 Cardiac Pulse

While photoplethysmography has been used for some time to measure the rate of blood vessel pulsations, particularly in a clinical environment (Millikan 1942) from a functional imaging perspective this cardiac pulse is considered to be a source of noise. It is particularly problematic when looking for the faster EROS signals (Gratton 1995). The fast optical signal occurs at much higher frequencies than the fundamental frequency of the cardiac pulse and higher residual

134

harmonics can corrupt the signal making the extraction of the required response very difficult. The current solution to this problem is the time-warped average pulse regression technique as proposed by Gratton and Corballis (Gratton 1995). It relies on extracting the heartbeat intervals, time warping them to a longer common timescale before averaging them to compute an average pulse template. This is temporally rescaled and regressed against each original pulse and subtracted to yield a corrected signal. The problem with this algorithm is that it makes the assumption that the variability in the shape of the pulse is negligible. The cardiac pulse features do vary to an extent that makes this particular algorithm difficult to implement in a robust fashion.

For the purposes of the optical BCI system, which relies on a slow varying vascular response, a simple solution is to use an IIR low pass filter to remove the pulse signal, revealing smoothed HbO and Hb signals. However this approach has proven insufficient in removing all remnants of the pulse signal (Gratton 1995) . As an alternative a pulse correction algorithm was developed and operates as follows. (i) The cardiac peaks are identified, to yield a set of heartbeat intervals. (ii) Under the assumption that the haemodynamic response is slowly and smoothly varying relative to the cardiac pulse signal, the mean of the average signal during each heartbeat interval is computed. (iii) The smooth pulse corrected signal is then generated by interpolation using a cubic spline against the original time vector.

The pulse correction algorithm effectively reduces the pulse artefact as shown in figure 6.14 while still preserving the slow-varying haemodynamic response. The algorithm is described in more detail below and source code is given in Appendix C.

i) Identify the cardiac peaks, yielding a set of heartbeat intervals H = {H_{780},H_{830}}. Where

$$H_{760} = \{I_1, I_2, ...I_N\}_{760} \qquad\qquad 6.2$$

$$H_{880} = \{I_1, I_2, ...I_N\}_{880} \qquad\qquad 6.3$$

and I is a sampled optical signal bounded between successive systoles recognized by periodic dips in the received optical signal. These periodic dips will repeat at heart rate frequencies , typically $0.5 - 2$ Hz.

ii) Compute the mean of the average signal during each heartbeat interval. The haemodynamic response is assumed to be slowly and smoothly varying relative to the cardiac pulse signal.

$$M_{760} = \left\{ \overline{I}_1, \overline{I}_2, \dots \overline{I}_N \right\}_{760}$$ 6.4

$$M_{880} = \left\{ \overline{I}_1, \overline{I}_2, \dots \overline{I}_N \right\}_{880}$$ 6.5

iii) Interpolate the set **M** using a cubic spline against the original time vector to obtain the smooth pulse corrected signal. The cubic spline is a piecewise continuous curve, passing through each element of the set **M**, with a separate polynomial curve across each time interval $[t_i, t_{i+1}]$ that is associated with each element of **H**, and with its own coefficients $[a_i\ b_i\ c_i\ d_i]$, described by equation 6.6.

$$S(t) = a_i(t - t_i)^3 + b_i(t - t_i)^2 + c_i(t - t_i) + d_i$$ 6.6

Where

$$S(t_i) = \overline{I}_i \text{ and } S(t_{i+1}) = \overline{I}_{i+1}$$ 6.7

Spectral analysis demonstrates that this technique tends to produce a smoother spectrum although for the purpose of the BCI such intensive signal processing was not required.
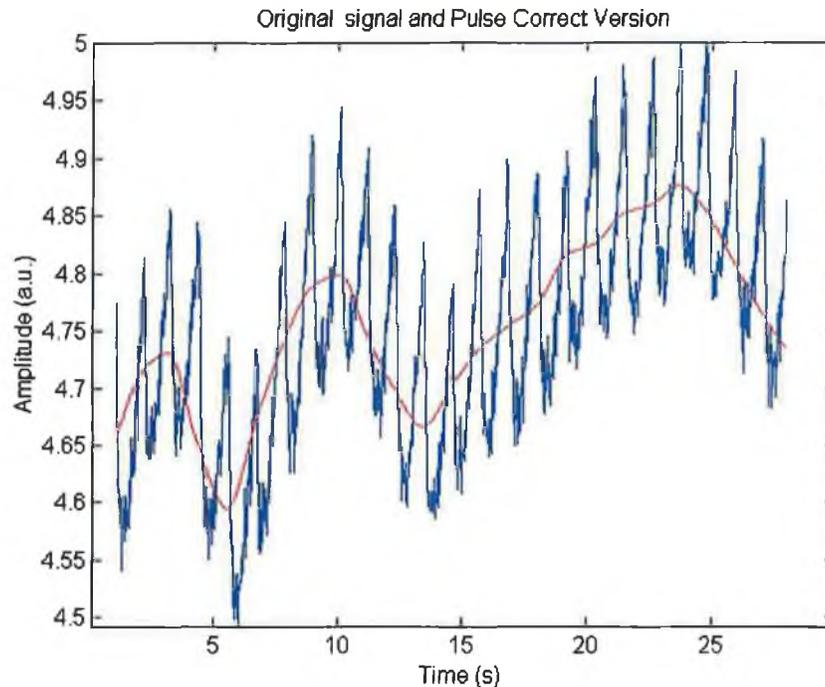
Figure 6.14 Detected NIR light signal (raw data) and pulse corrected signal using the described pulse correction algorithm.

6.5.3 Mayer wave

Spontaneous low frequency oscillations around 0.1Hz have been termed the Mayer wave (Elwell 1999). These oscillations, also referred to as vasomotion, V-signal and spontaneous oscillations, been reported by various studies using different techniques (Elwell 1999); Mayhew *et al.* 1996; Obrig *et al.* 2000). (Obrig *et al.* 2000) tabulates a summary of studies using different physiological measurement systems in different species. The origin of this signal is not clearly understood at present. It was thought to represent baroreceptor mediated blood pressure control and later interpreted to be originating from a central oscillator (Cooley *et al.* 1998). The magnitude of these oscillations renders them a significant noise source in functional activation studies (Elwell 1999), and particularly for optical brain computer interfacing where single-trial events are necessary to ensure optimum speed.

The following signal processing model can be used to reduce the influence of the Mayer wave. The model is based on the IEEE Standard 1057 algorithm for fitting the parameters of a sine wave to noisy data (IEEE 1994). The model assumes that the Mayer wave m(t), being quasi-periodic in nature, can be modelled by equation 6.8.

$$m(t) = \alpha \sin(\omega t + \phi)$$ 6.8

α is the amplitude, ω is the frequency of the oscillation and φ is its phase relative to time t=0. Based on data acquired from various subjects, this appears to be a reasonable assumption for small time intervals (10-20s). The assumption that α and ω are constant during the analysis windows has been shown to be true providing there are no gross changes in the subject's position such as moving from supine to seated (Tachtsidis *et al.* 2004).

The optical data containing the sequence $y_0,...,y_N$ taken at times $t_0,...,t_N$ can be modelled by

$$y_k(A,B,C,\omega) = A\cos\omega t_k + B\sin\omega t_k + C$$ 6.8

Where $A=\alpha\sin\varphi$ and $B=\alpha\cos\varphi$ are unknown constants, ω is the angular frequency of the oscillation and C is the residual signal.

For a given segment of data, the four unknown parameters can be found using a least squares fit algorithm, taking the frequency to be 0.1Hz as an initial guess for ω. In order to take into account the time-varying frequency and amplitude of the oscillations, a moving window of ten second duration is applied; yielding the best fit values of A, B, C and ω for each second in time. The algorithm presented here has been used to remove the Mayer wave (0.1Hz), but it could also be applied to any oscillatory noise function present, e.g. respiratory effects (0.3Hz), simply by using the frequency of the oscillation to get an initial estimate of the angular frequency ω. The source code implementing the sine-fit algorithm is given in Appendix C.

138

Applying this algorithm to single trials involving motor function can significantly reduce the effects of the Mayer wave, as shown in figure 6.15a. Data segments where no stimulus (hand movement) was present, but where the amplitude of the Mayer wave could be interpreted as an event occurrence are shown in figure 6.15b. If event classification of the optical BCI is carried out using a thresholding approach applying this algorithm can reduce the bit error rate.

In real-time application of the BCI this processing was not essential. Instead subjects were positioned in a supine posture during experimental trials which has been shown to reduce the influence of the Mayer wave.
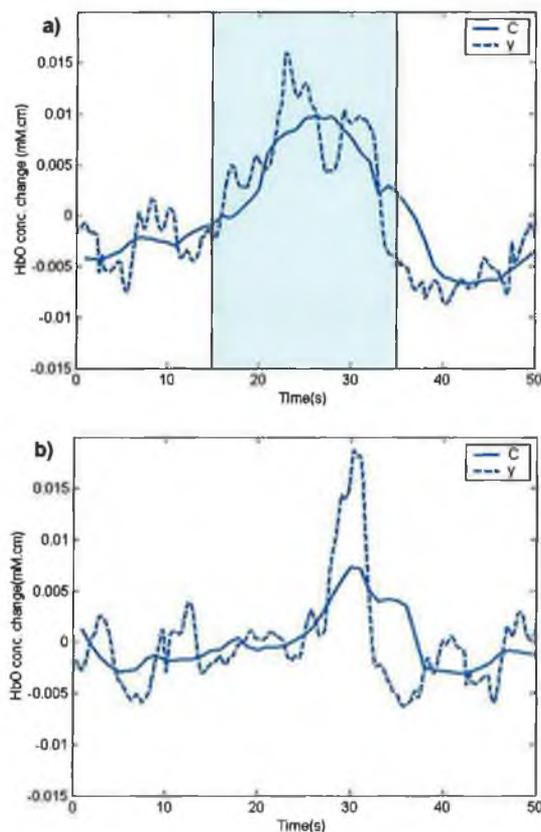
Figure 6.15 Oxy-haemoglobin concentration changes before (dashed line), and after signal processing algorithm applied (solid line). a) True positive - Stimulus (hand movement) occurs after 15s and lasts for 20s. b) False positive during rest.

6.6   Summary

NIRS is capable of monitoring cognitive functions such as visual, motor, auditory and problem-solving tasks (Rolfe 2000). Of these motor imagery is a well-established protocol for BCI control (Wolpaw 2000) and has potential use in controlling the optical BCI. As motor imagery and motor execution activate similar neural pathways, a study was conducted to investigate if NIRS can detect neural activity within the motor cortex during visualisation of movement.

Performing motor imagery is a straightforward task involving natural intent and is therefore ideal for BCI control. The optical response showing either blood volume changes or haemodynamic changes is presented for nine subjects in this chapter. Initial studies examined blood volume changes relating to detected light intensity from one side of the head. Later studies incorporated a second wavelength of light to discern blood oxygenation changes, and also investigated a bilateral response in both hemispheres. Inter-subject variability was observed in the recorded responses. In general, evidence of neural activation, i.e. increase in HbO and decrease in Hb, was more significant in the motor cortex contralateral to the hand involved in imagery.

Aside from motor imagery, other neural functions may also be harnessed for BCI control, which will be important for development of a multi-channel BCI. Activity in the frontal lobes can be detected resulting from various cognitive tasks. Mathematical calculation and verbal fluency tasks tend to activate the left frontal lobe while visuo-spatial activities activate the right frontal cortex. Other avenues to investigate include visual responses and the "oddball" response to infrequent events. These are protocols used in EEG-based BCIs and a fast optical response of similar time-course to the EEG responses may be needed.

Before the response can be translated to a BCI output, the optical signal must be processed in order to reduce the effects of number of noise sources. Multiple noise effects, including system noise, motion artifacts and physiological noise, corrupt the detected light signal in near-infrared imaging studies. Efforts can be made to minimize noise within the system, however physiological noise is inherent and can lead to event misclassification in optical BCIs. The noise arises primarily from the cardiac cycle, respiratory functions and the Mayer wave. The Mayer wave in particular must be taken into account because the magnitude and period of these oscillations can be similar to haemodynamic changes responding to functional activation.

The confirmation of mental imagery detection with NIRS makes a BCI based on this modality possible. The next chapter describes such a device.

Chapter 7

Optical Brain Computer Interfacing –
Applications and Performance

"Everything you can imagine is real."

(Pablo Picasso)

7.1   Introduction

In this chapter the experimental phenomena described in Chapter 6 will be
harnessed to develop a BCI. While NIRS has become customary in
neuropsychological studies, it has not yet been applied in this way. Appropriate
methods to characterise the response must be developed in order to identify
features in the signal. The optical BCI must detect and identify features, in real-
time, that result from mental processes such as motor imagery, and subsequently
translate these features to a control output. A prominent feature notable in the
results presented in Chapter 6 is the characteristic change in HbO concentration,
which could be used to distinguish the event of functional activation. This
chapter describes the applications that have been developed to operate in real-
time that give user feedback based on the changes in HbO levels. A number of
pilot studies involving a small number of subjects were performed in order to

determine the most suitable course of action. The pilot studies investigated different modes of operation, e.g. giving continuous or intermittent feedback regarding HbO signal changes, and different event classification approaches. Section 7.2 outlines the functionality of these trial applications. Section 7.3 discussed the ensuing application, "Mindswitch", that was based on the findings of these early studies. Mindswitch presents targets to the user for selection, which allows for its operation and performance to be assessed easily in terms of accuracy and speed.

7.2 Pilot studies

There are two modes of BCI operation – asynchronous and synchronous. In synchronous BCIs, the system is active only during some defined periods. Asynchronous BCIs do not rely on cues, instead they continuously analyse and classify mental activity giving the user an open amount of decision time (Mason and Birch 2000). The first pilot study operates in asynchronous mode, giving the user continual feedback regarding HbO signal changes. The second study integrates a second channel, but operates in synchronous mode, while the third study reverts to a single channel, also in synchronous mode.

7.2.1 Study 1 – Asynchronous single-channel OBCI

7.2.1.1 Introduction

The first approach was to give continuous feedback to the user based on HbO signal changes that the user could control through motor imagery. As a training strategy continuous visual feedback was displayed to the user by means of a circle expanding and contracting depending on the haemodynamic response. An event of functional activation was noted when there was an increase in oxy-

143

haemoglobin above a defined threshold. Such an event caused the circle to shrink (associated with clenching a ball in one's hand), as shown in figure 7.1. No significant change in oxy-haemoglobin levels caused the size of the circle to remain constant, while a decrease in oxy-haemoglobin caused the circle to be released, expanding back to its resting position. Three subjects participated in this study. Offline analysis of the responses detected from one subject are presented here.
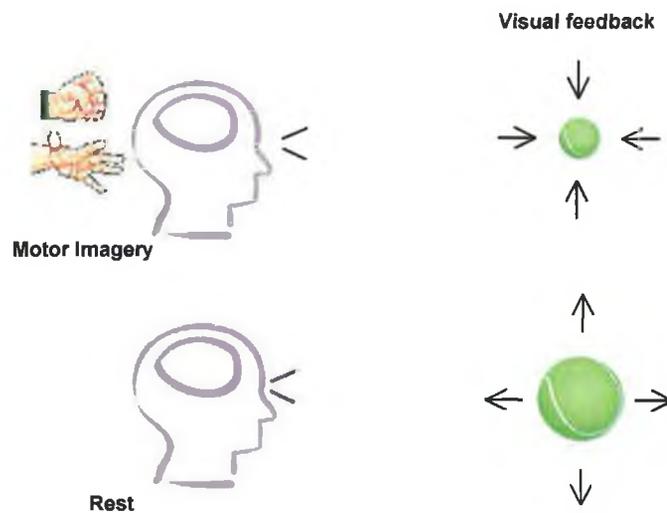
Figure 7.1 Visual feedback is given to the user. Imagination of fist clenching causes the virtual ball to contract, cessation of imagery causes the virtual ball to expand and return to its original size.

7.2.1.2 Methods

The optical response was measured using a single channel on the surface of the scalp above the motor cortex. The source and detector were placed at C3:1.5(-$\pi/2$) and C3:1.5($\pi/2$) respectively. The subject was asked to clench a ball or to visualise doing so using the hand contralateral to the side of optode placement. The average oxy-haemoglobin concentration level is calculated every second and a 20 second window of data is analysed. An event is noted if the average oxy-haemoglobin concentration is greater than a reference level, shown in figure 7.2. The reference is set to the maximum level occurring during the first 10s of the

window. This is done to take into account spontaneous low frequency oscillations that are inherent in the signal, as discussed in Chapter 6. Identification of an event is registered by the BCI and continuous visual feedback updated every second is presented to the user, as shown in figure 7.3. As the user imagines clenching a ball, a "virtual ball" on the screen shrinks and expands in response to changing haemoglobin levels. The purpose of using such feedback is to reinforce the mental imagery being used.
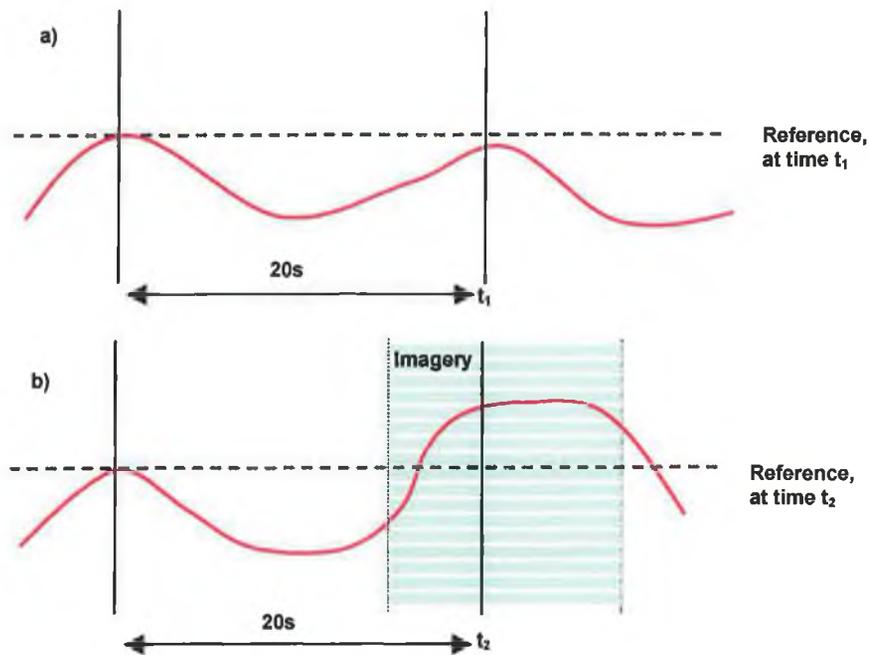
Figure 7.2 a) HbO level is less than reference at time t_1, therefore no event detected by BCI, b) HbO level is greater than reference at time t_2, therefore event noted by the BCI.

7.2.1.3   Results

In order to adequately assess the system performance a rigorous analysis was carried out off-line. The performance is assessed here based on results of motor imagery investigations presented in Chapter 6. The algorithm has been applied to the data as it performs in the real-time system described above. Figure 7.4 shows the HbO signal change with respect to a dynamic reference. The reference is updated every second, derived from the HbO level in the first 10s of the

previous 20s window of data. In order for an event to be acknowledged the HbO level must rise above the threshold, indicated by the dashed line.
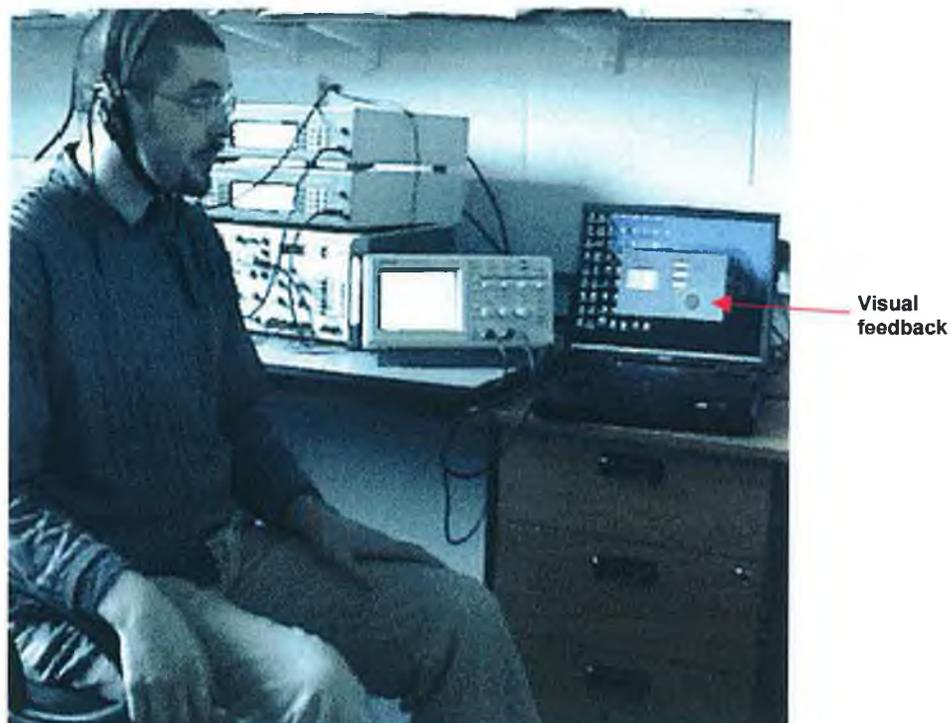
Figure 7.3 Optical BCI experimental set-up, visual feedback is presented on the computer monitor, by means of a green circle that shrinks and expands.

In assessing performance of asynchronous BCIs, events that have been correctly categorized, termed true positives (TP) should be noted but the number of false positives (FP) that occur during resting periods must also take into account. An evaluation of true and false positives is illustrated in figure 7.4. There are eight periods when the subject was instructed to perform imagery tasks, indicated by the shaded regions. Six of these are categorised as events by the algorithm and there is one false positive that occurs during a rest period (t=380s).

The accuracy can be expressed in terms of the difference between the ratio of true positives to events (E) and false positives to tests (events and false positives), known as the TF difference (Townsend *et al.* 2004).

$$TF\% = \left(\frac{TP}{E} - \frac{FP}{E+FP} \right) \cdot 100 \qquad 7.1$$

146

Ideally the TF difference would be 100%, if all events were classified correctly and if no false positives occurred. If the detected signal was random each parameter would be 50% and the TF difference 0%. The TF difference for the data shown in figure 7.4 is 64%.
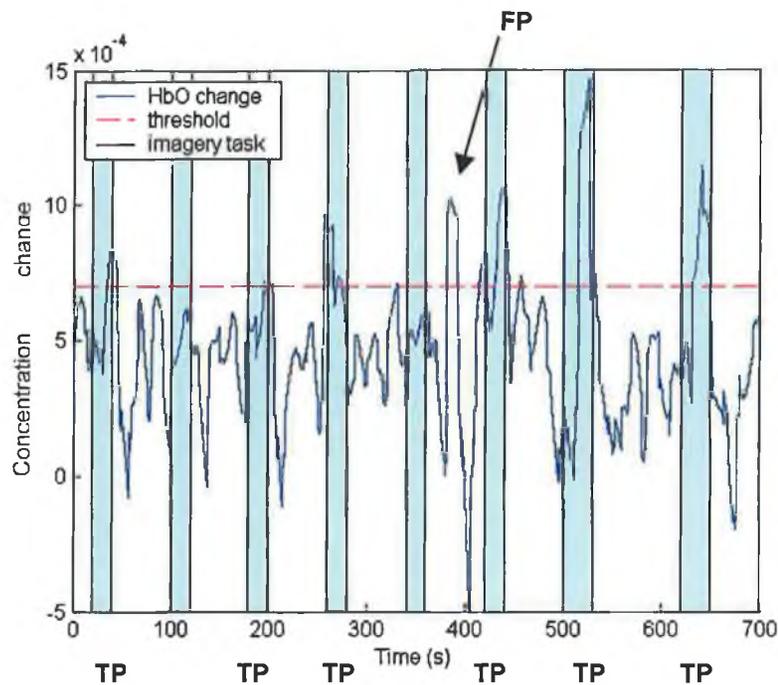
Figure 7.4 HbO signal change with respect its reference, used to evaluate true and false positives (TPs and FPs).

7.2.1.4   Discussion

On account of the 20s window required for this basic translation algorithm, the system has an information transfer rate of 2-3bits/min. Single channel systems with improved signal processing have potential data rates of up to 6bits/min, in order to allow approximately 5s for the response to register and 5s for the signal to return to a baseline state.

While the reference level is updated based on the signal level during the preceding rest period the threshold may also need to be adaptable. It could be defined in terms of the magnitude of a cardiac pulse cycle, i.e. monitor the peak-

to-peak amplitude of the cardiac pulse and set the threshold to be a multiple of this value. If the threshold is too low the number of false positives increases and in real-time functioning this can cause confusion and frustration for the user. To improve accuracy a synchronous approach could be taken, which would give an accuracy of 75% to the data presented in figure 7.4.

7.2.2 Study 2 – Synchronous dual-channel OBCI

7.2.2.1 Introduction

The purpose of this pilot study is to examine the possibility of employing two channels that the users can control. Detecting the optical response on the left and right motor cortex may provide two channels that the user can control using left and right hand movement imagery. This would increase the speed of the system, by increasing the number of bits per baud. Rather than giving continuous feedback a synchronous mode of operation is applied to give a better accuracy. This reduces the likelihood of false positives occurring, based on the analysis carried out in Study 1.

7.2.2.2 Methods

Following an initial rest period, the user is presented with a sequence of commands, to perform left or right hand motor imagery. An arrow appears for 15s indicating that the user should visualise left or right hand movements. In the last 5s of this period, i.e. 10s after its onset, a moving average is calculated each second and feedback is given to the user during these 5s. A rest period of 15s is then given before the next command, allowing the signals to return to baseline. The average signals during the rest period are calculated in the 10s preceding the next command. Thresholds are set for the left and right cortex. During each stimulus period the response recorded at the cortex contralateral to the given command was analysed for event classification, e.g. if the HbO signal change

148

detected at the right motor cortex during left hand imagery exceeds the threshold during the feedback period an event is noted, regardless of the response at the left motor cortex.
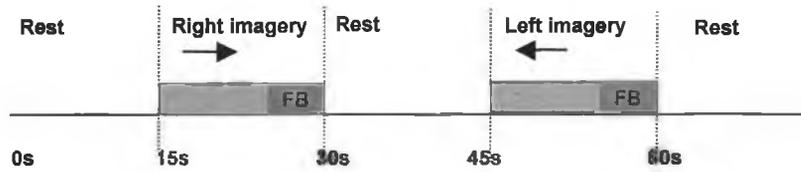
Figure 7.5 Sequence of events in the BCI application. Users are instructed to perform left or right hand imagery for a period of 15s, with rest periods of the same duration in-between tasks. User feedback is given in the last 5s of imagery task epochs.

7.2.2.3   *Results*

Each trial relies on the response from either the left or right cortex, therefore the performance is evaluated for each of these channels individually. The results are presented for a right-handed subject in table 7.1 and 7.2. The reported HbO changes are the results of 22 trials (11 left hand imagery, 11 right hand imagery). A correct event classification occurs if the HbO level exceeds a threshold. Classification of events involving right hand imagery proved successful in this study, with an accuracy of 73%. Left hand imagery tasks were less successful, with 36% accuracy.

Left hand Imagery		
Trial	Right cortex HbO change(threshold =0.0001)	Event classification
1	-0.0007	✗
2	0.0015	✓
3	-0.0001	✗
4	-0.0009	✗
5	-0.0002	✗
6	0.0015	✓
7	-0.001	✗
8	-0.0001	✗
9	-0.0012	✗
10	0.0007	✓
11	0.0025	✓
Accuracy		36%

Table 7.1 HbO changes measured at the right motor cortex during left hand imagery, ✓ signifies correct classification of an event, while ✗ means incorrect.

Right hand imagery		
Trial	Left cortex HbO change(threshold =0.0001)	Event classification
1	0.0001	✓
2	-0.0004	✗
3	0.0015	✓
4	-0.0007	✗
5	0.0005	✓
6	0.0001	✓
7	0.0001	✓
8	0.0006	✓
9	0.0014	✓
10	-0.001	✗
11	0.0005	✓
Accuracy		73%

Table 7.2 HbO changes measured at the right motor cortex during right hand imagery. ✓ signifies correct classification of an event, while ✗ means incorrect.

7.2.2.4   Discussion

The greater success of right hand imagery tasks may be due to the fact that the subject was right-handed. Imagery involving the dominant hand is generally easier to perform and generates a greater response (Dassonville *et al.* 1997). Another reason may be that the response over the non-dominant hemisphere is more localised needed more precise placement.   The use of fMRI before implementing a dual-channel BCI would greatly help locate regions of activation. This would particularly help identify lateral responses that would provide two differential signals. A problem with this dual-channel application is the existence of a bilateral response during both left and right hand movements (Porro *et al.* 2000). For differentiation of the two channels, the optodes must be placed in regions having a lateral response. In this way it would be possible to determine if the left hand, right hand, both or neither hand was involved in imagery, giving the user four options to communicate with at a time. Without fMRI imaging to yield such information, multiple NIR sources and detectors could be used to encompass a larger region of the cortex, providing a better insight into the functional activation topography.

7.2.3 Study 3 – 2x2 choice matrix

7.2.3.1   Introduction

With the absence of prior fMRI studies or a multiple imaging system the most practical solution is to use a single channel based on the most prominent response that can be measured. The simplest BCI requires a binary (yes/no) signal, which is achievable using such a single-channel system. The optical response that is detected at the left or right motor cortex, due to imagined hand movement, may be used to provide this binary channel. Alternatively an optical response measured at any other location that can be controlled at will, may also be used. This system was tested using cognitive tasks as a mental task strategy.

The main purpose of this application design was to illustrate how multiple choices could be handled using a single channel system e.g. this approach could be employed in a spelling application.

7.2.3.2 Methods

The binary signal can be used to make a selection from a number of presented items. A 2x2 matrix is presented to the user giving them the choice of four different colours, as shown in figure 7.6. The screenshot shown in figure 7.6 was projected onto a screen 2m in front of the subject. Each row and column is highlighted in turn for 15s, with rest periods of the same time frame in-between. The user must perform imagery tasks when their desired target is highlighted. This application was tested using mental calculation tasks. The experimental set-up is described in section 6.4.1. The HbO signal is evaluated during the rest period and during the last 10s of the stimulus (row/column being highlighted). The row is selected depending on which row caused a larger HbO signal change when that row was highlighted, and similarly for column selection. This avoids having to define thresholds for each user and trial, making it more flexible to implement.
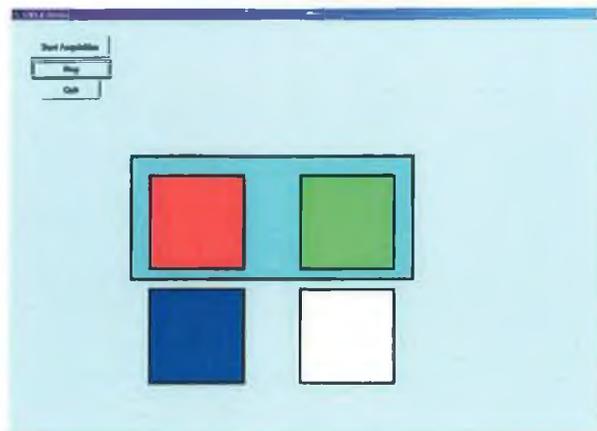
Figure 7.6 A 2x2 matrix of targets is presented to the user, with row 1 highlighted for selection.

7.2.3.3   Results

The optical response recorded during 6 target selection tasks is given in table 7.3, showing the HbO signal change that occurred when each row (R1, R2) or column (C1,C2) was highlighted compared to a baseline condition. The row and column with the larger signal change were selected, leading to a single target being selected. (R1,C1) corresponds to red, (R1,C2) green, (R2,C1) blue and (R2,C2) white as shown in figure 7.6.

Target	R1	R2	R1/R2	Row error	C1	C2	C1/C2	Column error	Selected Target	Target error
(R1,C1)	4.79E-04	3.00E-04	R1		2.87E-04	1.45E-04	C1		(R1,C1)	
(R1,C2)	2.12E-04	1.55E-04	R1		-4.01E-04	1.34E-04	C2		(R1,C2)	
(R2,C1)	2.65E-05	3.28E-04	R2		1.69E-04	-1.75E-04	C1		(R2,C1)	
(R2,C2)	1.06E-04	-4.13E-04	R1	X	-0.0011	7.09E-05	C2		(R1,C2)	X
(R2,C2)	-7.54E-04	2.55E-04	R2		5.07E-04	-1.42E-04	C1	X	(R2,C1)	X
(R2,C2)	4.31E-05	2.53E-04	R2		-2.93E-04	1.07E-04	C2		(R2,C2)	
Accuracy										67%

Table 7.3 HbO changes during target selection. Row 1 (R1) or Row 2 (R2) is selected depending on which one initiates a higher HbO change when highlighted, similarly for columns 1 and 2 (C1,C2). Artifacts were identified during off-line analysis and are noted in grey.

7.2.3.4   Discussion

Two decisions must be made for each target selection. Therefore although there are 2 incorrect decisions out of 12, i.e. an accuracy of 83%, the system appears to have an accuracy of 67% considering 4 out of 6 targets are selected correctly. Having just two targets for selection would make evaluation of the BCI performance more clear-cut. This would also increase the frequency of user feedback twofold – choosing one of two targets takes an interval of one minute, whereas choosing a row then column takes twice as long. Giving more frequent feedback would offer more prolific human-computer interaction, and showing a true accuracy rating may reduce feelings of frustration that can result from errors (Forrest *et al.* 2001).

153

A problem with recording cognitive responses on the frontal lobes is the effect of stress on cerebral blood flow in this location. The detected light intensity, measured at the forehead, has been shown to decrease during stressful situations, resulting from an increase in blood pressure and cerebral blood flow (Coyle *et al.* 2003c). Anxiety and frustration have a considerable effect on the optical response and hence BCI performance.

7.3   OBCI – Mindswitch

7.3.1 Introduction

This OBCI application is similar to Study 3, but a simpler array is presented. Two choices (a switch) are given to the user – a "Mindswitch". As with the approach taken in Study 3, Mindswitch compares two responses and chooses the more pronounced one. Although this takes more time than using thresholding, it is more flexible to implement, as a threshold need not be established for every user for every experimental run. 3 subjects (2 right-handed and one left-handed) participated in the evaluation of Mindswitch, using motor imagery as the mental strategy for controlling the application. The OBCI performance was evaluated over a number of days for one of the subjects.

7.3.2 Methods

Subjects resided comfortably in a supine position throughout experimental trials and optodes were placed above the motor cortex using the mechanical mounting system described in Section 5.4.3. Two target squares are presented to the user for selection – a red square and a white square. The sequence of procedures

involved in choosing a target is shown in figure 7.7. Selection of a target takes a total duration of 1 minute.

a) The first 15s is a resting period, establishing a baseline condition. In the last 5s of this period a command is given to the user by means of a small coloured square indicating which target must be selected.

b) In the next 15s the upper target, the red square, is highlighted. If the user wishes to select the highlighted target he/she must perform imagery tasks during this time.

c) The following 15s is another rest state allowing the HbO signal to return to baseline if necessary.

d) During the next 15s the lower target is highlighted, and again the user may perform imagery if the highlighted target is desired.

e) Rest follows, with the decision being presented to the user and the score updated (number of correct trials/total number of trials). 10 trials were carried out in each experimental run, allowing the subjects some respite in-between.

7.3.3 Results

The average signal changes for each trial is given in Appendix B, where a trial involves the sequence of events, (a) to (e), outlined in figure 7.7. Subject 1 participated in 60 trials over three days, with accuracy ranging from 65%-85%. Subject 2 participated in 10 trials, with accuracy of 70% and subject 3 participated in 20 trials at 50% accuracy. The data was analysed further offline and removal of baseline drifts in the signal improved the performance of nearly all experimental runs. Using offline analysis subject 1 achieved an accuracy of 70%-85%, subject 2 90%, and subject 3 80%. This demonstrates the importance
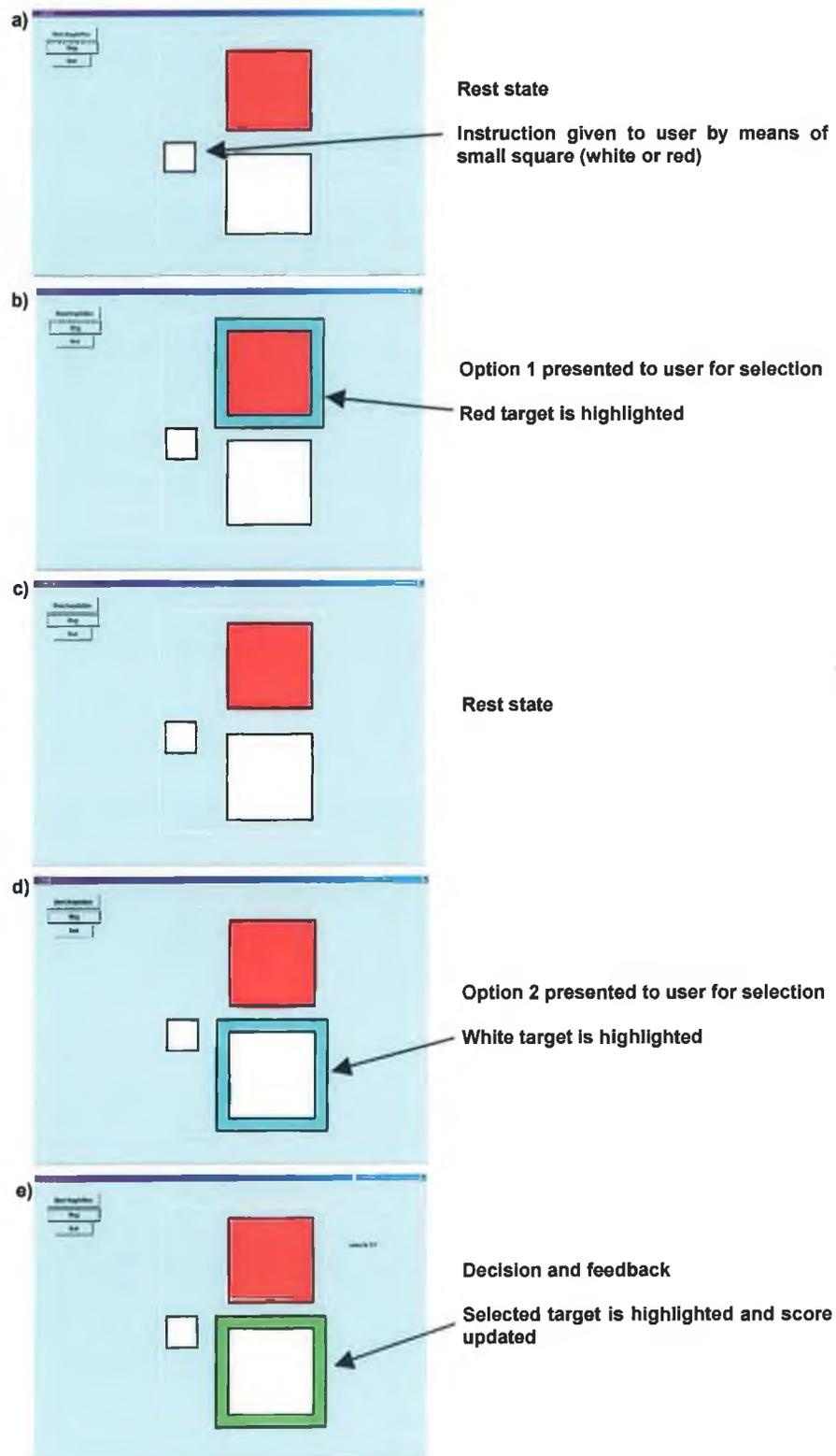
Figure 7.7 Sequence of operations in Mindswitch. (a) rest, (b) option 1 highlighted for selection, (c) rest, (d) option 2 highlighted for selection, (e) feedback showing target selection.

156

of signal processing methods to improve signal to noise ratios and improve classification accuracies.

7.3.4 Discussion

Subjects were able to achieve reasonable accuracy levels with minimal training, which is a critical factor for BCI use. The mental tasks required to operate the OBCI are straightforward and do not necessitate the learning of a completely new though process. Subjects 1 and 2 participated in motor imagery experiments, while Subject 3 received no prior training. Subjects reported a need to develop their own strategy for motor imagery including motor functions beyond hand movement, e.g. pedalling a bike with one leg, kicking footballs and sifting one's fingers though a bucket of grain. The use of continuous feedback as in the first pilot study may be useful for helping users to cultivate such strategies, using more rapid feedback. Mindswitch takes one minute to decide the users selection, and feedback is given upon each of these. The benefit of increasing feedback, e.g. during stimulus epochs, needs to be examined further. Feedback provided by the end result, as given by Mindswitch, has proved sufficient in EEG BCI systems. During system operations continual feedback may help maintain attention levels, but may also distract users from the essential aspects of their designated task (McFarland *et al.* 1998; Pfurstscheller 2004).

The speed of operation is 1bit/min, which is slower than some of the pilot studies that use thresholding. Mindswitch implements a comparison approach. The reason for this is that this which has resulted in a higher accuracy rate. Thresholding or feature classification methods could be used to achieve faster information transfer rates and for asynchronous mode implementation. In order to do this a more sophisticated signal processing needs to be implemented to prevent the occurrence of false positives due to physiological noise effects as discussed in Section 6.5. While physiological noise effects and motion artefacts obviously create errors, the occurrence of subject error must also be taken into consideration. Subjects reported that a lack of concentration or momentary confusion during the tasks led to erroneous target selections. Subjects also

reported a need to focus on thoughts that did not involve any movement during periods where an undesired target was being highlighted, however this can prove difficult as movement can be associated with so many concepts (de Lafuente and Romo 2004). To help users one possibility may be to integrate some graphical representations to emphasise or impede the motor imagery process.

7.4 Summary

The haemodynamic response resulting from mental imagery processes can be used as a control channel for a computer application. As this is the first time that NIRS signals have been used for this purpose, a number of pilot studies were carried out to discern a suitable strategy. Asynchronous and synchronous modes of operation were investigated. Synchronous mode was found to give a better accuracy. Both dual channel and single channel systems were investigated. This area needs further investigation due to the existence of bilateral responses in the cerebral hemispheres. Therefore the final application for assessing the performance of an optical BCI, "Mindswitch", in synchronous mode, uses a single channel placed on a region giving a pronounced optical response. To maximise performance optode placement is critical, and synchronizing placement and mental processes must be carefully established for each user. The system has the advantage that it does not rely on thresholding and therefore is quite flexible, however as it must compare two responses for each decision this reduces the speed of the system. Further development is needed to improve speed and accuracy. The great advantage of all the developed applications is that training is minimal, as the mental tasks involve natural and unambiguous processes.

Chapter 8

Conclusions

"One never notices what has been done, one can only see what remains to be done."

(Marie Curie, in a letter to her brother)

This chapter reviews the most important issues and contributions that are presented in this thesis. Some future directions of the presented work are also discussed.

The objectives of this thesis were to:

> ➤ Design a NIRS measurement system suitable for investigating functional brain activity.

> ➤ Investigate the nature of the haemodynamic response resulting from neural activation, with a view to harnessing such a response for BCI control. In particular to investigate if functional activation due to motor imagery tasks could be detected using NIRS techniques.

> ➤ Develop an application to analyse the haemodynamic response in real-time allowing the user to control the output though mental process alone.

8.1 Summary of achievements

The main achievements can be summarised as follows:

- ➢ Design and construction of a NIRS measurement system to detect neural activity due to various cognitive tasks
- ➢ Ascertaining the brain response during motor imagery tasks using optical techniques, consistent with investigations involving other functional imaging methods.
- ➢ Application of the measured signals to provide user feedback and development of a real-time BCI application which users can control with minimal training, achieving accuracy rates of up to 90%.
- ➢ Demonstration of the suitability of NIRS measurements for BCI development.

8.2 Future directions

Having demonstrated the feasibility of using NIRS as a signal acquisition tool for BCI systems, there remains much scope for development in a new field of optical BCI research. This section presents some suggested tactics that may help to enhance the quality of the detected signal, increase the speed of operation and improve accuracy in order to achieve a better overall system performance.

8.2.1 Localisation of brain function

Limitations of using single site measurements were found to be a major drawback in this study in locating regions of activation. The placement of optodes is critical to ensure correlation between mental processes and the detected signal. Moving the optodes by 0.5cm could be the difference between detecting a discernible or subdued response during brain activation. The

conventional 10-20 EEG measures serve as a guide for the placement of optodes, however the craniocerebral topography varies between individuals (Myslobodsky *et al.* 1990). To overcome this, fMRI studies could be carried out in advance to give accurate anatomical information regarding functional activation. Alternatively multiple sources and detectors could be employed to interrogate a larger region of the brain in order to locate a site of maximum response.

8.2.2 *Improving Information Transfer Rates*

The ultimate potential of optical brain computer interfaces will be dependent on increasing their throughput and accuracy to rates useful enough for their adaptation by their intended users. This may be done by integrating more control channels, by seeking an optical response correlated to neuronal activity, or the addition of complementary functional brain imaging modality.

8.2.2.1 *Multiple channels*

Further investigation is needed into the variety of mental tasks that can be used as control channels. An imaging system would prove more suitable than the current instrumentation in locating areas within the motor cortex that have lateral responses to left or right movements. A recent fMRI study has used four different tasks to provide 2-D cursor control (Yoo *et al.* 2004). The mental tasks were left and right hand movement imagery, mental calculation and mental speech generation. Such mental processes are detectable using NIRS techniques (Hoshi and Tamura 1993; Coyle *et al.* 2003a; Coyle *et al.* 2003b; Herrmann *et al.* 2003). This study has focused on motor imagery tasks involving the dominant hand as a single channel system. The nature of the haemodynamic response limits the information transfer rate as vascular changes occur over a number of seconds. Therefore more channels are needed to improve the communication rate of the BCI.

8.2.2.2   EROS

To achieve optimum speed, acquiring the fast optical signal and attaining an evoked optical response will be essential. A recent study revealed an EROS, showing a response of the order of milliseconds, correlating to the frequency of hand movement (Wolf *et al.*). Currently thousands of averages are required for its successful acquisition and the signal is highly localised. For EROS to be practical a robust and reliable method to measure it must first be accomplished.

8.2.2.3   *Multi-modal operation*

Another possibility to improve performance is to develop a hybrid system by integrating other brain monitoring modalities, such as EEG, with the optimal deployment of NIR techniques. Optical signals are ideal for multi-modal studies, as the light signal does not interfere with electrical or magnetic fields.

8.2.3 *Signal Integrity*

This study has focussed on the use of HbO concentration change, as the HbO response has appeared to be a more consistent measure than Hb changes throughout experiments. This may be because Hb concentration changes are generally of smaller magnitude, and more susceptible to cross-talk effects that can occur between these two chromophores. Cross-talk is mainly due to assumptions made in the modified Beer-Lambert law algorithm, as absorption changes are assumed to be global within the sampling region. While this assumption may hold for tissue such as muscle it does not hold for measurements in the adult head (Strangman *et al.* 2003). Brain activation is focal to a small region of the sampling volume, which leads to an underestimation of concentration changes known as a partial volume effect. Errors in the analysis of each wavelength due to the partial volume effect can lead to cross-talk between the chromophores. In order to overcome this problem the wavelengths used

should be carefully chosen, e.g. 760nm paired with 830nm is subject to less cross-talk than pairing 780nm with 830nm. A comprehensive study of optimising wavelength combinations is given in (Strangman *et al.* 2003). Another solution is to position probes as close as possible to the location of absorption changes. This could be done with the use of fMRI or selecting a recording location of maximum signal contrast in the case of a multi-optode imaging array.

Further investigations into reducing cross-talk and optimising signal quality should improve the integrity of the Hb signal change, which could then be used as an additional measure in event classification. Another avenue to investigate is to monitor cytochrome-c-oxidase concentration changes. Integrating a third wavelength of light into the system and modifying the algorithm accordingly would allow measurement of this respiratory enzyme. Cytochrome-c-oxidase has been reported as a more sensitive indicator of brain oxygen insufficiency than changes in haemoglobin oxygenation (Cooper *et al.* 1998) and could prove a useful marker of neural activity in BCI studies.

Another factor affecting the signal integrity is the effect of superficial layers on the detected signal. These layers of tissue are assumed to have a constant attenuation effect on the light signal however there is a slight effect due to extracerebral signal components (Kohl-Bareis *et al.* 2002). This can be minimised by using multiple source-detector arrangements with different inter-optode distances, which would result in different penetration depths, thereby isolating the effect of superficial layers of tissue.

8.2.4 *Signal Processing and Event classification*

Signal processing in brain computer interfaces involves maximising the signal-to-noise ratio (pre-processing) and characterisation of event-related brain activity (feature extraction).

163

Improved pre-processing is needed in the real-time system to remove the effects of baseline drift in the detected signal and also to reject artifacts. Offline analysis taking these effects into account significantly improved the accuracy of the system, discussed in Chapter 7. Another factor is the effect of physiological noise, in particular the Mayer wave. Adaptive filtering techniques could be employed to reduce its presence.

Event classification of single trials, rather than comparing the response to two different targets, would double the bit rate of the Mindswitch application. As the NIRS signal etiology is more similar to fMRI signals some of the approaches taken to identifying functional activation in fMRI signals could be implemented, e.g. correlation analysis with modelled haemodynamic response functions (Gembris *et al.* 2000).

8.2.5 *Clinical Investigations*

Future validation of the system must involve trials with paralysed subjects in order to investigate attributes of motor cortical function. Previous studies have shown motor cortex activation in severely paralysed subjects resulting from motor imagery tasks (Mao *et al.* 1998; Shoman *et al.* 2001). Clinical trials would be needed to examine the effects of fatigue and administered drugs on functional activation of the cerebral cortex and associated haemodynamic changes. BCIs utilizing the electrical signals from the brain have shown reduced performance due to fatigue, toxicity from infections, pain and analgesics (Kennedy *et al.* 2000). These studies in different subject populations under different experimental conditions are vital if an optical BCI is to be of use to its target users.

8.3   Concluding Remarks

This thesis demonstrates the suitability of an optical interrogation modality to provide a control input signal to a BCI. The great advantages of optical systems include safety, accessibility and non-invasiveness. The cognitive processes detectable with NIRS allow straightforward mental tasks to be used in controlling the optical BCI. Controlling the optical BCI involves natural thought processes, which minimizes user training. It is hoped that this work will foster further investigations into the application of NIRS signals for a new era of BCI development.

"Le scaphandre devient moins oppressant, et l'esprit peut vagabonder comme un papillon. Il y a tant a faire. On peut s'envoler dans l'espace ou dans le temps, partir pour la Terre de Feu ou la cour du roi Midas."

("My cocoon becomes less oppressive, and my mind takes flight like a butterfly. There is so much to do. You can wander off in space or in time, set out for Tierra del Fuego or for King Midas's court.")

(Jean-Dominique Bauby, Le Scaphandre et le Papillon)

Appendix A

Experiment 2 – Cerebral Oxygenation changes, using dual site measurements.

Subject 1

Mental Task	Stimulus duration (s)	# Trials	# Rejected trials
Left imagery	20	5	0
Right imagery	20	5	0

Table A.1 Details of trials for Subject 1.

	Left motor cortex		Right motor cortex	
Left imagery	HbO change	Hb change	HbO change	Hb change
trial 1	0.0025	-0.0002	0.0065	0.0002
trial 3	0.0176	-0.0044	0.0215	-0.0098
trial 5	0.0230	-0.0066	0.0195	-0.0121
trial 7	0.0199	-0.0056	0.0212	-0.0113
trial 9	0.0036	-0.0002	0.0060	-0.0014
mean response	0.0133	-0.0034	0.0149	-0.0069
Signrank	0.0625	0.0625	0.0625	0.1250

Table A.2 Subject 1 - HbO/Hb changes during right imagery tasks.

167

	Left motor cortex		Right motor cortex	
Right imagery	HbO change	Hb change	HbO change	Hb change
trial 2	-0.0015	0.0003	-0.0019	0.0006
trial 4	0.0129	-0.0032	0.0146	-0.0056
trial 6	0.0195	-0.0063	0.0074	-0.0053
trial 8	-0.0022	0.0006	0.0010	0.0004
trial 10	0.0040	-0.0008	-0.0009	0.0001
mean response	0.0065	-0.0019	0.0040	-0.0020
Signrank	0.3125	0.3125	0.4375	0.8125

Table A.3 Subject 1 - HbO/Hb changes during right imagery tasks.

Subject 2

Mental Task	Stimulus duration (s)	# Trials	# Rejected trials
Left imagery	20	5	0
	10	5	0
	5	5	0
Right imagery	20	5	0
	10	5	0
	5	5	0

Table A.4 Details of trials for Subject 2.

Left imagery	Left motor cortex		Right motor cortex	
	HbO change	Hb change	HbO change	Hb change
trial 1 (20s)	0.0022	-0.00036	0.0003	0.00024
trial 3 (20s)	0.0009	-0.00084	0.0011	-0.00031
trial 5 (20s)	0.0026	-0.00044	0.0018	-0.00020
trial 7 (20s)	0.0007	-0.00040	0.0012	0.00000
trial 9 (20s)	0.0017	-0.00032	0.0020	-0.00003
trial 11 (10s)	0.0022	-0.00058	0.0010	-0.00004
trial 13 (10s)	0.0018	-0.00045	0.0020	-0.00028
trial 15 (10s)	0.0004	-0.00023	-0.0006	0.00029
trial 17 (10s)	0.0012	-0.00037	0.0008	-0.00003
trial 19 (10s)	-0.0004	0.00018	-0.0032	0.00062
trial 21 (5s)	0.0020	-0.00058	0.0023	-0.00030
trial 23 (5s)	-0.0001	0.00004	0.0002	-0.00005
trial 25 (5s)	0.0017	-0.00042	0.0018	-0.00005
trial 27 (5s)	0.0002	-0.00003	0.0002	-0.00005
trial 29 (5s)	0.0002	-0.00018	0.0005	0.00004
mean	0.0012	-0.00033	0.0008	-0.00001
Signrank	**0.0006**	**0.0006**	**0.0215**	**0.35750**

Table A.5 Subject 2 - HbO/Hb changes during left imagery tasks.

Right imagery	Left motor cortex		Right motor cortex	
	HbO change	Hb change	HbO change	Hb change
trial 2 (20s)	0.0018	-0.00017	0.0024	-0.00061
trial 4 (20s)	-0.0001	0.00059	-0.0020	0.00066
trial 6 (20s)	0.0016	-0.00065	0.0013	-0.00038
trial 8 (20s)	-0.0010	-0.00012	-0.0023	0.00043
trial 10 (20s)	0.0006	0.00018	-0.0002	-0.00018
trial 12 (10s)	0.0008	-0.00024	0.0011	-0.00034
trial 14 (10s)	0.0022	-0.00058	0.0017	-0.00050
trial 16 (10s)	0.0001	0.00002	-0.0007	0.00015
trial 18 (10s)	0.0004	0.00002	0.0015	-0.00008
trial 20 (10s)	-0.0006	0.00023	-0.0001	0.00001
trial 22 (5s)	-0.0019	0.00055	-0.0010	0.00028
trial 24 (5s)	0.0010	-0.00033	-0.0007	0.00027
trial 26 (5s)	0.0009	-0.00014	0.0016	-0.00022
trial 28 (5s)	0.0010	-0.00030	0.0007	-0.00018
trial 30 (5s)	0.0001	-0.00010	-0.0014	0.00036
mean	0.0005	-0.00007	0.0001	-0.00002
Signrank	**0.1070**	**0.38940**	**0.7197**	**0.84690**

Table A.6 Subject 2 - HbO/Hb changes during right imagery tasks.

Subject 3

Mental Task	Stimulus duration (s)	# Trials	# Rejected trials
Left imagery	15	15	3
Right imagery	15	15	3

Table A.7 Details of trials for Subject 3.

Left imagery	Left motor cortex		Right motor cortex	
	HbO change	Hb change	HbO change	Hb change
trial 1	-0.0005	0.0313	-0.0007	0.0694
trial 3	0.0014	-0.1821	0.0015	-0.1206
trial 5	-0.0001	-0.0179	-0.0001	-0.0313
trial 7	-0.0005	0.0392	-0.0009	0.2047
trial 9	-0.0001	-0.0341	-0.0002	0.0101
trial 11	0.0020	-0.2112	0.0015	-0.2242
trial 13	-0.0005	0.0428	-0.0010	0.2092
trial 15	0.0002	-0.0494	-0.0001	0.1638
trial 17	-0.0016	0.1669	-0.0012	-0.0420
trial 19	0.0002	-0.0239	0.0001	0.1083
trial 21	0.0011	-0.1176	0.0007	-0.0277
trial 23	0.0018	-0.1886	0.0025	-0.1500
mean	0.0003	-0.0454	0.0002	0.0141
Signrank	0.57	0.23	0.84	0.85

Table A.8 Subject 3 - HbO/Hb changes during left imagery tasks.

Right imagery	Left motor cortex		Right motor cortex	
	HbO change	Hb change	HbO change	Hb change
trial 2	0.0001	-0.0160	0.0003	0.0109
trial 4	-0.0004	0.0453	-0.0010	0.3491
trial 6	0.0015	-0.1544	0.0019	-0.0525
trial 8	-0.0007	0.0271	-0.0007	0.0927
trial 10	0.0005	-0.0445	0.0006	0.0634
trial 12	0.0001	-0.0128	-0.0001	0.0617
trial 14	0.0001	-0.0303	0.0001	-0.0728
trial 16	0.0006	-0.0872	0.0008	0.0236
trial 18	0.0001	0.0020	-0.0002	0.1781
trial 20	0.0014	-0.1210	0.0025	-0.1435
trial 22	-0.0010	0.1049	-0.0015	0.2559
trial 24	0.0005	-0.0171	0.0001	0.0559
mean	0.0002	-0.0253	0.0002	0.0685
Signrank	**0.26**	**0.27**	**0.62**	**0.26**

Table A.9 Subject 3 - HbO/Hb changes during right imagery tasks.

Subject 4

Mental Task	Stimulus duration (s)	# Trials	# Rejected trials
Left imagery	20	5	2
	10	5	1
	5	5	2
Right imagery	20	5	0
	10	5	5
	5	5	3

Table A.10 Details of trials for Subject 4.

171

	Left motor cortex		Right motor cortex	
Left imagery	HbO change	Hb change	HbO change	Hb change
trial 1 (20s)	-0.0016	0.0002	-0.0069	0.0011
trial 3 (20s)	0.0015	0.0001	-0.0014	0.0003
trial 5 (20s)	0.0038	0.0013	-0.004	0.0008
trial 7 (10s)	-0.0086	-0.0026	0.0075	-0.0019
trial 9 (10s)	0.007	0.0007	-0.0012	0.0004
trial 11 (10s)	0.0007	-0.001	-0.0047	0.0007
trial 13 (10s)	-0.0014	-0.0002	0.0022	-0.0004
trial 15 (5s)	0.0054	0.0007	0.003	-0.0003
trial 17 (5s)	0.0031	0.0001	0.0029	-0.0002
trial 19 (5s)	-0.0098	0.0036	0.0032	-0.0002
mean	1E-05	0.00029	6E-05	0.00003
Signrank	**0.8457**	**0.4316**	**1**	**0.625**

Table A.11 Subject 4 - HbO/Hb changes during left imagery tasks.

	Left motor cortex		Right motor cortex	
Right imagery	HbO change	Hb change	HbO change	Hb change
trial 2 (20s)	0.0001	0.0002	0.0014	0
trial 4 (20s)	-0.0025	0.0003	-0.0055	0.0008
trial 6 (20s)	-0.004	-0.0008	0.0026	-0.0006
trial 8 (20s)	-0.0017	0.0006	-0.0047	0.0003
trial 10 (20s)	0.0145	0.002	-0.0058	0.0011
trial 16 (5s)	-0.0038	-0.0005	0.0017	-0.0003
trial 18 (5s)	0.0115	0.0024	-0.0031	0.0017
mean	0.0020	0.0006	-0.0019143	0.0004
signtest	1	0.4531	1	0.6875
Signrank	**1**	**0.375**	**0.2188**	**0.2188**

Table A.12 Subject 4 - HbO/Hb changes during right imagery tasks.

Appendix B

"Mind-switch" Performance

Subject 1

Day 1, Experimental Run 1

Command	HbO change - online				HbO change – offline			
	Option 1 RED	Option 2 WHITE	Online selection	Error	Option 1 RED	Option 2 WHITE	Offline selection	Error
R	0.6138	-0.9261	R		0.4185	-0.5294	R	
R	0.3444	-0.3612	R		0.7673	-0.3553	R	
W	0.3678	0.486	W		0.163	0.4036	W	
W	-0.5418	-0.0081	W		-0.5075	0.0275	W	
R	-0.2517	0.1509	W	X	-0.1957	0.1364	W	X
R	0.5901	-0.0697	R		0.4651	-0.1443	R	
W	-0.6976	-0.3049	W		-0.5568	0.1083	W	
W	-0.4228	-0.0832	W		0.0644	0.186	W	
R	-0.1702	-0.4734	R		-0.0251	-0.3195	R	
W	-0.2764	-0.0995	W		-0.2122	0.2185	W	
Accuracy				90%				90%

Table B.1 Subject 1, Experiment 1 - HbO changes using on-line and off-line analysis, during target selection. Option causing the larger HbO signal change is selected. X signifies incorrect classification.

Day 1, Experimental Run 2

	HbO change – online				HbO change - offline			
Command	Option 1 RED	Option 2 WHITE	Online selection	Error	Option 1 – RED	Option 2 - WHITE	Offline selection	Error
W	-0.182	-0.3208	R	X	0.185	-0.5453	R	X
W	-0.6544	-0.3348	W		-0.3283	0.0946	W	
W	-0.2866	0.8886	W		-0.227	0.5094	W	
W	-0.742	0.312	W		-0.3062	0.1274	W	
R	-0.1683	-0.1951	R		0.0516	-0.2105	R	
W	-0.5625	-0.3426	W		-0.3924	-0.2363	W	
W	-0.0798	-0.3139	R		-0.3693	-0.0763	W	
R	0.3885	-0.4394	R		0.158	-0.8211	R	
W	-0.9855	-0.1904	W		-0.4273	-0.0186	W	
W	-0.0248	-0.9926	R	X	-0.4594	-0.5128	R	X
Accuracy				80%				80%

Table B.2 Subject 1, Experiment 2 - HbO changes using on-line and off-line analysis, during target selection. Option causing the larger HbO signal change is selected. X signifies incorrect classification.

Day 2, Experimental Run 3

	HbO change - online				HbO change - online			
Command	Option 1 RED	Option 2 WHITE	Online selection	Error	Option 1 – RED	Option 2 - WHITE	Offline selection	Error
W	-1.6	-1.1	W		-0.4546	0.1693	W	
W	-0.9464	-0.5423	W		-0.225	0.1271	W	
W	-0.5914	0.4634	W		-0.0896	0.6364	W	
R	-0.1941	-0.6233	R		-0.0274	-0.5669	R	
W	-0.344	-0.414	R	X	-0.3461	0.0318	W	X
W	-0.1506	0.5675	W		0.3705	0.5844	W	
R	-0.3369	0.2858	W	X	-0.3995	0.3582	W	X
W	0.2469	0.8938	W		0.1729	0.8454	W	
W	-0.5169	0.0487	W		-0.2905	0.2227	W	
R	-0.0503	-0.5254	R		-0.0423	-0.3161	R	
Accuracy				80%				80%

Table B.3 Subject 1, Experiment 3 - HbO changes using on-line and off-line analysis, during target selection. Option causing the larger HbO signal change is selected. X signifies incorrect classification.

174

Day 2, Experimental Run 4

Command	HbO change – online			Error	HbO change - offline			Error
	Option 1 RED	Option 2 WHITE	Online selection		Option 1 – RED	Option 2 - WHITE	Offline selection	
W	0.0927	-0.4221	R	X	0.3394	0.0254	R	X
R	-0.2139	-0.2329	R		-0.0285	-0.2863	R	
W	-0.1965	-0.0223	W		-0.1436	0.1654	W	
W	-0.4327	0.0846	W		-0.2592	0.1425	W	
R	0.0603	-0.235	R		0.0851	-0.1413	R	
W	0.1989	0.003	R	X	0.3677	0.2405	R	X
W	-0.7924	0.0223	W		-0.7115	-0.0699	W	
R	-0.2786	-0.1506	W	X	-0.2564	-0.0308	W	X
W	-0.1907	0.0738	W		-0.1304	0.0825	W	
W	-0.1607	-0.0596	W		-0.1438	0.0006	W	
Accuracy				70%				70%

Table B.4 Subject 1, Experiment 4 - HbO changes using on-line and off-line analysis, during target selection. Option causing the larger HbO signal change is selected. X signifies incorrect classification.

Day 3, Experimental Run 5

Command	HbO change - online			Error	HbO change			Error
	Option 1 RED	Option 2 WHITE	Online selection		Option 1 – RED	Option 2 - WHITE	Offline selection	
W	-0.2739	0.1984	W		-0.0446	0.207	W	
W	0.0796	-0.0147	R	X	0.032	0.1844	W	
W	0.7939	-0.0733	R	X	0.2546	-0.0502	R	X
R	0.3239	-0.0666	R		0.0709	-0.0373	R	
W	-0.6566	-0.0656	W		-0.0065	0.1718	W	
W	-0.4201	0.0378	W		-0.0906	0.2391	W	
R	0.3269	0.472	W	X	0.392	0.3395	R	
W	0.0479	-0.7073	R	X	-0.4021	-0.2309	W	
W	0.7881	0.1688	R	X	0.5769	0.3339	R	X
R	0.1425	-0.2192	R		0.0773	0.0885	W	X
Accuracy				50%				70%

Table B.5 Subject 1, Experiment 5 - HbO changes using on-line and off-line analysis, during target selection. Option causing the larger HbO signal change is selected. X signifies incorrect classification.

Day 3, Experimental Run 6

	HbO change – online				HbO change - offline			
Command	Option 1 RED	Option 2 WHITE	Online selection	Error	Option 1 – RED	Option 2 - WHITE	Offline selection	Error
W	0.0706	0.5485	W		0.0894	0.2921	W	
R	0.0472	-0.3643	R		0.1834	-0.5319	R	
R	0.6735	0.0869	R		0.0357	0.0718	W	X
R	0.6736	-0.7444	R		0.2915	-0.5704	R	
W	1.1	-0.715	R	A	0.7812	-0.605	R	A
W	-0.8935	-0.1699	W		-0.7727	0.2709	W	
W	0.3327	-0.189	R	X	0.0032	0.0066	W	
W	-0.538	-0.536	W		-0.2627	0.0145	W	
R	-0.104	-0.2427	R		-0.0801	-0.2767	R	
R	-0.216	0.3404	W	X	-0.0922	0.1037	W	X
Accuracy				78%				78%

Table B.6 Subject 1, Experiment 6 - HbO changes using on-line and off-line analysis, during target selection. Option causing the larger HbO signal change is selected. X signifies incorrect classification.

Subject 2

Experimental Run 1

	HbO change - online				HbO change - offline			
Command	Option 1 RED	Option 2 WHITE	Online selection	Error	Option 1 – RED	Option 2 - WHITE	Offline selection	Error
W	-0.6871	0.5571	W		-0.0974	0.6068	W	
W	0.4038	1.5	W		0.2468	0.971	W	
W	-0.2483	1	W		0.1324	0.7896	W	
R	1.3	0.1151	R		0.7696	0.0852	R	
W	0.5849	0.007	R	X	0.0809	0.2787	W	
W	0.4185	0.2107	R	X	0.6391	0.2259	R	X
R	1.8	-0.22	R		0.0012	0.0001	R	
W	-0.00001	0.1181	W		0.2848	0.403	W	
W	0.5527	0.3372	R	X	0.59	0.7554	W	
R	1.6	-0.1292	R		-0.2049	-0.2065	R	
Accuracy				70%				90%

Table B.7 Subject 2, Experiment 1 - HbO changes using on-line and off-line analysis, during target selection. Option causing the larger HbO signal change is selected. X signifies incorrect classification.

176

Subject 3

Experimental Run 1

Command	HbO change - online			Error	HbO change - offline			Error
	Option 1 RED	Option 2 WHITE	Online selection		Option 1 – RED	Option 2 - WHITE	Offline selection	
W	-0.2359	-0.1865	W		-0.2465	-0.0947	W	
W	-0.0366	0.1146	W		-0.0407	-0.0024	W	
W	0.1585	0.1141	R	X	0.1553	0.2496	W	
R	0.172	0.2238	W	X	-0.0647	0.1061	W	X
R	0.182	0.1235	R		0.2106	-0.1392	R	
W	0.1902	-0.2664	R	X	0.1513	-0.007	R	X
W	0.5319	-0.3381	R	X	0.5407	0.2058	R	X
R	-0.1575	0.121	W	X	-0.0585	0.1078	W	A
W	0.1016	0.1915	W		-0.0565	0.2603	W	
W	0.1804	0.231	W		0.0804	0.2868	W	
Accuracy				50%				78%

Table B.8 Subject 3, Experiment 1 - HbO changes using on-line and off-line analysis, during target selection. Option causing the larger HbO signal change is selected. X signifies incorrect classification.

Experimental Run 2

Command	HbO change - online			Error	HbO change - offline			Error
	Option 1 RED	Option 2 WHITE	Online selection		Option 1 – RED	Option 2 - WHITE	Offline selection	
W	0.0434	-0.0536	R	X	-0.8889	-0.4718	W	
R	0.3822	0.1392	R		-0.3975	0.2788	W	X
W	-0.0061	0.6151	W		0.5811	0.7696	W	
W	0.2705	-0.1395	R	X	-0.3201	0.6768	W	
R	1.4	-0.4885	R		1.5	0.1332	R	
W	0.364	0.465	W		0.5724	-0.2973	R	X
W	0.1048	1.3	W		-0.6487	0.7724	W	
R	0.1336	0.464	W	X	2.5	1.4	R	
W	-0.8125	-1.7	R	X	0.2809	0.7324	W	
W	0.2516	-0.2167	R	X	-0.1062	0.3984	W	
Accuracy				50%				80%

Table B.9 Subject 3, Experiment 2 - HbO changes using on-line and off-line analysis, during target selection. Option causing the larger HbO signal change is selected. X signifies incorrect classification.

Appendix C

The following Matlab and Visual C++ code was used to implement some of the algorithms described in this thesis:

pulsecorr.m   Pulse correction algorithm using cubic spline interpolation.

mark_peaks.m   Algorithm used by pulsecorr.m to identify peaks in the signal relating to the cardiac pulse.

sinefit.m   Implementation of IEEE Standard 1057 sine wave fit algorithm used in reducing the effect of the Mayer wave.

Hbcalculate.m   Implementation of Beer-Lambert Law algorithm to find Hb and HbO concentration changes given the intensity changes of two wavelengths of light at 760nm and 880nm.

mindswitchDlg.cpp   Implementation of the Mindswitch application within a Visual C++ programming workspace for Windows Dialogue.

C.1 pulsecorr.m

```
function [y]= pulsecorr(x)
%[y]= pulsecorr(x)
%pulse correction algorithm using cubic spline interpolation
% Last updated July 2005

[peak_value_n,peak_time_n]=mark_peaks(x);        % identify cardiac peaks
r=length(peak_time_n);                           % number of heartbeat intervals
samplerate=100;                                  % data sampled at 100Hz
t=(1:length(x))'/100;                            % time vector of original signal x
for l=1:(r-1)                                     % mean of each heart-beat interval
  mop(l)=mean(x(peak_time_n(l):peak_time_n(l+1)));
end

starttime=peak_time_n(1);
```

```
y=interp1(peak_time_n(1:(r-1)),mop,peak_time_n(1):peak_time_n(r-1),'cubic');    %    interpolate
using a cubic spline

figure
plot(t(peak_time_n(1):peak_time_n(r-1)),x(peak_time_n(1):peak_time_n(r-1)))
hold on
plot(t(peak_time_n(1):peak_time_n(r-1)),y(1:peak_time_n(r-1)-peak_time_n(1)+1),'r')
title('Original  signal and Pulse Correct Version')
xlabel('Time (s)'), ylabel('Amplitude')
```

C.2   mark_peaks.m

```
function [peak_value,peak_time]=mark_peaks(input)
% mark_peaks identifies peaks in the cardiac pulse and their time index
% Last updated July 2005

N=input;
[nm,ni]=min(N(1:50));   %start analysis at first crest in the signal
start_point=ni;end_index=start_point+105; % 100Hz samling rate, examine 1.05s intervals
peak_time=[];
peak_value=[];

while (end_index+105<length(N))
  beg_index=start_point;
  end_index=beg_index+105;
  buff=N(beg_index:end_index);
  [new_peak_value,new_peak_time]=max(buff); % find maximum over 105 samples
  new_peak_time=new_peak_time+beg_index-1;  % time index of peak value
  peak_time=[peak_time new_peak_time];
  peak_value=[peak_value new_peak_value];
  start_point=peak_time(end)+20;  % start analysis of next interval 20 samples after last peak
end
```

C.3 sinefit.m

```
function [a1, b1, c1, w1] = sinefit(y,f,Ao,Bo,Co)
% [x]= sinefit(y,f,Ao,Bo,Co)
%sinefit.m uses the IEEE Standard 1057 algorithm to fit the parameters of a sine wave to a
%dataset y where y(a1,b1,c1,w1)= a1*cos(w1*t) + b1*sin(w1*t) + c1
%The algorithm is implemented according to Händel, P. (2000), Evaluation of a standardized
%sine wave fit algorithm.IEEE Nordic Signal Processing %Symposium, Sweden 453-456.
% Last updated July 2005


N=length(y);
iteration=100;
A=zeros(1,iteration);, B=zeros(1,iteration);, C=zeros(1,iteration);, delta_w=zeros(1,iteration);
w=zeros(1,10);
x=[A; B; C; delta_w];
D=zeros(N,4);
A(1)=Ao;, B(1)=Bo;, C(1)=Co;, w(1)=2*pi*f;, delta_w(1)=0; % initial guesses for the variables
t=1:N;
t=t/100;   % sampling frequency at 100Hz
done=0;
i=1;


while i<(iteration-1)&done==0,
        i=i+1;
        w(i)=w(i-1)+delta_w(i-1);

        for k=1:N,
                D(k,:) = [cos(w(i) * t(k)) sin(w(i) * t(k))    1    -A(i-1) * t(k) * sin(w(i) *
                t(k))+B(i-1) * t(k) * cos(w(i) * t(k))] ;
        end

                            M=inv(D'*D)*D';
        x(:,i)=M*y';
        A(i)=x(1,i);, B(i)=x(2,i);, C(i)=x(3,i);, delta_w(i)=x(4,i);

        if (A(i)-A(i-1)<0.001) & (B(i)-B(i-1)<0.001) &(C(i)-C(i-1)<0.001) &
```

180

```
                        (D(i)-D(i-1)<0.001)
                                done=1;
                        else
                                done=0;
                        end
end


a1=A(i);, b1=B(i);, c1=C(i);, w1=w(i);
```

C.4 Hbcalculate.m

```
function [delta_Hb, delta_HbO]= Hbcalculate1(red_sig,nir_sig,Ay,d)
% [delta_Hb, delta_HbO]= Hbcalculate(red,nir,Ay,d)
% Ay - age of subject
% d - interoptode distance
% red - 760nm signal
% nir - 880nm signal
% Calculates Hb and HbO concentration changes given light intensity changes at 760nm and
% 880nm, implemented as described in Cope, M. (1991). The Application of Near Infrared
% Spectroscopy to Non Invasive Monitoring of Cerebral Oxygenation in the Newborn Infant.
% Department of Medical Physics and Bioengineering. London, University College London.
% Last updated July 2005

if(nargin==0)
 disp('USAGE:  Hbcalculate(red,nir,Ay,d)');
 return;
end


if (nargin==2)
Ay=35;                    %age of subject
d=3;                          %inter-optode distance
end


B_780=5.13+0.07*Ay^0.81;%DPF at 780nm, age of subject is Ay
Bn_760=1.12;              %pathlength factor normalised to 780nm
Bn_880=0.84;
data_length=length(red_sig);
delta_OD_880=zeros(1,data_length-1);
delta_OD_760=zeros(1,data_length-1);
```

181

```matlab
if min(red_sig)<=0          %add offset if signal is less than 0
    red_sig=abs(min(red_sig))+red_sig+1;
end
if min(nir_sig)<=0
    nir_sig=abs(min(nir_sig))+nir_sig+1;
end


for i=1:data_length-1
    delta_OD_880(i)=log10(nir_sig(i)/nir_sig(1));          %change in attenuation
    delta_OD_760(i)=log10(red_sig(i)/red_sig(1));
end


delta_K1=delta_OD_880/(B_780*d);
delta_K2=delta_OD_760/(B_780*d);
delta_K=[delta_K1;delta_K2];
%ext_coef_HbO_880=1.2846;%spec. extinction coefficient(mM-1 cm-1)
%ext_coef_Hb_880=0.8412;
%ext_coef_HbO_760=0.6096;
%ext_coef_Hb_760=1.6745;
alpha=[1.2846*Bn_880 0.8412*Bn_880; 0.6096*Bn_760 1.6745*Bn_760];
alpha_transpose = alpha';
M=(inv(alpha_transpose*alpha))*alpha_transpose;
C=(inv(alpha_transpose*alpha))*alpha_transpose*delta_K;
delta_HbO=C(1,:);
delta_Hb=C(2,:);
delta_HbO=delta_HbO(1)-delta_HbO;
delta_Hb=delta_Hb(1)-delta_Hb;
```

C.5 mindswitchDlg.cpp


```cpp
// mindswitchDlg.cpp : implementation file
// Last updated July 2005
#include "stdafx.h"
#include <iostream.h>
#include <windows.h>
#include "math.h"
#ifdef _DEBUG
```

```
#define new DEBUG_NEW
#undef THIS_FILE
static char THIS_FILE[] = __FILE__;
#endif
// CMindswitchDlg dialog
CMindswitchDlg::CMindswitchDlg(CWnd* pParent /*=NULL*/)
        : CDialog(CMindswitchDlg::IDD, pParent)
{       //{{AFX_DATA_INIT(CMindswitchDlg)
                m_statusCommand = _T("");
        //}}AFX_DATA_INIT
        m_hIcon = AfxGetApp()->LoadIcon(IDR_MAINFRAME);
}


void CMindswitchDlg::DoDataExchange(CDataExchange* pDX)
{       CDialog::DoDataExchange(pDX);
        //{{AFX_DATA_MAP(CMindswitchDlg)
        DDX_Text(pDX, IDC_STATIC_Command, m_statusCommand);
        DDX_Text(pDX, IDC_STATIC_Score, m_statusScore);
        DDX_Text(pDX, IDC_STATIC_count, m_statusCount);
        DDX_Text(pDX, IDC_STATIC_Channelnum, m_statusChannel);
        DDX_Text(pDX, IDC_EDIT_Frequency, m_SelectFrequency);
        DDX_Text(pDX, IDC_EDIT_Buffer, m_SelectBufferSize);
        //}}AFX_DATA_MAP
}
BEGIN_MESSAGE_MAP(CMindswitchDlg, CDialog)
        //{{AFX_MSG_MAP(CMindswitchDlg)
        ON_WM_PAINT()
        ON_WM_QUERYDRAGICON()
        ON_BN_CLICKED(IDC_BUTTON1_StartDataAquisition,
OnBUTTON1StartDataAquisition)
        ON_BN_CLICKED(IDC_BUTTON4_Quit, OnBUTTON4Quit)
        ON_BN_CLICKED(IDC_BUTTON2_StopDataAcquisition,
        OnBUTTON2StopDataAcquisition)
        ON_BN_CLICKED(IDC_BUTTON1_getchannelnum, OnBUTTON1getchannelnum)
        //}}AFX_MSG_MAP
END_MESSAGE_MAP()
// CMindswitch message handlers
BOOL CMindswitchDlg::OnInitDialog()
{       CDialog::OnInitDialog();
        SetIcon(m_hIcon, TRUE);                    // Set big icon
```

```cpp
        SetIcon(m_hIcon, FALSE);                    // Set small icon
        state=0;//status REST
        score=0;
        trial=0;
        m_LogicalDevice=0;
        m_LogicalChannel=0;    //Use channel 0 by default
        number_of_channels=4; //default number of channels to measure
        SamplingRate=10; //sampling freq in Hertz
        m_samples=number_of_channels*SamplingRate;                    //samples_per_sec
        samples_per_channel=m_samples/number_of_channels;
        m_DLmsg=RegisterWindowMessage(DL_MESSAGE);//register DriverLINX messages
        m_DriverInstance=OpenDriverLINX(m_hWnd,"kmbpio");
        m_pSR = (DL_ServiceRequest*) new DL_ServiceRequest;
        memset(m_pSR,0,sizeof(DL_ServiceRequest));//allocate memory for the service request
        DL_SetServiceRequestSize(*m_pSR); //reset the members of the service request
        m_pSR->device=m_LogicalDevice; // Device - number assigned in DriverLINX config.
        m_pSR->operation=INITIALIZE;
        m_pSR->mode=OTHER;
        m_pSR->subsystem=DEVICE;
        m_pSR->hWnd=m_hWnd;
        DriverLINX(m_pSR);
        showMessage(m_pSR); //Show DriverLINX errors, if any
        return TRUE;  // return TRUE  unless you set the focus to a control
}


void CMindswitchDlg::OnPaint()
{       if (IsIconic())
        {       CPaintDC dc(this); // device context for painting
                SendMessage(WM_ICONERASEBKGND, (WPARAM) dc.GetSafeHdc(), 0);
                // Center icon in client rectangle
                int cxIcon = GetSystemMetrics(SM_CXICON);
                int cyIcon = GetSystemMetrics(SM_CYICON);
                CRect rect;
                GetClientRect(&rect);
                int x = (rect.Width() - cxIcon + 1) / 2;
                int y = (rect.Height() - cyIcon + 1) / 2;
                dc.DrawIcon(x, y, m_hIcon);                // Draw the icon
        }
        else
        {       CWnd *CrtHandle = GetDlgItem(IDC_CRT);
```

184

```
RECT rect;
int decisionl,decisionr,decisiont,decisionb;
HPEN hpen;
HBRUSH hbrush;
COLORREF colorref;
COLORREF colorgreen;
COLORREF colorred;
COLORREF colorwhite;
COLORREF colorhighlight;
int height,width;

colorref = RGB(0,0,0);
colorred = RGB(255,0,0);
colorgreen= RGB(0,210,0);
colorwhite=RGB(255,255,255);
colorhighlight=RGB(0,200,200);
CrtHandle->GetWindowRect(&rect);          //Get coordinates of CRT
ScreenToClient(&rect);                    //Get client coordinates
height=(rect.bottom-rect.top)/2;
width=(rect.right-rect.left)/2;
CPaintDC dc(this);
hbrush=CreateSolidBrush(colorhighlight);
hpen=CreatePen(PS_SOLID,5,colorref);
SelectObject(dc,hbrush);
SelectObject(dc,hpen);

if(state==1 && active==TRUE) //highlight row 0, top rectangle
        {Rectangle(dc,rect.left+180,rect.top,rect.right,rect.bottom-height);
        if (command_row==0)
                {hbrush=CreateSolidBrush(colorred);
                SelectObject(dc,hbrush);
                Rectangle(dc,rect.left+20,rect.top+height-
                100,rect.left+120,rect.bottom-height);}
        else
                {hbrush=CreateSolidBrush(colorwhite);
                 SelectObject(dc,hbrush);
                Rectangle(dc,rect.left+20,rect.top+height,rect.left+120,
                rect.bottom-height+100); }}

else if (state==2 && active==TRUE) //highlight row 1, bottom rectangle
```

```
                    {Rectangle(dc,rect.left+180,rect.top+height,rect.right,rect.bottom);
                    if (command_row==0)
                            {hbrush=CreateSolidBrush(colorred);
                            SelectObject(dc,hbrush);
                            Rectangle(dc,rect.left+20,rect.top+height-
                            100,rect.left+120,rect.bottom-height);}
                    else
                            {hbrush=CreateSolidBrush(colorwhite);
                            SelectObject(dc,hbrush);
                            Rectangle(dc,rect.left+20,rect.top+height,rect.left+120,
                            rect.bottom-height+100); }}
        else if (state==3) //decide on selected target
                    {
                    if (row==0)
                            {decisiont=rect.top;
                            decisionb=rect.top+height;
                            decisionl=rect.left+180;
                            decisionr=rect.right;}
                    else
                            {decisiont=rect.top+height;
                            decisionb=rect.bottom;
                            decisionl=rect.left+180;
                            decisionr=rect.right;}

                    hbrush=CreateSolidBrush(colorgreen);
                    SelectObject(dc,hbrush);
                    Rectangle(dc,decisionl,decisiont,decisionr,decisionb);

                    if (command_row==0)
                            {hbrush=CreateSolidBrush(colorred);
                            SelectObject(dc,hbrush);
                            Rectangle(dc,rect.left+20,rect.top+height-
                            100,rect.left+120,rect.bottom-height);}
                    else
                            {hbrush=CreateSolidBrush(colorwhite);
                            SelectObject(dc,hbrush);
                            Rectangle(dc,rect.left+20,rect.top+height,rect.left+120,
                            rect.bottom-height+100);}
        }
```

```
else
    {if (iteration>25)
        {if (command_row==0)
            {hbrush=CreateSolidBrush(colorred);
            SelectObject(dc,hbrush);
            Rectangle(dc,rect.left+20,rect.top+
            height-100,rect.left+120,rect.bottom-height);}
        else
            {hbrush=CreateSolidBrush(colorwhite);
            SelectObject(dc,hbrush);
            Rectangle(dc,rect.left+20,rect.top+height,
            rect.left+120, rect.bottom-height+100); }
        hbrush=CreateSolidBrush(colorred);
        SelectObject(dc,hbrush);
        Rectangle(dc,rect.left+220,rect.top+40,rect.right-40,
        rect.top+height-40); //red
        hbrush=CreateSolidBrush(colorwhite);
        SelectObject(dc,hbrush);
        Rectangle(dc,rect.left+220,rect.bottom-height+40,
        rect.right-40,rect.bottom-40); //white
    }
    else
        {hbrush=CreateSolidBrush(colorred);
        SelectObject(dc,hbrush);
        Rectangle(dc,rect.left+220,rect.top+40,rect.right-40,
        rect.top+height-40); //red
        hbrush=CreateSolidBrush(colorwhite);
        SelectObject(dc,hbrush);
        Rectangle(dc,rect.left+220,rect.bottom-height+40,
        rect.right-40,rect.bottom-40); //blue}
    }
    hbrush=CreateSolidBrush(colorred);
    SelectObject(dc,hbrush);
    Rectangle(dc,rect.left+220,rect.top+40,rect.right-40,
    rect.top+height-40); //red
    hbrush=CreateSolidBrush(colorwhite);
    SelectObject(dc,hbrush);
    Rectangle(dc,rect.left+220,rect.bottom-height+40,
    rect.right-40,rect.bottom-40); //white
DeleteObject(hpen);
```

```
                    DeleteObject(hbrush);
        //          CDialog::OnPaint();
        }
}


HCURSOR CMindswitchDlg::OnQueryDragIcon()
{       return (HCURSOR) m_hIcon;        }


void CMindswitch::showMessage(DL_ServiceRequest *SR)
{       SR->operation=MESSAGEBOX;
        DriverLINX(SR);             }


void CMindswitchDlg::clearBuffers(DL_ServiceRequest *SR)
{       /*Make sure the service request exists first, */
        if(SR!=NULL)
        {       /*If the service request exists, make sure there is a buffer list*/
                if(SR->lpBuffers!=NULL)
                {/*If the buffer list exists, is there actually a pointer to a buffer?*/
                if(SR->lpBuffers->BufferAddr[0]!=NULL)
                        {/*De-allocate the buffer, and clear its pointer*/
                        BufFree(SR->lpBuffers->BufferAddr[0]);
                        SR->lpBuffers->BufferAddr[0]=NULL;
                        // clear the other two buffers as well
                        BufFree(m_pSR->lpBuffers->BufferAddr[1]);
                        m_pSR->lpBuffers->BufferAddr[1]=NULL;
                        BufFree(m_pSR->lpBuffers->BufferAddr[2]);
                        m_pSR->lpBuffers->BufferAddr[2]=NULL;}
                /*Delete the buffer list, we don't need it anymore*/
                delete(SR->lpBuffers);
                SR->lpBuffers=NULL;}
        }
}


void CMindswitchDlg::OnBUTTON1StartDataAquisition()
{       iteration=0; //count no. of buffer filled events
        outFile.open("output.txt",ios::out);
        outFileHb.open("HbHbOconc.txt",ios::out);
        outFileavg.open("avgHbHbO.txt",ios::out);
        clearBuffers(m_pSR);       //de-allocate any exisiting buffers in the service request
        //number_of_channels=m_Number_of_Channels;
```

```
m_pSR->operation=START; //Start the acquisition
m_pSR->subsystem=AI; //using the AI subsystem
m_pSR->mode=INTERRUPT; //use interrupt mode/DMA mode
m_pSR->start.typeEvent=COMMAND; //Start on command
m_pSR->timing.typeEvent=RATEEVENT; //timing determined by the rate generator
m_pSR->stop.typeEvent=COMMAND; //Stop on command
m_pSR->channels.nChannels=2; //A start/stop channel range will be used
m_pSR->channels.chanGain[0].channel=m_LogicalChannel;//starting channel
m_pSR->channels.chanGain[0].gainOrRange=Gain2Code(m_LogicalDevice,AI,-1.0);
                                                     //Use bipolar unity gain
m_pSR->channels.chanGain[1].channel=m_LogicalChannel+number_of_channels-1;
                                                     //stop on channel no.
m_pSR->channels.chanGain[1].gainOrRange=Gain2Code(m_LogicalDevice,AI,-1.0);
m_pSR->channels.numberFormat=tNATIVE; //use the native format (integer counts)
/*  Declare three buffers, create a buffer list pointer for 3 buffers, set the size of the buffer (in
bytes) to hold the number of samples*/
m_pSR->lpBuffers=(DL_BUFFERLIST*) new BYTE[DL_BufferListBytes(3)];
m_pSR->lpBuffers->notify=NOTIFY; //enable the buffer filled message
m_pSR->lpBuffers->nBuffers=3; //uses 3 buffers
m_pSR->lpBuffers->bufferSize=Samples2Bytes(m_LogicalDevice,AI,
m_LogicalChannel,m_samples);
m_pSR->lpBuffers->BufferAddr[0]=BufAlloc(GBUF_INT,m_pSR->lpBuffers-
>bufferSize); //Allocate Buffer 0 based on the size we just specified
m_pSR->lpBuffers->BufferAddr[1]=BufAlloc(GBUF_INT,m_pSR->lpBuffers-
>bufferSize);
m_pSR->lpBuffers->BufferAddr[2]=BufAlloc(GBUF_INT,m_pSR->lpBuffers->
bufferSize);
HbOwindow1= new double [20*samples_per_channel];
Hbwindow1= new double [20*samples_per_channel];
/* the rate information for the RATEEVENT typeEvent */
SamplePeriod=1/((float)SamplingRate*number_of_channels);
m_pSR->timing.u.rateEvent.channel=DEFAULTTIMER;
//DEFAULTTIMER is a symbol representing the default counter/timer channel used for pacing.
m_pSR->timing.u.rateEvent.mode=RATEGEN; //Set the timer mode to rate mode
m_pSR->timing.u.rateEvent.clock=INTERNAL1; //Internal clocking will be used
m_pSR->timing.u.rateEvent.gate=DISABLED; //no gating will be used
m_pSR->timing.u.rateEvent.period
=Sec2Tics(m_LogicalDevice,AI,INTERNAL1,SamplePeriod);
DriverLINX(m_pSR); //Execute the service request to start the acquisition
showMessage(m_pSR); //show any errors
```

m_task=m_pSR->taskId; } //Save the task ID of the AI task so it can be stopped later

```
LRESULT CMindswitchDlg::WindowProc(UINT message, WPARAM wParam, LPARAM lParam)
{       if(message==m_DLmsg)
        { //Did DriverLINX post a message?
        switch(wParam)
                {case DL_BUFFERFILLED: //Buffer filled message?
                // determine the index of the buffer that if full
                        m_bufnum=getBufIndex(lParam); //Get index of the full buffer
                        done(m_bufnum); //if so, call the done() function to process the results
                        break;
                case DL_DATALOST:
                        showMessage(m_pSR);
                        // call a handler for this condition
                        break;}
        }
return CDialog::WindowProc(message, wParam, lParam);
}


void CMindswitchDlg::done(int bufNum)
{       float *readings;
        double *red,*nir,*Hb,*HbO;
        int temp_index;
        int loop_count;
        int i;
        static int movetime;
        static bool active=TRUE;
        static bool goleft=TRUE;
        temp_index=0;

        readings = new float[m_samples]; // temporary array to hold the converted readings
        red=new double[samples_per_channel]; //red channel1 760nm
        nir=new double[samples_per_channel];        //nir channel1 880nm
        Hb=new double[samples_per_channel];
        HbO=new double[samples_per_channel];
        CString str;
        char chanIndex[30],command[10],countdown[10],scoreboard[10];
        int index;
        m_pSR->operation=CONVERT; //Convert the raw counts in the buffer to voltages
```

190

```
m_pSR->mode=OTHER;  //Convert is not a polled, interrupt, or DMA operation
m_pSR->start.typeEvent=DATACONVERT; //Set the start type to convert the data
m_pSR->start.u.dataConvert.startIndex=0; //start at index 0 of the buffer
m_pSR->start.u.dataConvert.nSamples=m_samples; //number of samples to convert
m_pSR->start.u.dataConvert.numberFormat=tSINGLE; //convert to tSINGLE (float)
m_pSR->start.u.dataConvert.scaling=1.0f; //no scaling will be used
m_pSR->start.u.dataConvert.offset=10.0f; // offset of 10, avoids taking negative log
m_pSR->start.u.dataConvert.wBuffer=bufNum; //
m_pSR->start.u.dataConvert.lpBuffer=readings; //Readings into the temporary buffer
DriverLINX(m_pSR); //Execute the conversion
showMessage(m_pSR); //Show any errors
m_listBox.ResetContent(); //Clear the listbox
loop_count=0;
i=0;
int j=0;
while(i<m_samples)
{       for(index=0;index<number_of_channels;index++)
        {       temp_index=i+index-(number_of_channels*loop_count);
                strcpy(chanIndex,"chan #: ");
                str.Format("%d",temp_index);
                strcat(chanIndex,str);
                strcat(chanIndex," ");  // build a string of indexed chans
                str.Format("%8.3f",readings[index+i]); // float reading into a string
                        strcat(chanIndex,str);  // add the reading onto end
                m_listBox.AddString(chanIndex); //Add the string to the listbox
                outFile<<readings[index+i]<<"\t";

        if(index==0)                    //red channel 1 data
                red[j]=readings[index+i];
        else if(index==1) //nir channel 1 data
                nir[j]=readings[index+i];               }
  outFile<<"\n";
  j++;
  loop_count++;
  i=i+number_of_channels;               }

for(i=0;i<samples_per_channel;i++)                      //change in attenuation/(DPF*d)
        {nir[i]=(log10(nir[i]))/19.3;  //b780*d=19.13 default  (log I/Io)/B780*d
        red[i]=(log10(red[i]))/19.3;}
if(iteration==0)
```

191

```
                {tempHb1=0;
                tempHbO1=0;
                HbO_initial=(1.2168*nir[0]) + (-0.4585*red[0]);
                Hb_initial=(-0.443*nir[0]) + (0.7001*red[0]);}
        else{}


        for(i=0;i<samples_per_channel;i++)
                {HbO[i]= HbO_initial - ((1.2168*nir[i]) + (-0.4585*red[i]));
                outFileHb<<HbO[i]<<"\t";
                Hb[i]= Hb_initial - ((-0.443*nir[i]) + (0.7001*red[i]));
                outFileHb<<Hb[i]<<"\t";  }
        int window_index;                       //keep data for the past 20s
        if(iteration<20)             // for time t=0 to t=20 store the values into the window arrays
                {for (i=0;i<samples_per_channel;i++)
                        { window_index=(iteration)*samples_per_channel;
                        HbOwindow1[window_index+i]=HbO[i];
                        Hbwindow1[window_index+i]=Hb[i];}
                movetime=0; }
        else      //from time t=20 shift all the values over to the left by one second,
                {for (i=0;i<(samples_per_channel*19);i++)
                        {HbOwindow1[i]=HbOwindow1[i+samples_per_channel];
                        Hbwindow1[i]=Hbwindow1[i+samples_per_channel];}
                for (i=0;i<samples_per_channel;i++) //put current value into array
                        {HbOwindow1[samples_per_channel*19+i]=HbO[i];
                Hbwindow1[samples_per_channel*19+i]=Hb[i];}    }
        if ((iteration>19)&&(iteration%15==0)&&(active==FALSE)) //give commands
                        {movetime=0;
                        state=state+1;
                        baseline=0;
                        for (i=100;i<199;i++)
                                {baseline=baseline+HbOwindow1[i];}
                        baseline=baseline/100; //average of 10s rest
                          active=TRUE;   }
        else if((iteration>19)&&(iteration%15==0)&&(active==TRUE))
                        {resttime=0;
                        active=FALSE;
                        movetime=0;}
        else      {}


        if ((active==TRUE)&&(iteration>19)) //user is presented with flashing option
```

192

```
                        movetime=movetime+1;
else if ((active==FALSE)&&(iteration>19)) //user rests
            {           resttime=resttime+1;
                        if (resttime>5 && state==3) // if decision has been made
                        state=0;
                        else
                        state=state; //still more options to be presented          }
else
                        movetime=0;


srand( (unsigned)time( NULL ) );
int colourchoice;
if ((state==0) &&(resttime==10)) //give command to user
            {colourchoice=rand();
            if (colourchoice%3==0)
                        command_row=0;
            else
                        command_row=1;}


if (movetime==15) //after 15s of user input, compare signal with baseline
            {motor=0;
            for(i=100;i<199;i++)
            {motor=motor+HbOwindow1[i];}
            motor=motor/100; //channel 1
            if (motor>baseline)
                        RIGHT=TRUE;
            else
                        RIGHT=FALSE;
            if(state==1)                        //state 1 - top rectangle flashing
                        option1=motor-baseline;
            else                        //state 2 - bottom rectangle flashing
                        {option2=motor-baseline;
                        if (option1>option2)
                                row=0;
                        else
                                row=1;
                        trial+=1;
                        if (row==command_row)
                                score+=1;
                        else
```

```
                              score=score;
                   strcpy(command," score is ");
                   str.Format("%d",score);
                   strcat(command,str);
                   strcat(command,"/");
                   str.Format("%d",trial);
                   strcat(command,str);
                    m_statusCommand.Format("%s",command);
                    state=3; //decision time
                    }
          }
          else {}
          outFileavg<<state<<"\t"; //****
          outFileavg<<option1<<"\t"; //****
          outFileavg<<option2<<"\t"; //****
          outFileavg<<row<<"\t"; //****
          outFileavg<<command_row<<"\n"; //****

          UpdateData(FALSE); //Update the listbox display
           this ->Invalidate(TRUE); // update user feedback
          iteration+=1;
          delete [] readings; //clear the temporary buffer to avoid memory leaks
          delete [] red;
          delete [] nir;
          delete [] Hb;
          delete [] HbO;

}

void CMindswitchDlg::OnBUTTON2StopDataAcquisition()
{        // stop the active AI task
         m_pSR->taskId=m_task; // restore the task ID
         m_pSR->operation=STOP;
         m_pSR->start.typeEvent=NULLEVENT;
         m_pSR->mode=INTERRUPT;
         DriverLINX(m_pSR);
         showMessage(m_pSR);
                 outFile.close();
                 outFileHb.close();
                 outFileavg.close();          }
```

```cpp
void CMindswitchDlg::OnBUTTON4Quit()
{       clearBuffers(m_pSR); //de-allocate any existing buffers
        delete m_pSR;  //de-allocate the memory used by the service request
        m_pSR=NULL;
        CloseDriverLINX(m_DriverInstance); //close the DriverLINX driver
        m_DriverInstance=NULL;//make sure m_driverInstance isn't pointing to anything
        HbOwindow1=NULL;
        Hbwindow1=NULL;
        OnOK();        }
```

Appendix D

Glossary

Amyotrophic Lateral Sclerosis (ALS)
A chronic, progressive disease marked by gradual degeneration of the nerve cells in the central nervous system that control voluntary muscle movement. The disorder causes muscle weakness and atrophy; symptoms commonly appear in middle to late adulthood, with death in two to five years. The cause is unknown, and there is no known cure. Also called Lou Gehrig's Disease, or Motor Neuron Disease. Literally, amytrophic lateral sclerosis means without muscle nourishment, side (of spinal cord) hardening.

Autoregulation
The capacity of an organ to regulate its blood supply according to its functional or metabolic needs.

Arteriole
An arteriole is a blood vessel that extends and branchs out from an artery and leads to capillaries.

Bilateral
On both sides

Capillary
A tiny blood vessel that connects the smallest arteries to the smallest veins and allows exchange of oxygen and other materials between blood cells and body tissue cells

Cerebral hypoxia

The term cerebral hypoxia technically refers to a lack of oxygen supply to the cerebral hemispheres, but it is more typically used to refer to a lack of oxygen supply to the entire brain. Brain cells are extremely sensitive to oxygen deprivation. Some brain cells actually start dying less than 5 minutes after their oxygen supply is cut. As a result, brain hypoxia can kill or cause severe brain damage rapidly.

Chromophore
A compound that absorbs light in the spectral region of interest

Contralateral
On the opposite side

Coronal section
Vertical slice dividing into front and back halves

Distal
Far from

Dopamine
A neurotransmitter present in regions of the brain that regulate movement, emotion, motivation and feelings of pleasure.

Edema
An increase in the volume of fluid in the spaces between the body's cells

Haemodynamic
Relating to the physical aspects of the blood circulation. Adequate blood circulation is a necessary condition for adequate supply of oxygen to all tissues.

Homeostasis
The term is most often used in the sense of biological homeostasis (homeo meaning similar, stasis meaning standing or stopping). Multicellular organisms require a homeostatic internal environment, in order to live. Complex systems,

such as a human body, must have homeostasis to maintain stability and to survive. These systems do not only have to endure to survive; they must adapt themselves and evolve to modifications of the environment.

In situ
"In place" in Latin. A term used in biology, where it means to examine the phenomenon exactly in place where it occurs, i.e. without removing it in some special medium etc.

Ipsilateral
on the same side

Irradiance
The density of radiant flux incident on a given area, typically measured as a unit of power per unit area (e.g. W/m^2)

Ischemia
A decrease in the blood supply to a bodily organ, tissue, or part caused by constriction or obstruction of the blood vessels.

Medial
Towards the midline

Lamina
Any thin, flat layer of membrane or other bulkier tissue

Locked-in syndrome
A condition in which a patient is aware and awake, but cannot move or communicate due to complete paralysis of the body

Proximal
Near to

Radiolabel

Any compound that has been joined with a radioactive substance for, e.g., certain imaging methods.

Transverse section

Horizontal section parallel to ground

Vascular

Relating to the channels that carry body fluids, usually used in connection with the blood vessels.

Vasodilation

Widening of the diameter of a blood vessel in order to decrease the resistance to blood flow

Ventral

Front end

Vestibular system

The vestibular system, or balance system, is the sensory system that provides the dominant input about our movement and orientation in space. Together with the cochlea, the auditory organ, it is situated in the vestibulum in the inner ear.

References

Arridge, S. R., M. Cope and D. T. Delpy (1992). "The theoretical basis for the determination of optical pathlengths in tissue: temporal and frequency analysis." *Physics in Medicine and Biology* **37**(7): 1531-1560.

Baraldi, P., C. A. Porro, M. Serafini, G. Pagnoni, C. Murari, R. Corazza and P. Nichelli (1999). "Bilateral representation of sequential finger movements in human cortical areas." *Neuroscience Letters* **269**: 95-98.

Barinaga, M. (1997). "What Makes Brain Neurons Run?" *Science* **276**: 196-198.

Bauby, J. (1997). The Diving Bell and the Butterfly : A Memoir of Life in Death, Knopf.

Beisteiner, R., P. Hoellinger, G. Lindinger, W. Lang and A. Berthoz (1995). "Mental representations of movements. Brain potentials associated with imagination of hand movements." *Electroencephalography and Clinical Neuropsychology* **96**: 183-193.

Benaron, D. A., S. Hintz, A. Villringer, D. Boas, A. Kleinschmidt, J. Frahm, C. Hirth, H. Obrig, J. van Houten, E. Kermit, W. Cheong and D. Stevenson (2000). "Noninvasive Functional Imaging of Human Brain Using Light." *Journal of Cerebral Blood Flow and Metabolism* **20**: 469-477.

Berne, R. M. and M. N. Levy (2000). Cardiovascular Physiology, Mosby.

Biomedical Optics Research Group at University College London, Specific extinction spectra of tissue chromophores, http://www.medphys.ucl.ac.uk /research/borg/research.htm.

Birbaumer, N., A. Kuebler, N. Ghanayim, T. Hinterberger, J. Perelmouter, J. Kaiser, I. Iversen, B. Kotchoubey, N. Neumann and H. Flor (2000). "The Thought Translation Device (TTD) for Completely Paralyzed Patients." *IEEE Transactions on Rehabilitation Engineering* 8(2): 190-202.

Boas, D., D. H. Brooks, E. L. Miller, C. A. DiMarzio, M. Kilner, R. J. Gaudette and Q. Zhang (2001). "Imaging the Body with Diffuse Optical Tomography." *IEEE Signal Processing Magazine* 18: 57-75.

Boas, D., M. A. Franceshini, A. K. Dunn and G. Strangman (2002). Noninvasive Imaging of Cerebral Activation with Diffuse Optical Tomography. In-Vivo Optical Imaging of Brain Function. R. Frostig, CRC Press.

Boas, D., K. Chen, D. Grebert and M. A. Franceshini (2004). "Improving the diffuse optical imaging spatial resolution of the cerebral hemodynamic response to brain activation in humans." *Optics Letters* 29(13): 1306-1308.

British Standards (1994). BS EN 60825-1, Safety of Laser Products.

Burke, D., T. Ward and A. de Paor (2001). "Image processing used to harness blinking as a channel of communication and control for physically disabled people." *Medical Biological Engineering and Computation* 39(3): 285-287.

Buxton, R. B. and L. R. Frank (1997). "A model for the coupling between cerebral blood flow and oxygen metabolism during neural stimulation." *Journal of Cerebral Blood Flow and Metabolism* 17: 64-72.

Buxton, R. B. (2001). "The Elusive Initial Dip." *Neuroimage* 13: 953-958.

Buxton, R. B., K. Uludag, D. J. Dubowitz and T. T. Liu (2004). "Modeling the hemodynamic response to brain activation." *Neuroimage* 23: S220-S233.

Center, R. U. M. (2005). Health Information - Nervous System Disorders Online Resources http://www.rush.edu/rumc/page-P00797.html.

Chance, B. and A. Villringer (1997). "Non-invasive optical spectroscopy and imaging of human brain function." *Trends in Neuroscience* **20**(10): 435-442.

Chance, B., M. Cope, E. Gratton, N. Ramanujam and B. Tromberg (1998). "Phase measurement of light absorption and scatter in human tissue." *Review of Scientific Instruments* **69**(10): 3457-3481.

Chance, B., S. Nioka, S. Sadi and C. Li (2003). Oxygenation and Blood Concentration Changes in Human Subject Prefrontal Activation by Anagram Solutions. Oxygen Transport in Tissue XXIII. D. Wilson, Kluwer Academic/Plenum Publishers.

Cooley, R. L., N. Montano, C. Cogliati, P. van de Borne, W. Richenbacher, R. Oren and V. K. Somers (1998). "Evidence for a central origin of the low frequency oscillation in RR-internal variability." *Circulation* **98**: 556-561.

Cooper, C. E., D. T. Delpy and E. M. Nemoto (1998). "The relationship of oxygen delivery to absolute haemoglobin oxygenation and mitochondrial cytochrome oxidase redox state in the adult brain: a near-infrared spectroscopy study." *Journal of Biochemistry* **332**: 627-632.

Cope, M. and D. T. Delpy (1988). "A system for the long-term measurement of cerebral blood and tissue oxygenation in newborn infants by near infra-red transillumination." *Medical and Biological Engineering and Computing* **26**: 289-294.

Cope, M. (1991). The Application of Near Infrared Spectroscopy to Non Invasive Monitoring of Cerebral Oxygenation in the Newborn Infant. Department of Medical Physics and Bioengineering. London, University College London.

Coyle, S., C. Markham, W. Lanigan and T. Ward (2005). A mechanical mounting system for functional near-infrared spectroscopy brain imaging studies. Opto-Ireland 2005, non-paginated CD-ROM.

Coyle, S., T. Ward and C. Markham (2004a). Physiological Noise in Near-infrared Spectroscopy: Implications for Optical Brain Computer Interfacing. The 26th Annual International Conference of the IEEE Engineering in Medicine and Biology Society, San Francisco, non-paginated CD-ROM.

Coyle, S., T. Ward and C. Markham (2004b). "An Optical Brain Computer Interface." *Biomedizinische Technik, Proceedings of the 2nd International Brain-Computer Interface Workshop and Training Course* **49**: 45-46.

Coyle, S., T. Ward, C. Markham and G. McDarby (2003a). "On the suitability of Near-Infrared Systems for Next Generation Brain Computer Interfaces." World Congress on Medical Physics and Biomedical Engineering, Sydney, Australia, non-paginated CD-ROM.

Coyle, S., T. Ward and C. Markham (2003b). Cerebral Blood Flow Changes related to Motor Imagery, using Near-infrared Spectroscopy (NIRS). World Congress on Medical Physics and Biomedical Engineering, Sydney, non-paginated CD-ROM.

Coyle, S., T. Ward, C. Markham, B. Roche, G. McDarby and S. F. McCloone (2003c). The use of Near-Infrared Spectroscopy in measuring general autonomic arousal. World Congress on Medical Physics and Biomedical Engineering, Sydney, Australia, non-paginated CD-ROM.

Coyle, S., T. Ward and C. Markham (2003d). "Brain-Computer Interfaces: A Review." *Interdisciplinary Science Reviews* **28**(2): 112-118.

Coyle, S., T. Ward, C. Markham and G. McDarby (2003e). "On the suitability of Near-Infrared Systems for Next Generation Brain Computer Interfaces." *Physiological Measurement Special Issue: World Congress on Medical Physics and Biomedical Engineering 2003* **25**: 815-822.

Crammond, D. J. (1997). "Motor Imagery: never in your wildest dream." *Trends in Neuroscience* **20**(2): 54-57.

Dassonville, P., X. Zhu, K. Ugurbil, S. Kim and J. Ashe (1997). "Functional activation in motor cortex reflects the direction and the degree of handedness." *Proceedings of the National Academy of Science* **94**: 14015-14018.

de Lafuente, V. and R. Romo (2004). "Language abilities of motor cortex." *Neuron* **41**(2): 178-180.

Decety, J. and D. H. Ingvar (1990). "Brain Structures Participating in Mental Simulation of Motor Behaviour: A Neuropsychological Interpretation." *Acta Psychologica* **73**: 13-34.

Decety, J., M. Jeannerod, D. D and G. Baverel (1993). "Central activation of autonomic effectors during mental simulation of motor actions in man." *Journal of Physiology* **461**(1): 549-563.

Decety, J., D. Perani, M. Jeannerod, V. Bettinardi, B. Tadary, R. Woods, J. C. Mazziotta and F. Fazio (1994). "Mapping motor representations with positron emission tomography." *Nature* **371**: 600-602.

de Charms, R. C., K. Christoff, G. H. Glover, J. M. Pauly, S. Whitfield and J. D. E. Gabrieli (2004). "Learned regulation of spatially localized brain activation using real-time fMRI." *NeuroImage* **21**: 436-443.

Dechent, P., K. Merboldt and J. Frahm (2004). "Is the human primary motor cortex involved in motor imagery?" *Cognitive Brain Research* **19**: 138-144.

Dobelle, W. H. (2000). "Artificial vision for the blind by connecting a television camera to the visual cortex." *ASAIO Journal* **46**: 3–9.

Donchin, E., K. M. Spencer and R. Wijesinghe (2000). "The Mental Prosthesis: Assessing the Speed of a P300-Based-Brain-Computer Interface." *IEEE*

Transactions on Rehabilitation Engineering **8**(2): 174-179.

Donoghue, J. P. (2002). "Connecting cortex to machines: recent advances in brain interfaces." *Nature Neuroscience Supplement* **5**: 1085-1088.

Duncan, A., J. H. Meek, M. Clemence, C. E. Elwell, L. Tyszczuk, M. Cope and D. T. Delpy (1995). "Optical pathlength measurements on adult head, calf and forearm and the head of the newborn infant using phase resolved optical spectroscopy." *Physics in Medicine and Biology* **40**: 295-304.

Duncan, A., J. H. Meek, M. Clemence, C. E. Elwell, P. Fallon, L. Tyszczuk, M. Cope and D. T. Delpy (1996). "Measurement of Cranial Optical Path Length as a Function of Age Using Phase Resolved Near Infrared Spectroscopy." *Pediatric Research* **39**(5): 889-893.

Edvinsson, L. and D. N. Krause, (Eds.) (2002). Cerebral Blood Flow and Metabolism. Philadelphia, Lippincott Williams and Wilkins.

Elfgren, C. I. and J. Risberg (1998). "Lateralized frontal blood flow increases during fluency tasks: influence of cognitive strategy." *Neuropsychologica* **36**(6): 502-512.

Elwell, C. E. (1995). A practical users guide to near-infrared spectroscopy, UCL Reprographics, London, UK.

Elwell, C. E., R. Springett and E. Hillman (1999). "Oscillations in Cerebral Haemodynamics - Implications for Functional Activation Studies." *Advances in Experimental Medicine and Biology* **471**: 57-65.

Fallgatter, A. J. and W. K. Strik (1998). "Frontal brain activation during the Wisconsin Card Sorting Test assessed with two-channel near-infrared spectroscopy." *European Archives of Psychiatry and Clinical Neuroscience* **248**: 245-249.

Farwell, L. A. and E. Donchin (1988). "Talking off the top of your head: toward

205

a mental prosthesis utilizing event-related brain potentials." *Electroencephalography and Clinical Neurophysiology* **70**: 510-523.

Forrest, G., T. Zikov and Y. Zhou (2001). Evaluation of an Asynchronous Switch Application using Frustration Metrics for Potential use in Biological Driven Switches (especially EEG). Proceedings of Human Interface Technologies, 16-22.

Fox, P. T. and M. E. Raichle (1986). "Focal physiological uncoupling of cerebral bloof flow and oxidative metabolism during somatosensory stimulation in human subjects." *Proceedings of the National Academy of Science* **83**: 1140-1144.

Fox, P. T., Raichle M.E., Mintun M.A., Dence C., (1988). "Nonoxidative Glucose Consumption During Focal Physiologic Neural Activity." *Science* **241**: 462-464.

Franceschini, M. A., S. Fantini, J. H. Thompson, J. P. Culver and D. Boas (2003). *"Hemodynamic evoked response of the sensorimotor cortex measured noninvasively with near-infrared optical imaging."* Psychophysiology *40: 548–560.*

Fritsch, G. and E. Hitzig (1870). "On the Electrical Excitability of the Cerebrum." as quoted in Mind, Brain and Adaptation in the Nineteenth Century: Cerebral Localisation and its Biological Content from Gall to Ferrier, Young, R.M. Oxford University Press (1990).

Fukui, Y., Y. Ajichi and E. Okada (2003). "Monte Carlo prediction of near-infrared light propagation in realistic adult and neonatal head models." *Applied Optics* **42**(16): 2881-2887.

Gauger, G. E. (1980). "Communication in the Locked-in Syndrome." *Transactions of the American Society of Artificial Internal Organs* **26**: 527-529.

Gembris, D., J. G. Taylor, S. Schor, W. Frings, D. Suter and S. Posse (2000).

"Functional Magnetic Resonance Imaging in Real-Time (FIRE):Sliding-Window Correlation Analysis and Reference-Vector Optimization." *Magnetic Resonance in Medicine* **43**: 259-268.

Gjedde, A., S. Ohta, H. Kuwabara and E. Meyer (1991). Is oxygen diffusion limiting for blood-brain transfer of oxygen? Brain Work and Mental Activity, Alfred Benzon Symposium 31, Copenhagen. N. Lassen, D. H. Ingvar, M. E. Raichle and L. Friberg, Blackwell Science: 177-184.

Gratton, G. and M. Fabiani (2001). "Shedding light on brain function: the event-related optical signal." *Trends in Cognitive Science* **5**(8): 357-363.

Gratton, G., M. Fabiani, T. Elbert and B. Rockstroh (2003). "Seeing right through you: Applications of optical imaging to the study of the human brain." *Psychophysiology* **40**(4): 487-491.

Guyton, A. C. (1987). Human Physiology and Mechanisms of Disease, W.B. Saunders Company.

Hebden, J. C. and D. T. Delpy (1997). "Diagnostic Imaging with light." *The British Journal of Radiology* **70**: S206-S214.

Hebden, J. C. (2003). "Advances in optical imaging of the newborn infant brain." *Psychophysiology* **40**: 501-510.

Herrmann, M. J., A. C. Ehlis and A. J. Fallgatter (2003). "Frontal activation during a verbal fluency task as measured by near-infrared spectroscopy." *Brain Research Bulletin* **61**: 51-56.

Hillman, E. (2002). Experimental and theoretical investigations of near infrared tomographic imaging methods and clinical applications, PhD thesis, University of London.

Hinterberger, T., S. Schmidt, N. Neumann, J. Mellinger, B. Blankertz, G. Curio and N. Birbaumer (2004). "Brain-computer communication with slow cortical potentials: Methodology and critical aspects." *IEEE Transactions on Biomedical Engineering* **51**(6): 1011-1018.

Homan, R., J. Herman and P. Purdy (1987). "Cerebral location of international 10-20 system electrode placement." *Electroencephalography and Clinical Neurophysiology* **66**(376-382).

Hoshi, Y. and M. Tamura (1993). "Detection of dynamic changes in cerebral oxygenation coupled to neuronal function during mental work in man." *Neuroscience Letters* **150**: 5-8.

Hoshi, Y., I. Oda, Y. Wada, Y. Ito, Y. Yamashita, M. Oda, K. Ohta, K. Yamada and M. Tamura (2000). "Visuospatial imagery is a fruitful strategy for the digit span backward task: a study with near-infrared optical tomography." *Cognitive Brain Research* **9**: 339-342.

Hubel, D. H. (1979). "The Brain." *Scientific American* **241**(3): 39-47.

ICNIRP Guidelines (1997). "Guidelines on Limits of Exposure to Broad-Band Incoherent Optical Radiation (0.38 to 3μm)."

ICNIRP Guidelines (2000). Revision of the Guidelines on Limits of Exposure to Laser Radiation of Wavelengths between 400nm and 1.4μm.

IEEE (1994). Standard for digitizing waveform recorders, IEEE Standard 1057.

Izzetoglu, K., G. Yurtsever, A. Bozkurt, B. Yazici, S. Bunce, K. Pourrezaei and B. Onaral (2003). NIR Spectroscopy Measurements of Cognitive Load Elicited by GKT and Target Categorization. 36th Hawaii Internaitonal Conference on System Science, Hawaii, non-paginated.

Jasper, H. H. (1958). "The ten-twenty electrode system of the International

Federation." *Electroencephalography and Clinical Neurophysiology* **10**: 371-375.

Jeannerod, M. and J. Decety (1995). "Mental motor imagery: a window into the representational stages of action." *Current Opinion in Neurobiology* **5**: 727-732.

Jeannerod, M. (1995). "Mental Imagery in the Motor Cortex." *Neuropsychologica* **33**(11): 1419-1432.

Jobsis, F. F. (1977). "Non-invasive infrared monitoring of cerebral and myocardial oxygen sufficiency and circulatory parameters." *Science* **198**: 1264-1267.

Jobsis, F. F. (1999). "Discovery of the Near-Infrared Window into the Body and the Early Development of Near-Infrared Spectroscopy." *Journal of Biomedical Optics* **4**(4): 392-396.

Kanji, G. K. (2002). 100 Statistical Tests. London, SAGE Publications.

Kauhanen, L., P. Rantanen, J. A. Lehtonen, I. Tarnanen, H. Alaranta and M. Sams (2004). "Sensorimotor cortical activity of tetraplegics during attempted finger movements." *Biomedizinische Technik,Proceedings of the 2nd International Brain-Computer Interface Workshop and Training Course* **49**(1): 59-60.

Keenan, R., S. Horovitz, A. Maki, Y. Yamahita, H. Koizumi and J. Gore (2002). "Simultaneous Recording of Event-Related Auditory Oddball Response Using Transcranial Near Infrared Optical Topography and Surface EEG." *Neuroimage* **16**: 587-592.

Kennedy, P. R., A. E. Bakay, M. Moore, K. Adams and J. Goldwaithe (2000). "Direct Control of a Computer from the Human Central Nervous System." *IEEE Transactions on Rehabilitation Engineering* **8**(2): 198-202.

Kohl, M., C. Nolte, H. R. Heekeren, S. Horst, U. Scholz, H. Obrig and A. Villringer (1998). "Determination of the wavelength dependence of the differential pathlength factor from near-infrared pulse signals." *Physics in Medicine and Biology* **43**: 1771-1782.

Kohl-Bareis, M., H. Obrig, Steinbrink J., K. Uludag and A. Villringer (2002). "Noninvasive monitoring of cerebral blood flow by a dye bolus method: separation of brain from skin and skull signals." *Journal of Biomedical Optics* **7**(3): 464-470.

Krauledat, M., G. Dornhege, B. Blankertz, G. Curio and K. Müller (2004). "The berlin brain-computer interface for rapid response." *Biomedizinische Technik* **49**(1): 61-62.

Krepki, R., B. Blankertz, G. Curio and K. Mueller (2003). The Berlin Brain-Computer Interface(BBCI) towards a new communication channel for online control of multimedia applications and computer games. 9th International Conference on Distributed Multimedia Systems (DMS'03).
Kuebler, A., B. Kotchoubey, J. Kaiser, E. W. Wolpaw and N. Birbaumer (2001). "Brain-computer communication: Unlocking the Locked In." *Psychological Bulletin* **127**(3): 358-375.

Lacourse, M. G., J. Turner, E. Randolph-Orr, S. L. Schandler and M. J. Cohen (2004). "Cerebral and cerebellar sensorimotor plasticity following motor imagery-based mental practice of a sequential movement." *Journal of Rehabilitation Research and Development* **41**(4): 505-524.

Laitinen, L. (2003). Neuromagnetic sensorimotor signals in brain computer interfaces. Department of Electrical and Communications Engineering. Helsinki, Helsinki University of Technology.

Lalor, E., S. P. Kelly, C. Finucane, R. Burke, R. Reilly and G. McDarby (2004). "Brain Computer Interface Based on the Steady State VEP for Immersive Gaming Control." *Biomedizinische Technik* **49**: 63-64.

Lancraft, T., F. Frierson, E. Sun and Y. Ivlev (2002). Interactions: Exploring the Functions of the Human Body , Regulation: The Nervous and Endocrine Systems (CD package - Software), Wiley.

Lebid, S., R. O'Neill, C. Markham, T. Ward and S. Coyle (2005). Multi-timescale measurements of brain responses in visual cortex during functional stimulation using time-resolved spectroscopy. Opto-Ireland, Dublin.

Leung, T. S., C. E. Elwell, J. R. Henty and D. T. Delpy (2003). Simultaneous measurement of cerebral tissue oxygenation over the adult frontal and motor cortex during rest and functional activation. Oxygen Transport in Tissue XXIII. D. Wilson, Kluwer Academic/Plenum Publishers: 385-389.

Leuthardt, E. C., G. Schalk, J. R. Wolpaw, J. G. Ojemann and M. D.W. (2004). "A brain–computer interface using electrocorticographic signals in humans." *Journal of Neural Engineering* **1**: 63-71.

Lotze, M., P. Montoya, M. Erb, E. Huelsmann, H. Flor, U. Klose, N. Birbaumer and W. Grodd (1999). "Activation of Cortical and Cerebellar Motor Areas during Executed and Imagined Hand Movements: An fMRI Study." *Journal of Cognitive Neuroscience* **11**(5): 491-501.

Luo, Q., S. Nioka and B. Chance (1996). Imaging on Brain Model by a Novel Optical Probe - Fiber Hairbrush. OSA TOPS on Advances in Optical Imaging and Photon Migration, Orlando, Florida.

MacKenzie, I. S. (1991). Fitts' law as a performance model in human-computer interaction., University of Toronto, Ontario, Canada.

Maki, A., Y. Yamashita, Y. Ito, E. Watanabe, Y. Mayanagi and H. Koizumi (1995). "Spatial and temporal analysis of human motor activity using noninvasive NIR topography." *Medical Physics* **22**(12): 1997-2005.

Maki, A., Y. Yamashita, E. Watanabe and H. Koizumi (1996). "Visualising

human motor activity by using non-invasive optical topography." *Frontiers in Medical and Biological Engineering* 7(4): 285-297.

Malonek, D. and A. Grinvald (1996). "Interactions Between Electrical Activity and Cortical Microcirculation Revealed by Imaging Spectroscopy: Implications for Functional Brain Mapping." *Science* 272: 551-554.

Malonek, D., U. Dirnagl, U. Lindauer, K. Yamada, I. Kanno and G. A. (1997). "Vascular imprints of neuronal activity: Relationships between the dynamics of cortical blood flow, oxygenation, and volume changes following sensory stimulation." *Proceedings of the National Academy of Science* 94: 14826-14831.

Mao, H., R. Muthupillai, P. R. Kennedy, C. A. Popp and A. W. Song (1998). "Clinical application of fMRI: Motor cortex activation in a paralysed patient." *Medicamundi* 42(3): 19-22.

Martin, G. N. (1997). Human Neuropsychology. London, Prentice Hall.

Mason, S. G. and G. E. Birch (2000). "A Brain-Controlled Switch for Asynchronous Control Applications." *IEEE Transactions on Biomedical Engineering* 47(10): 1297-1307.

Mayhew, J. E. W., S. Askew, Y. Zheng, J. Porill, W. G.W.M, P. Redgrave, D. M. Rector and H. R.M (1996). "Cerebral Vasomotion: A 0.1Hz Oscillation in Reflected Light Imaging of Neural Activity." *Neuroimage* 4: 183-193.

McFarland, D., L. M. McCane and J. R. Wolpaw (1998). "EEG-Based Communication and Control: Short-Term Role of Feedback." *IEEE Transactions on Rehabilitation Engineering* 6(1): 7-11.

McNaught, A. D. and A. Wilkinson (1997). IUPAC Compendium of Chemical Terminology, Blackwell Science.

Middendorf, M., G. McMillan, G. Calhorn and K. S. Jones (2000). "Brain-

Computer Interfaces Based on the Steady-State Visual-Evoked Response." *IEEE Transactions on Rehabilitation Engineering* **8**(2): 211-214.

Millikan, G. A. (1942). "The oximeter, an instrument for measuring continuously the oxygenation saturation of arterial blood in man." *Review of Scientific Instruments* **13**: 434-444.

Montcel, B., M. Torregrossa and P. Poulet (2004). Optode positioning in time-resolved neurological near-infrared imaging. BIOMED Topical Meeting of the Optical Society of America, Miami Beach. USA.

Myslobodsky, M. S., R. Coppola, J. Bar-Ziv and D. R. Weinberger (1990). "Adequacy of the International 10-20 Electrode System for Computed Neurophysiologic Topography." *Journal of Clinical Neurology* **7**(4): 507-518.

Ngai, A. C., K. R. Ko, S. Morii and W. H.R. (1988). "Effect of sciatic nerve stimulation on pial arterioles in rats." *American Journal of Physiology, Heart and Circulatory Physiology* **254**: H133-H139.

Niedermeyer, E. and F. H. Lopes da Silva (1999). Electroencephalography: basic principles, clinical applications and related fields. Baltimore, MD, Lippincott, Williams and Wilkins.

Obermaier, B., C. Neuper, C. Guger and G. Pfurstscheller (2001). "Information Transfer Rate in a Five-Classes Brain-Computer Interface." *IEEE Transactions on Neural Systems and Rehabilitation Engineering* **9**(3): 283-288.

Obrig, H., N. Neufang, R. Wenzel, M. Kohl, J. Steinbrink, K. Einhaeupl and A. Villringer (2000). "Spontaneous Low Frequency Oscillations of Cerebral Hemodynamics and Metabolism in Human Adults." *Neuroimage* **12**: 623-639.

Ogawa, S., T. M. Lee, A. R. Kay and D. W. Tank (1990). "Brain magnetic resonance imaging with contrast dependent on blood oxygenation." *Proceedings of the National Academy of Science* **87**: 9869-9872.

Okada, E., M. Firbank, M. Schweiger, S. R. Arridge, M. Cope and D. D.T. (1997). "Theoretical and experimental investigation of near-infrared light propagation in a model of the adult head." *Applied Optics* **36**(1): 21-31.

Okada, E. and D. T. Delpy (2003). "Near-Infrared light propagation in an adult head model I. Modeling of low level scattering in the cerebrospinal fluid layer." *Applied Optics* **42**(16): 2906-2914.

Patterson, M. S., B. Chance and B. C. Wilson (1989). "Time resolved reflectance and transmittance for the non-invasive measurement of tissue optical properties." *Applied Optics* **28**(12): 2331-2336.

Penfield, W. and H. H. Jasper (1954). Epilepsy and the Functional Anatomy of the Human Brain. Boston, Little, Brown & Co.

Pfurstscheller, G., C. Neuper, G. R. Mueller, B. Obermaier, G. Krausz, A. Schloegl, R. Scherer, B. Graimann, C. Keinrath, D. Skliris, M. Woertz, G. Supp and C. Schrank (2003). "Graz-BCI: State of the Art and Clininical Applications." *IEEE Transactions on Neural Systems and Rehabilitation Engineering* **11**(2): 177-180.

Pfurstscheller, G. (2004). "Importance of motor imagery and of feedback by observation of a moving object in BCI research." *Biomedizinische Technik* **49**: 23-28.

Pfurtscheller, G. and C. Neuper (1997). "Motor imagery activates primary sensorimotor area in humans." *Neuroscience Letters* **239**: 65-68.

Pfurtscheller, G., C. Neuper, D. Flotzinger and M. Pregenzer (1997). "EEG-based discrimination between imagination of right and left hand movement." *Electroencephalography and Clinical Neuropsychology* **103**: 642-651.

Pfurtscheller, G., C. Neuper, C. Guger, W. Harkam, H. Ramoser, A. Schloegl, B. Obermaier and M. Pregenzer (2000). "Current Trends in Graz Brain–Computer Interface (BCI) Research." *IEEE Transactions on Rehabilitation Engineering* **8**(2): 216-219.

Philipkoski, K. (2005). "Patients Put on Thinking Caps." *Wired News* http://www.wired.com/news/medtech/0,1286,66259,00.html.

Picton, T. W. (1992). "The P300 Wave of the Human Event-Related Potential." *Journal of Clinical Neurophysiology* **9**(4): 456-479.

Polikoff, J., Bunnell H.T. and B. W. (1995). Toward a P300-based Computer Interface. Proceedings of the RESNA '95 Annual Conference, Arlington Va., RESNAPRESS.

Porro, C. A., V. Cettolo, M. P. Francesato and P. Baraldi (2000). "Ipsilateral involvement of primary motor cortex during motor imagery." *European Journal of Neuroscience* **12**: 3059-3063.

Posner, M. I. and M. E. Raichle (1996). Images of Mind. New York, Scientific American Library.

Prahl, S. A., M. Keijzer, S. L. Jacques and A. J. Welch (1989). A Monte Carlo Model of Light Propagation in Tissue. Dosimetry of Laser Radiation in Medicine and Biology. D. S. G. Mueller, Eds.,, SPIE Series. **IS 5**: 102-111.

Profio, A. E. (1989). "Light Transport in Tissue." *Applied Optics* **28**(12): 2216-2222.

Quaresima, V., M. Ferrari, M. C. P. van der Sluijs, J. Menssen and W. Colier (2002). "Lateral frontal cortex oxygenation changes during translationa and language switching revealed by non-invasive near-infrared multi-point measurements." *Brain Research Bulletin* **59**(3): 235-243.

Raichle, M. E. (1994). "Visualising the Mind." *Scientific American*: 36-42.

Raichle, M. E. (1998). "Behind the scenes of funcional brain imaging: A historical and physiological perspective." *Proceedings of the National Academy of Science* **95**: 765-772.

Rinne T, G. Gratton, M. Fabiani, N. Cowan, E. Maclin, A. Stinard, J. Sinkkonen, K. Alho, R. Naatanen (1999). "Scalp-recorded optical signals make sound processing in the auditory cortex visible?" Neuroimage 10(5):620-4

Roland, P. E. and L. Friberg (1985). "Localization of Cortical Areas Activated By Thinking." *Journal of Neurophysiology* **53**(5): 1219-1243.

Rolfe, P. (2000). "In Vivo Near-Infrared Spectroscopy." *Annual Review of Biomedical Engineering* **2**: 715-754.

Roth, M., J. Decety, M. Raybaudi, R. Massarelli, C. Delon-Martin, C. Segebarth, S. Morand, A. Gemignani, M. Décorps and M. Jeannerod (1996). "Possible involvement of primary motor cortex in mentally simulated movement: a functional magnetic resonance imaging study." *Cognitive Neuroscience* **7**: 1280-1284.

Rousche, P. J. and R. A. Normann (1998). "Chronic recording capability of the Utah Intracortical Electrode Array in cat sensory cortex." *Journal of Neuroscience Methods* **82**: 1-15.

Roy, C. S. and C. S. Sherrington (1890). "On the regulation of the blood-supply of the brain." *Journal of Physiology (London)* **11**: 85-108.

Rush University Medical Centre (2005). Overview of Nervous System Disorders http://www.rush.edu/rumc/page-P00797.html.

Ryer, A. (1997). Light Measurement Handbook, http://www.intl-light.com/handbook.

Sato, N., B. Hagihara, T. Kamada and H. Abe (1976). "A Sensitive Method for the Quantitative Estimation of Cytochromes a and a3 in Tissues." *Analytical Biochemistry* **74**: 105-117.

Schloegl, A., C. Neuper and G. Pfurtscheller (1997). Subject specific EEG patterns during motor imaginary. IEEE/EMBS 19th International Conference, Chicago, IL.

Schroeter, M. L., S. Zysset, T. Kupka, F. Kruggel and D. Y. von Cramon (2002). "Near-infrared Spectroscopy can detect brain activity during a color-word matching stroop task in an event-related design." *Human Brain Mapping* **17**: 61-71.

Serby, H., E. Yom-Tov and G. F. Inbar (2005). "An Improved P300 Based Brain Computer Interface." *IEEE Transactions on Neural Systems and Rehabilitation Engineering* **13**(1): 89-98.

Serruya, M. D., Hatsopoulos N.G., Paninski L., Fellows M.R. and Donoghue J.P. (2002). "Instant neural control of a movement signal." *Nature* **416**: 141-142.

Shoman, S., E. Halgren, E. M. Maynard and R. A. Normann (2001). "Motor-cortical activity in tetraplegics." *Nature* **413**: 793.

Spinney, L. (2003). "Hear my Voice." *New Scientist* **22**: 36-39.

Steinbrink, J., H. Wabnitz, H. Obrig, A. Villringer and H. Rinneberg (2001). "Determining changes in NIR absorption using a layered model of the hunan head." *Physics in Medicine and Biology* **46**: 879-896.

Steinmetz, H., G. Fuerst and B. Meyer (1989). "Craniocerebral topography within the international 10-20 system." *Electroencephalography and Clinical Neurophysiology* **72**: 499-506.

Stepnoski , R. A., LaPorta, A., Raccuia-Behling, F., Blonder, G.E., Slusher, R.E.,

Kleinfeld, D. (1991). "Noninvasive detection of changes in membrane potential in cultured neurons by light scattering." *Proceedings of the National Academy of Science USA* **88**: 9382-9386.

Stevens, C. F. (1979). "The Neuron." *Scientific American* **241**(3): 49-59.

Strangman, G., D. Boas and J. P. Sutton (2002). "Non-Invasive Neuroimaging Using Near-Infrared Light." *Biological Psychiatry* **52**: 679-693.

Strangman, G., M. A. Franceschini and B. D.A. (2003). "Factors affecting the accuracy of near-infrared spectroscopy concentration calculations for focal changes in oxygenation parameters." *Neuroimage* **18**: 865-879.

Sutter, E. E. (1992). "The Brain Response Interface: Communication through visually-induced electrical brain responses." *Journal of Microcomputer Applications* **15**: 13-45.

Sutton, S., M. Braren, J. Zubin and E. R. John (1965). "Evoked-Potential Correlates of Stimulus Uncertainty." *Science* **150**(3700): 1187-1188.

Syré, F., H. Obrig, J. Steinbrink, M. Kohl, R. Wenzel and V. A. (2000). "Are VEP Correlated Fast Optical Changes Detectable in the Adult by Non-invasive Near Infrared Spectroscopy (NIRS)?" *Advances in Medicine and Biology* **471**.

Tachtsidis, I., C. E. Elwell, S. L. Leung, C. Lee, M. Smith and D. T. Delpy (2004). "Investigation of cerebral haemodynamics by near-infrared spectroscopy in young healthy volunteers reveals posture-dependent spontaneous oscillations." *Physiological Measurement* **25**: 437-445.

Talwar, S. K., S. Xu, E. S. Hawley, S. A. Weiss, K. A. Moxon and J. K. Chapin (2002). "Rat navigation guided by remote control." *Nature* **417**: 37-38.

Taylor, D. M., S. I. Helms Tillery and A. B. Schwartz (2002). "Direct Cortical Control of 3D Neuroprosthetic Devices." *Science* **296**: 1829-1831.

Tegic Communications (2005). http://www.t9.com/

Toga, A. W. and J. C. Mazziotta (2000). Brain Mapping - The Systems, Academic Press.

Toga, A. W. and J. C. Mazziotta (2002). Brain Mapping - The Methods, Academic Press.

Toronov, V., M. A. Franceschini, M. Filiaci, S. Fantini and M. Wolf (2000). "Near-infrared study of fluctuations in cerebral hemodynamics during rest and motor stimulation: Temporal analysis and spatial mapping." *Medical Physics* **27**(4): 801-815.

Tortora, G. J. and S. R. Grabowski (2003). Principles of Anatomy and Physiology, Wiley.

Townsend, G., B. Grainmann and G. Pfurtscheller (2004). "Continuous EEG classification during motor imagery - Simulation of an asynchronous BCI." *IEEE Transactions on Neural Systems and Rehabilitation Engineering* **12**(2): 258-365.

van der Zee, P. (1993). Measurement and modelling of the optical properties of biological tissue in the near-infrared Ph.D,, University of London.

Vargas, C. D., E. Olivier, L. Craighero, L. Fadiga, J. R. Duhamel and A. Sirigu (2004). "The Influence of Hand Posture on Corticospinal Excitability: A Transcranial Magnetic Stimulation Study." *Cerebral Cortex* **14**: 1200-1206.

Vaughan, T. M., W. J. Heetderks, L. T. Trejo, W. R. Rymer, M. Weinrich, M. Moore, A. Kuebler, B. H. Dobkin, N. Birbaumer, E. Donchin, E. W. Wolpaw and J. R. Wolpaw (2003). "Brain-Computer Interface Technology: A Review of the Second International Meeting." *IEEE Transactions on Neural Systems and Rehabilitation Engineering* **11**(2): 94-109.

Vidal, J. J. (1977). "Real-time detection of brain events in EEG." *IEEE Proc.,*

Special Issue on Biological Signal Processing and Analysis **65**: 633-664.

Villringer, A., J. Planck, C. Hock, L. Schleinkofer and U. Dirnagl (1993). "Near infrared spectroscopy(NIRS): a new tool to study hemodynamic changes during activation of brain function in human adults." *Neuroscience Letters* **154**: 101-104.

Weinman, J. A. and S. T. Shipley (1972). "Effects of Multiple Scattering on Laser Pulses Transmitted through Clouds." *Journal of Geophysics Research* 77(36): 7123-7128.

Weiskopf, N., R. Veit, M. Erb, K. Mathiak, W. Grodd, R. Goebel and N. Birbaumer (2003). "Physiological self-regulation of regional brain activity using real-time functional magnetic resonance imaging (fMRI): methodology and exemplary data." *NeuroImage* 19(3): 577-586.

Weiss, R. (2003). Monkeys Control Robotic Arm With Brain Implants. Washington Post: AO1.

Wessberg, J., C. R. Stambaugh, J. D. Kralik, P. D. Beck, M. Laubach, J. K. Chapin, J. Kim, S. J. Biggs, M. A. Srinivasan and M. A. L. Nicolelis (2000). "Real-time prediction of hand trajectory by ensembles of cortical neurons in primates." *Nature* **408**: 361-365.

Wolf, M., U. Wolf, V. Toronov, A. Michalos, L. A. Paunescu, J. H. Choi and E. Gratton (2002). "Different Time Evolution of Oxyhemoglobin and Deoxyhemoglobin Concentration Changes in the Visual and Motor Cortices during Functional Stimulation: A Near-Infrared Spectroscopy Study." *Neuroimage* **16**: 704-712.

Wolf, M., U. Wolf, J. H. Choi, R. Gupta, L. P. Safonova, A. Michalos and E. Gratton (2002). "Functional Frequency-Domain Near-Infrared Spectroscopy Neuronal Signal in the Motor Cortex." *NeuroImage* **17**: 1868–1875.

Wolpaw, J., Farland, D., (1994). "Multichannel EEG-based brain computer communication." *Electroencephalography and Clinical Neurophysiology* **90**: 444-449.

Wolpaw, J., N. Birbaumer, W. Heetderks, D. Farland, P. Peckham, G. Schalk, E. Donchin, L. Quatrano, C. Robinson and T. Vaughan (2000). "Brain-Computer Interface Technology: A Review of the First International Meeting." *IEEE Transactions on Rehabilitation Engineering* **8**(2): 164-173.

Wolpaw, E. W., N. Birbaumer, D. McFarland, G. Pfurstscheller and T. Vaughan (2002). "Brain computer interfaces for communicaiton and control." *Clinical Neurophysiology* **113**: 767-791.

Wolpaw, J., Mc Farland D.J., Vaughan T.M., Schalk G. (2003). "The Wadsworth Center Brain-Computer Interface (BCI) Research and Development Program." *IEEE Transactions on Neural Systems and Rehabilitation Engineering* **11**(2): 204-207.

Wolpaw, J. R. and D. McFarland (2004). "Control of a two-dimensional movement signal by a non-invasive brain-computer interface in humans." *Proceedings of the National Academy of Science* **101**(51): 17849-17854.

Woodard, H. Q. and D. R. White (1986). "The composition of body tissue." *The British journal of Radiology* **59**: 1209-1219.

Wyatt, J. S., M. Cope, D. T. Delpy, C. E. Richardson, A. D. Edwards, S. Wray and E. O. R. Reynolds (1990). "Quantitation of Cerebral Blood Volume in Human Infants by Near-infrared Spectroscopy." *Journal of Applied Phyisology* **68**: 1086-1091.

Yoo, S., T. Fairneny, N. Chen, S. Choo, L. P. Panych, H. Park, S. Lee and F. A. Jolesz (2004). "Brain-computer interface using fMRI: spatial navigation by thoughts." *Neuroreport* **15**(10): 1591-1595.

Young, R. M. (1990). Mind, Brain and Adaptation in the Nineteenth Century: Cerebral Localization and Its Biological Context from Gall to Ferrier (History of Neuroscience), Oxford University Press.